SAO/NASA JOINT INVESTIGATION OF ASTRONOMICAL VIEWING QUALITY AT MT. HOPKINS OBSERVATORY: 1969-1971

M. R. PEARLMAN, J. L. BUFTON, D. HOGAN,
D. KURTENBACH, and K. GOODWIN

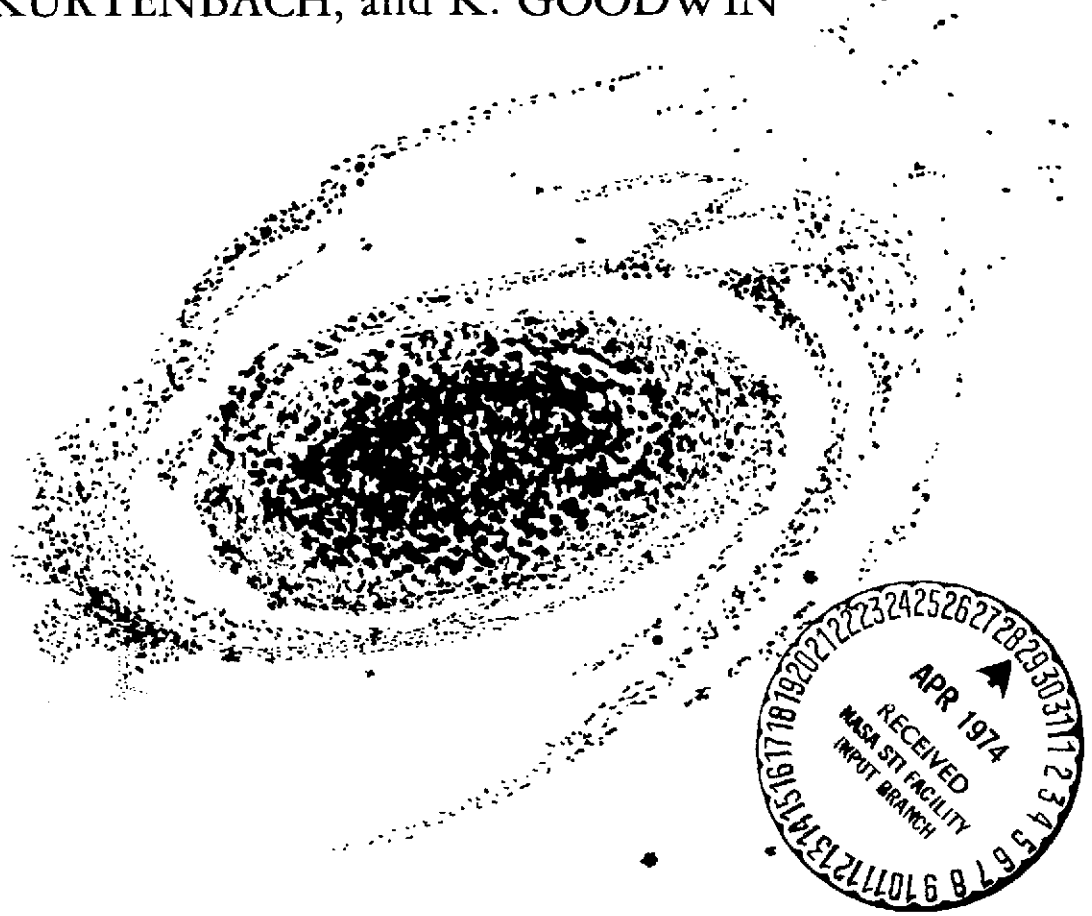

Smithsonian Astrophysical Observatory
SPECIAL REPORT 357

TABLE OF CONTENTS

TABLE OF CONTENTS (Cont.)

ILLUSTRATIONS

TABLES

ABSTRACT

Quantitative measurements of the astronomical seeing conditions have been made with a stellar-image monitor system at the Mt. Hopkins Observatory in Arizona. The results of this joint SAO–NASA experiment indicate that for a 15-cm-diameter telescope, image motion is typically 1 arcsec or less and that intensity fluctuations due to scintillation have a coefficient of irradiance variance of less than 0.12 on the average.

Correlations between seeing quality and local meteorological conditions are investigated. Local temperature fluctuations and temperature gradients were found to be indicators of image-motion conditions, while high-altitude-wind conditions were shown to be somewhat correlated with scintillation-spectrum bandwidth.

The theoretical basis for the relationship of atmospheric turbulence to optical effects is discussed in some detail, along with a description of the equipment used in the experiment. General site-testing comments and applications of the seeing-test results are also included.

RESUME

Les mesures quantitatives des conditions astronomiques de visibilité ont été prises à l'observatoire du Mont Hopkins, en Arizona, à l'aide d'un système de contrôle d'image stellaire. Les résultats de cette expérience commune du SAO et de la NASA indiquent que, pour un téléscope de 15 cm de diamètre, le mouvement typique de l'image est de 1 seconde d'arc maximum et que les fluctuations d'intensité dues à la scintillation ont un coefficient de variation d'irradience inférieur, en moyenne, à 0,12.

On étudie les corrélations qui existent entre la qualité de visibilité et les conditions météorologiques locales. On a trouvé que les fluctuations de température locale et les gradients de température indiquaient les conditions de mouvement de l'image, alors que les conditions de vent en haute altitude étaient, dans une certaine mesure, corrélatifs de la largeur de bande du spectre de scintillation.

On discute, de façon assez detaillée, le fondement théorique du rapport entre la turbulence atmosphérique et les effets optiques, et l'on decrit le matériel utilisé pour l'expérience. Sont également inclus, des commentaires généraux relatifs aux essais sur place et aux applications des résultats de l'essai de visibilité.

КОНСПЕКТ

Были проведены количественные измерения астрономических условий видимости пользуясь монитором звездного изображения в обсерватории Маунт Гопкинс в Аризоне. Результаты этого эксперимента совместно проведенного Смитсонианской Астрофизической Обсерваторией и Национальным комитетом по астронавтике и исследованию космического пространства указывают что для 15 см телескопа, движение изображения типично является 1 арк-сек или меньше и что флуктуации интенсивности вызываемые мерцанием имеют коэффициент дисперсии лучеискускания в среднем меньше 0,12.

Исследуются корреляции между качеством видимости и местными метеорологическими условиями. Местные колебания температуры и градиенты температуры были найдены как указатели условий движения изображений, в то время как ветровые условия на большой высоте были показаны в некоторой степени соответствующими с шириной полосы спектра мерцания.

Обсуждаются довольно детально, теоретическая основа связи атмосферной турбулентности с оптическими эффектами одновременно с описанием оборудования используемого в опыте. Также включены общие замечания о испытаниях станций и применяемости результатов испытаний видимости.

SAO/NASA JOINT INVESTIGATION OF ASTRONOMICAL VIEWING QUALITY AT MT. HOPKINS OBSERVATORY: 1969–1971

M. R. Pearlman, J. L. Bufton,* D. Hogan, D. Kurtenbach, and K. Goodwin

1. INTRODUCTION

During the period of June 1969 to February 1971, a series of experiments was performed, under sponsorship of the National Aeronautics and Space Administration (NASA) Headquarters, by the Smithsonian Astrophysical Observatory (SAO) at its Mt. Hopkins Observatory. The purpose was to obtain quantitative information on the astronomical "seeing" characteristics of the Mt. Hopkins site for future NASA and SAO use and, if possible, to relate these characteristics to local meteorological parameters. Data on nighttime stellar-image motion and scintillation were obtained with a stellar-image-monitor system supplied by NASA Goddard Space Flight Center (GSFC). Temperature-fluctuation measurements were made with a sensing device supplied by the Jet Propulsion Laboratory (JPL). Local measurements of temperature, temperature gradients, humidity, and wind velocity and direction were made and radiosonde data recorded on site. The analysis of the data was carried out jointly by SAO and NASA.

The series of experiments were divided into two phases. In Phase I, the specific goal was to monitor almost daily the astronomical seeing characteristics of the Mt. Hopkins site for a long period of time. Stellar data were taken three nights a week. Data collection began during June 1969 and continued until April 1970 except during July and August. The stellar data from Phase I were compared with gross meteorological data. Because of a lack of any strong correlations between seeing conditions

This work was supported in part by ~~grant~~ Contract NAS 12-2129 from the National Aeronautics and Space Administration.

*Goddard Space Flight Center, Laser Technology Branch, Code 723.

and meteorological data, plans for Phase II were modified to include longer stellar data runs on fewer observing nights and increased use of simultaneously acquired meteorological and temperature-fluctuation measurements. The JPL measurements of thermal fluctuation were begun in October 1970 and were employed to good advantage during the second phase, which extended from September 1970 to February 1971.

The results of the experiments indicate that the seeing conditions at the Mt. Hopkins Observatory are better than 1 arcsec on the average and that intensity fluctuations due to scintillation have a coefficient of irradiance variance (CIV) of less than 0.12 on the average. We find very little correlation with gross meteorological conditions such as temperature, humidity, and wind at the site. However, we find that local temperature fluctuations and temperature gradients are indicators of image-motion conditions and that mild correlations exist between scintillation-spectrum bandwidth and high-altitude winds.

We feel that our quantitative results and experience in comparing stellar-image data and local meteorological indicators should be of interest to investigators who are planning future programs at the Mt. Hopkins site and to those who, in general, are concerned with characterizing optical propagation effects on the vertical path at any other site. In particular, data of this type can be used to estimate the atmospheric channel performance for both coherent and pulsed-laser communication systems of high data rate. A discussion of these applications is included in this report.

2. THEORETICAL BACKGROUND AND EXPERIMENT RATIONALE

2.1 Relationship of Atmospheric Turbulence to Optical Effects

Astronomical "seeing" effects or degradation of stellar-image quality arises when an initially plane wave from a distant optical source such as a star is subjected to the temporal and spatial variability of the atmosphere before reaching a detector. As the initially plane wave encounters regions of atmospheric turbulence, local fluctuations in refractive index caused by the density fluctuations associated with turbulence scatter the wave. The results are immediate phase degradation (wavefront deformation) and subsequent amplitude fluctuations at distances far enough from the scattering point for interference effects to occur. At any point in the free atmosphere, typical density changes are of the order of 0.01 mg/cm^3, which corresponds to changes in refractive index of a few parts in 10^6 at visible wavelengths. The dimensions of the turbulence-induced density structures, which are most effective in this scattering process, range from a few centimeters to the order of meters. The effect of scattering at many points along the propagation path results in composite optical effects that are observed at ground level and that are commonly referred to as astronomical seeing.

When visible stellar radiation is collected by an optical system, these seeing effects manifest themselves in the image plane as scintillation (intensity variations of the entire image), image motion (movement of image center of gravity), and blurring (changes in image size and shape). Image motion and blurring, which are direct results of phase fluctuation, are total columnar effects. They are dependent not on the location of the turbulence along the propagation, but only on the total integrated influence. On the other hand, scintillation is in effect a diffraction process, with turbulent structure far from the receiver playing the most important role.

Both scintillation and phase effects have spatial structure that can be observed at the receiver. As the aperture stop and collecting optics of the system are increased in diameter, so that it is no longer a point receiver, the observed image effects reflect

a spatial averaging of the starlight phase and irradiance pattern sampled by the aperture. The magnitude of scintillation decreases with increasing aperture. When the aperture diameter exceeds the correlation length of the irradiance structure (8 to 10 cm), dictated by atmosphere quality and observation geometry, the effects of scintillation are significantly reduced. For small apertures, the dominant effect of the phase structure sampled is image motion, which is a result of the entire incident wavefront being tilted. As aperture diameter is increased, tilts in various regions of the aperture become uncorrelated, and the image undergoes more complex changes in size and shape, which lead to blurring. Aperture diameter common to stellar astronomy are in the range of 1 to 2 m, where scintillation effects are quite small; and the most serious degradation of image resolution is blurring rather than image motion. For convenience and economy of operation, we used a relatively small optical system (15-cm-diameter refractor) to facilitate the measurement of scintillation for our stellar-image data measurement. In our experiment, the primary phase-structure effect was image motion. Accordingly, the following discussions will primarily treat scintillation and image motion; however, some discussion on image blurring and the effects at large telescope diameters will also be included.

The turbulence process in the atmosphere is quite random in nature and thus produces an ensemble of spatial and temporal fluctuations for the observed optical effects. Accordingly, any description of this process must be statistical. For most situations that occur in the free atmosphere, the turbulence process itself has been found to be locally stationary, homogeneous, and isotropic; here, locally refers to that region of space and time for which the description of turbulence remains the same. Within each locality, an inertial subrange of turbulence-element sizes is said to exist. The inertial subrange is bounded on the upper end by an "outer scale," whose dimensions are characteristic of those processes responsible for the flow of energy into the turbulence process. The minimum or "inner scale" is dictated by the processes in which turbulence energy is dissipated as viscous friction. Energy is input to the system as turbulence of large scale and cascades down adiabatically to form the inertial subrange. The difference from one locality to another is simply the strength of turbulence, or scale factor, that multiplies the description of the inertial subrange. In addition to changes with time (nonstationarity), the nature of the atmospheric turbulence

changes significantly with altitude above the Earth's surface, but only moderately with horizontal displacements through the atmosphere. An overly simplified model of turbulence distribution would be a series of horizontal slabs or strata of well-developed turbulence slowly changing in time and interspersed with calm air.

The widely accepted Obukhov-Kolmogorov turbulence theory (Obukhov, 1941) states that within each inertial subrange, the spatial distribution of turbulence sizes and related physical properties obey identical power-law descriptions. The structure function, i.e., the mean-square difference of a quality of the turbulence, such as refractive index between two points as a function of the separation of the points $(\vec{r}_1, \vec{r}_2)$, is a complete statistical description. For visible radiation, temperature is the most important property that affects refractive index. The velocity fluctuations of turbulence cause temperature fluctuations as cold and warm parcels of air are mixed. Since the atmosphere will not support local pressure gradients, density and thus refractive-index fluctuations follow directly from the temperature fluctuations. The Obukhov-Kolmogorov theory expresses the temperature-structure function,

$$D_T(r) \equiv \langle [T(\vec{r}_2) - T(\vec{r}_1)]^2 \rangle = C_T^2 \, r^{2/3} \tag{1}$$

for $\ell_i \ll r = |\vec{r}_2 - \vec{r}_1|_o$, where $T(\vec{r})$ = ambient temperature at point $\vec{r}$, r = spatial separation, ℓ_i = inner scale, ℓ_o = outer scale, and C_T^2 is temperature-structure coefficient, a strength factor for the temperature fluctuations. From one locality to another, C_T^2 changes but the $r^{2/3}$ dependence remains. The inner scale, ℓ_i, is about 1 cm near ground level and is thought to increase slowly to about 10 cm at 10-km altitude. The outer scale, ℓ_o, has been estimated to be roughly equal to height above ground for the near-Earth environment and to be on the order of about 1 km at high altitude. For the narrow, nearly vertical propagation path that we are concerned with, the important variations in C_T^2 are with altitude above ground and with time. The dependence on altitude h will be denoted here as $C_T^2(h)$, and it will be understood that the coefficient value applies to a particular time or time average of a measurement.

The effect of temperature fluctuations (of strength $C_T^2(h)$) on refractive index is obtained by a straightforward application of the general formula (U.S. Air Force Research Center, 1960) for refractive index and the ideal gas law. The result for radiation in the visible or near infrared is given by

$$C_n^2(h) \approx \left[\frac{80P(h)}{T(h)^2} \times 10^{-6}\right]^2 C_T^2(h) \quad , \tag{2}$$

where P is the atmospheric pressure (mb), T is the temperature (K), and $C_n^2(h)$ is the strength factor or the refractive-index-structure coefficient. This is the desired connecting link between turbulence strength and optical refractive-index effects. It is now necessary to express the observed optical effects of scintillation and image motion in terms of $C_n^2(h)$, and for this, we must turn to wave-propagation theory.

Many theoretical treatments have addressed the problem of optical wave propagation through a turbulent medium. The most successful of these have relied on approximate solutions to the scalar wave equation,

$$\nabla^2 U(r) + k^2 N(r) U(r) = 0 \quad , \tag{3}$$

with U(r) = wavefunction (electromagnetic wave), $k = 2\pi/\lambda$, the free-space wavenumber, and N(r) = index of refraction. For a stellar source, the incident, normalized plane wave can be represented as

$$U(r) = \frac{A(r)}{A_0} \exp\left[ik\phi(r)\right] = \exp\left[ik\phi + \log_e\left(\frac{A}{A_0}\right)\right] \quad , \tag{4}$$

with A(r) = amplitude and $\phi(r)$ = phase. As a wave propagates toward Earth, it is perturbed by the turbulence in a multiplicative manner. As a result, quantities in the exponent add; and, after scattering from many points in the turbulence field, a gaussian distribution is implied by the central limit theorem for ϕ and $\log_e (A/A_0)$. This property has aided the calculation of statistical quantities dependent on phase and amplitude. The "Rytov approximation" has been used by Tatarski (1961) and others to linearize the wave equation by neglecting small terms in the plane-wave formulation of the scalar wave. This theoretical development is widely accepted for weakly scattered fields. For strong scattering, often observed over horizontal near-ground propagation paths in the daytime, a scattering saturation effect not predicted by the theory is observed. For the case here, i.e., near-vertical paths at night, no saturation effects are observed and the theory is thought to be valid. Where appropriate

below, the Rytov solutions for the statistical quantities necessary to explain scintillation and image motion will be quoted.

2.2 Scintillation

Total image intensity and the resulting fluctuations (i.e., scintillation) result from the irradiance pattern of starlight sampled by the telescope aperture. Irradiance varies with both position and time in the aperture plane. As noted above, the quantity log amplitude $[\log_e(A/A_0)]$ should obey gaussian statistics. Log amplitude can be defined in terms of irradiance,

$$\log_e\left(\frac{A}{A_0}\right) = \ell(x,t) = \frac{1}{2}\log_e\frac{I(x,t)}{I_0}\ (x,t) \quad , \tag{5}$$

where $\ell(x,t)$ is instantaneous log amplitude at point x in the aperture plane, $I(x,t)$ is corresponding irradiance, and I_0 is average irradiance. An expression for log-amplitude variance, σ_ℓ^2, follows (Tatarski, 1961, chapter 13) from the Rytov formulation and the Obukhov-Kolmogorov turbulence theory:

$$\sigma_\ell^2 = 0.56\ k^{7/6}\ \sec^{11/6}\theta \int_0^\infty C_N^2(h)\ h^{5/6}\ dh \quad , \tag{6}$$

where $k = 2\pi/\lambda$ and θ = stellar zenith angle. This equation is valid for a point detector – i.e., a telescope with aperture small enough so that the instantaneous irradiance is everywhere constant within the aperture. The wavelength dependence, $k^{7/6}$, predicts that σ_ℓ^2 is reduced by 20% in passing from 0.45 μm to 0.55 μm. While σ_ℓ^2 is reduced in magnitude at the higher wavelength, analysis (Tatarski, 1971) has shown that spectral correlation of σ_ℓ^2 remains high for this separation of wavelengths. The angular dependence in σ_ℓ^2 reflects the $h^{5/6}$ weighting and the air mass through which starlight must pass before reaching the telescope. This angular dependence breaks down for large zenith angles owing to the increased role of chromatic dispersion and to the resultant multipath effects through spatially uncorrelated turbulence. The dependence of σ_ℓ^2 on the strength of turbulence involves the 5/6 moment of altitude, showing the strong influence of even relatively low turbulence at high altitudes and the deemphasis of high turbulence conditions near the surface.

A photomultiplier tube or other square-law device is normally used in field work to obtain data on the stellar image. Electric-current output from this device is proportional to irradiance, not amplitude; and it is sometimes more convenient to handle the data in terms of irradiance statistics. The ratio of rms image-intensity fluctuations to the average value is a fundamental measure of irradiance statistics, called the coefficient of irradiance variance:

$$\mathrm{CIV} = \sigma_I / I_0 \quad , \tag{7}$$

where σ_I^2 = irradiance variance = $\langle (I - I_0)^2 \rangle$. The connection with log-amplitude statistics is

$$\mathrm{CIV}^2 = \exp(4\sigma_\ell^2) - 1 \approx 4\sigma_\ell^2 \quad , \tag{8}$$

where the approximation holds for the typically observed values of σ_ℓ^2 much less than 1.

The time structure of the irradiance pattern is best described by the autocorrelation function and its Fourier transform – i.e., the spectral-density function. Typical frequency content of scintillation is of the low-pass filter type extending from dc to frequencies of several hundred Hertz. The bandwidth of these spectra can be specified as the frequency value at which the spectral density function has fallen to 50% or, alternately, 10% of its maximum value. The bandwidth and, indeed, the shape of each spectrum are tied directly to the components $V_N(h)$ (component of mean horizontal wind speed $V_o(h)$, which carries the existing turbulence perpendicular to the line of sight). The quantity $V_N(h)$ can be computed from $V_o(h)$ with the additional knowledge of stellar zenith angle θ, azimuth angle α, and mean wind direction β (see Young, 1969),

$$V_N(h) = \frac{V_o(h)}{\sec\theta} \left[1 + \tan^2\theta \, \sin^2(\alpha - \beta)\right]^{1/2} \quad . \tag{9}$$

The size of the turbulence elements at each altitude that are most effective in contributing to scintillation is given by Fresnel diffraction theory as $\sqrt{\lambda h \sec\theta}$. Thus, the frequency at which each layer of wind speed is most effective in contributing to irradiance spectral density is proportional to

$$\frac{V_N(h)}{\sqrt{\lambda h \sec\theta}} \quad . \tag{10}$$

From this proportionality, it can be seen, for instance, that very low frequencies of scintillation should be associated with low wind speed at high altitude. Alternately, high wind speed and lower altitude contribure more to the high frequencies of scintillation. Modest correlations were found in our experiments between CIV spectral bandwidths and wind speeds at selected altitudes.

As the telescope aperture is increased in diameter from the point detector necessary for equation (6) to hold, the strength of scintillation, measured either by σ_ℓ^2 or by CIV, decreases rapidly at first and then more slowly as the spatial correlation distance of irradiance in the aperture plane is exceeded. For large apertures, the scintillation bandwidth is decreased while dependence on zenith angle to the star is increased. The spatial correlation distance of irradiance is determined by noting the separation distance at which the correlation between scintillation observed by two point detectors falls to 1/e of that observed at zero separation. Once again, by use of Fresnel diffraction theory, this distance can be associated with an altitude h_0 that is most effective in producing the strongest scintillations,

$$\text{spatial correlation distance} \approx \sqrt{\lambda h_o \sec\theta} \quad . \tag{11}$$

Experimental values for correlation distance are typically 8 to 10 cm for zenith viewing. For values of λ in the visible region, h_o is on the order of 10 to 20 km, where we expect significant turbulence due to the favorable meteorology of the tropopause and jet stream. This is additional evidence linking scintillation effects to turbulence at high altitude.

There are several theories for prediction of aperture-averaging effects for scintillation. They all result in a functional dependence on aperture diameter, correlation distance, and σ_ℓ^2 for a point detector. Unfortunately, at present no one theory can explain all the observed effects, especially for apertures larger than 1 m in diameter. Tatarski (1961) develops a general expression for aperture dependence that relies explicitly on the correlation coefficient of the fluctuations in log amplitude. Assuming

a case where C_n^2 is constant, he shows that the log-amplitude variance, and thus CIV depends on aperture D through the relation $(D/\sqrt{\lambda L})^{-7/3}$. With arguments from geometric optics, Reiger (1963) finds a similar dependence on aperture for scintillation.

Experimental work by Protheroe (1954), Tatarski (1961, 1971), and others shows the CIV or σ_ℓ zenith-angle dependence to vary with aperture as:

aperture diameter	dependence
3 in.	$(\sec\theta)^{0.9}$
6 in.	$(\sec\theta)^{1.2}$
12.5 in.	$(\sec\theta)^{1.4}$

Protheroe's data have been used to develop the following equation for a 15-cm (6-in.) aperture:

$$\sigma_\ell^2/(15\text{ cm}) \approx 0.09 k^{7/6} \sec^{2.4}\theta \int_0^\infty C_n^2(h)\, h^{5/6}\, dh \quad . \tag{12}$$

The CIV data taken in this experiment at Mt. Hopkins with a 6-in. telescope agree well with the $(\sec\theta)^{1.2}$ dependence observed by the above investigators.

2.3 Image Motion

Movement of the image center of gravity results from a linear phase change or tilt in the incoming wavefront. In the limit of a point detector, all phase changes appear linear. For a finite aperture, however, phase changes in different parts of the aperture become more uncorrelated as aperture diameter increases. Any image motion is then due to a resultant tilt after spatial averaging in the aperture plane. The uncorrelated phase changes also result in blurring of the image.

An expression for image-motion variance σ_m^2 (in square radians) can be derived by the Rytov method of Tatarski (1961), the Obukhov-Kolmogorov turbulence spectrum, and the modifications by Hufnagel (1966a) to include a circular aperture. The result,

$$\sigma_m^2 = 0.56\, D^{-1/3} \sec\theta \int_0^\infty C_n^2(h)\, dh \quad , \tag{13}$$

is independent of wavelength and applies only to motion in one dimension of the image plane. Under the assumption of isotropic image motion, the total two-dimensional image-motion variance is $2\sigma_m^2$. The aperture diameter dependence $D^{-1/3}$ is weak; only a decrease of a factor of 2 in σ_m^2 is predicted when D increases by a factor of 10. The dependence on air mass (sec θ) is linear, and the dependence of turbulence strength is a straightforward integration over $C_n^2(h)$ along the propagation path. It should be noted that equation (13) depends on theory that is valid only for $D \gtrsim \sqrt{\lambda h_o \sec\theta}$, the irradiance correlation coefficient. For smaller apertures, the $D^{-1/3}$ dependence holds but the constant multiplier will be reduced. In addition, the inner and outer bounds on D, for which (13) applies, are determined by the inner ℓ_i and outer ℓ_o turbulence scale sizes, respectively, which, as noted before, vary with altitude and with time. With these factors and limitations in mind, equation (13) should be an adequate prediction for the one-dimensional motion measured by the 15-cm-diameter telescope used in this experimental study. Data taken by Kolchinskii (1969) and in this experiment at Mt. Hopkins show a zenith-angle dependence that agrees well with this relation.

Several theoretical treatments based on different approximations for the spectral density of image motion have resulted in expressions involving the normal wind component $V_N(h)$ and turbulence strength $C_n^2(h)$. Observed spectra indicate extremely low-frequency behavior for image motion. Most energy is contained below 5 Hz, with typically less than 1% of the motion above 20 Hz. To predict such low frequencies, the theoretical treatments require low wind velocities of only a few meters per second. These velocities generally occur at ground level or above 20 km. Since image motion is equally weighted to all regions of turbulence depending only on the value of $C_n^2(h)$ and since owing to the rarefied air, little turbulence is expected above 20 km, the implication is that image motion is associated with turbulence near ground level.

2.4 Image Blurring

Specification of image size or profile is the final step in a description of the atmospherically distorted stellar image. Size determination and the whole investigation

of image quality are handled easily through the use of optical transfer-function techniques. The modulation transfer function (MTF) of an optical system is a measure of reduction in contrast suffered by each Fourier component of the object after transmission through the entire imaging system. It is a function of a transform variable, the image-plane spatial frequency f. The variable f has dimensions of cycles per unit length. Multiplication by system focal length allows spatial frequency to be expressed in cycles per radian of the field of view. This will be denoted as ω and is easily related to cycles per second of arc.

The image blurring to be expected in telescopes of aperture diameter greater than 15 cm can be estimated from the MTF; all data reported here were obtained with such telescopes. The observed MTF of $M(\omega)_o$ for starlight observations is the product of the telescope MTF, which is $M(\omega)_T$, and the atmospheric MTF, which is $M(\omega)_A$:

$$M(\omega)_o = M(\omega)_T \, M(\omega)_A \quad . \tag{14a}$$

If the averaging time of the experimental determination of $M(\omega)_o$ is small, as it is in short-exposure photography, all effects of image motion are frozen out. The resultant image is sharper, differing from the diffraction-limited case by only the contribution of residual atmospheric blur. Laboratory calibrations and field measurements at Mt. Hopkins with the 15-cm telescope revealed little if any image degradation beyond that already present in the telescope optics. This is essentially a restatement that atmospherically induced phase degradation appears primarily as image motion in telescopes of diameter 15 cm or smaller. The net result is that $M(\omega)_A$ for the short-term time average can be approximated by unity. For long-term time averages, as is the case in a long-exposure photograph or in an image viewed through a large-diameter telescope, $M(\omega)_A$ becomes the product of the short-term atmospheric MTF and an MTF constructed from image motion,

$$M(\omega)_M = \exp\left[-\left(4\pi^2 \frac{\sigma_m^2}{2} \omega^2\right)\right] \quad , \tag{14b}$$

as reported by Hufnagel (1966a). Although this result is constructed with σ_m^2, or one-dimensional image-motion variance observed through the aperture of 15-cm diameter, it specifies the atmospheric contribution to long-term image degradation by virtue of the short-term $M(\omega)_A$ being nearly unity for the 15-cm aperture. Image profile due to atmospheric effects is obtained by applying the inverse Fourier transform,

$$I(s) = 2\pi \int_0^\infty \omega M(\omega)_M \, J_0(2\pi \, s\omega) \, d\omega \quad , \tag{15}$$

where s is seconds of arc in the focal plane. Inserting equation (14) in equation (15) and approximating the integral yields

$$I(s) = \frac{1}{2\pi \, \sigma_m^2} \exp\left[-\left(\frac{s^2}{2\sigma_m^2}\right)\right] \quad . \tag{16}$$

This is a gaussian shape with variance σ_m^2. Thus, the rough estimate of image size (diameter at half maximum) in a large telescope is just $2\sigma_m$, where σ_m is rms image motion expressed in seconds of arc.

2.5 Turbulence Profiles and Relationship of Meteorology to Turbulence Structure

The common factor in the foregoing wave-propagation theory is an integral expression containing $C_n^2(h)$, the refractive-index structure constant as a function of altitude. Lack of both experimental and theoretical knowledge of this profile is the single greatest obstacle to full understanding of vertical propagation. If the profile were known, optical-propagation theory could be tested in any number of interesting experiments, and astronomical seeing could be predicted in advance. What experimental data are available suggest that turbulence strength is usually greatest in the first kilometer comprising the atmospheric boundary layer, with occasional but persistent layers of secondary strength at high altitudes in the troposphere and lower stratosphere. The near-ground turbulence is found to be quite dependent on local terrain, local meteorology, and time of day, while the upper altitude structure is more constant in time and space.

Data on boundary-layer turbulence have been reported by Coulman (1969), Tsvang (1969), and Lawrence, Ochs, and Clifford (1970). These data were obtained by measuring, from balloon and aircraft platforms, the profiles of microthermal statistics and thus $C_n^2(h)$. More recently, Bufton, Minott, Fitzmaurice, and Titterton (1972) extended balloon-borne temperature-sensor measurements to the region of the tropopause. All these investigators report wide fluctuations in $C_T^2(h)$ and thus $C_n^2(h)$, which indicate that the turbulence process is quite nonstationary. It is only with time averages on the order of minutes that an average profile or envelope of the fluctuations of $C_n^2(h)$ can be constructed. The average profile can then be used effectively to predict optical propagation effects. In the absence of other data, this consideration has lead several researchers to construct a turbulence-profile model, i.e., a functional dependence for the average behavior of $C_N^2(h)$. Model parameters can then be adjusted for correct prediction of ground-based stellar data. A particularly useful model is that reported by Hufnagel (1966b) and shown in Figure 1. His curve is for nighttime atmospheric conditions; it exhibits a near-ground maximum of 2×10^{-14} $m^{-2/3}$, an exponential-like decrease to 10^{-17} $m^{-2/3}$ at 1000 m, a relatively constant range of minimum values to about 10 km, and then a sharp bump of height 2×10^{-16} $m^{-2/3}$ at 12 km. Brookner (1971) describes this profile analytically as

$$C_N^2(h) = 2.5 \times 10^{-13}\, h^{-1}\, e^{-h/320} + 2 \times 10^{-16}\, \delta(h - 12\ \text{km}) \quad . \tag{17}$$

The exponential decrease near ground level corresponds reasonably well to observed $C_N^2(h)$ data, but the delta-function spike at 12 km does not. Actually, high-altitude thermal-sensor data reported by Bufton et al. (1972) and extensive radar backscatter measurements reported by Hardy and Katz (1969) reveal many thin, highly turbulent layers distributed over the altitude range of 4 to 15 km. The delta-function model has a magnitude equal to the integrated effect of these multiple layers and is centered near the midpoint of their distribution; however, it does not have the correct distribution for upper altitude turbulence.

Any model proposed should reflect probable meteorological factors at the origin of turbulence. As noted previously, essentially all refractive-index variations are accounted for by small-scale temperature fluctuations. These in turn can be related to the pertinent larger scale meteorological parameters. The intent is not to construct

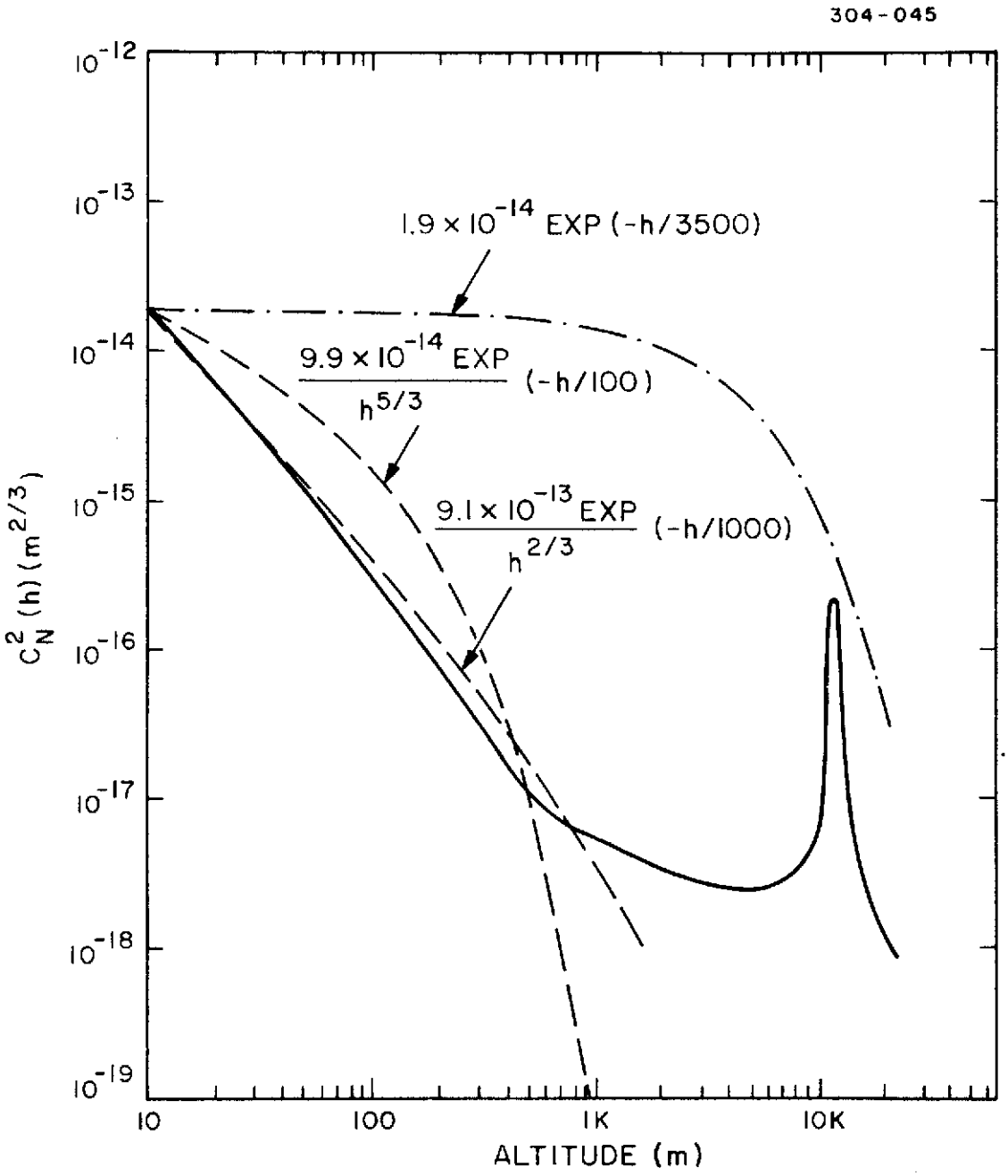

Figure 1. Model of turbulent profile (Hufnagel, 1966b).

an actual profile from meteorological parameters but to show their influence and to select for measurement those parameters that would provide a useful estimate of turbulence conditions.

The strength of the turbulence along the observation path, or $C_T^2(h)$, is a measure of the spatial fluctuations in the temperature field. In the presence of a wind field, this spatial temperature structure is observed as temporal fluctuation at fixed reference points. The first obvious quantity to investigate, then, is temperature fluctuation in the vicinity of the site and along the vertical observation column. From equation (13), we expect a linear relation (correlation) between temperature fluctuations and σ_m. Investigations using microthermal sensors near ground level have been carried out by Coulman (1965) and others (Tsvang, 1969; Ochs, 1967). A sensing device that measures the average value of the peak temperature fluctuations was used with some success in the present experiment.

Another approach to explain seeing conditions in terms of meteorological parameters is based on the connection between C_T^2 and the small-scale processes involved in turbulence activity. From Tatarski (1961, chapter 10),

$$C_T^2 \propto \overline{N}\epsilon^{-1/3} \quad , \tag{18}$$

where $\overline{N}$ is the rate at which temperature variations in the atmosphere are dissipated by molecular activity, and ϵ is the analogous dissipation rate for turbulent kinetic energy.

Numerous measurements of ϵ are available for at least the lower altitudes. Typical values, as quoted by Hufnagel and Stanley (1964), show a decrease from 300 cm^2/sec^3 at ground level to 0.07 cm^2/sec^3 at 10 km and then an abrupt rise, although the data for this region are scarce and quite inconsistent.

The quantities N and ϵ can be expressed in terms of gradients of temperature and wind velocity (Tatarski, 1961):

$$\overline{N}(h) = D\left[\frac{\partial\theta(h)}{\partial h}\right]^2 \tag{19}$$

and

$$\epsilon(h) = K_D \left[\frac{\partial \bar{u}(h)}{\partial h}\right]^2 \quad , \tag{20}$$

where

$\theta(h)$ = potential temperature (K) = $T(h) - \Gamma$,
$T(h)$ = actual temperature (K) ,
Γ = adiabatic lapse rate, which is equal to -9.8 K/km ,
$\bar{U}(h)$ = mean wind speed,
D = coefficient of molecular diffusion, and
K_D = coefficient of turbulent diffusion .

We then expect that gradients of temperature and wind velocity (shear) will be fruitful quantities to investigate when we look for correlations with image motion.

The vertical gradient of the potential temperature, or the relationship between $\frac{\partial T}{\partial h}$ and Γ, is in fact a measure of static thermal stability. In particular,

$$\begin{aligned}
&\frac{\partial T}{\partial h} < \Gamma \quad , \quad \text{unstable} \ , \\
&\frac{\partial T}{\partial h} = 0 \quad , \quad \text{neutral} \ , \\
&\frac{\partial T}{\partial h} > \Gamma \quad , \quad \text{stable, and} \\
&\frac{\partial T}{\partial h} > 0 \quad , \quad \text{inversion} \ .
\end{aligned} \tag{21}$$

In the atmosphere at night, the temperature lapse rate is often inverted near the ground and neutral or stable at higher altitudes. Values of $\partial \bar{U}/\partial h$ are the least well known. As Hulett (1967) pointed out, small-scale shears between layers a few tens of meters apart are not often included in the reported data. Yet shears of this dimension probably have most influence on optical effects.

The three parameters of equations (18), (19), and (20) are height dependent and also are functions of one another. Thus, it is difficult to isolate a single cause of turbulence. Tatarski (1961) has shown, however, that $C_T^2(h)$ can be expressed as

$$C_T^2(h) = L_o^{4/3} \left[\frac{\partial \bar{\theta}(h)}{\partial h}\right]^2 \quad , \tag{22}$$

where L_o is a measure of the outer scale of the turbulence. As noted previously, this outer scale is roughly equal to the height above ground for regions near the surface and is on the order of 1 km for higher altitudes.

For some specific cases, $C_T^2(h)$ has been determined analytically for at least the boundary region near the ground.

Values of $\bar{N}$, ϵ, and hence $C_T^2(h)$ in the atmospheric boundary layer are strongly dependent on the atmosphere-terrain interaction. Tatarski (1961) and others have looked at this region for the simplest case in which air moves in a flat plane. Under the assumption that buoyancy forces are small (i.e., mean temperature varies slowly with height), the wind velocity can be shown to vary logarithmically:

$$\bar{U}(h) \propto \log (h/h_o) \quad , \qquad h \gg h_o \quad ,$$

where h_o is a scale length characteristic of terrain roughness. For ease of computation, Tatarski (1961) assumes a slowly varying temperature profile of the form

$$\bar{T}(h) = T_o + T_* \log (h/h_o) \quad ,$$

where T_* is a logarithmic lapse rate assumed to be small compared to T_o. Using arguments based on the Obukhov-Kolmogorov turbulence structure, Tatarski shows that

$$C_T^2(h) \propto T_*^2$$

and that

$$C_T(h) \propto \frac{\bar{T}(h_1) - \bar{T}(h_2)}{h^{1/3} \log (h_1/h_2)} \quad , \qquad \text{for } h_1 < h_2 \quad . \tag{23}$$

The proportionality has been checked experimentally by Tatarski, who finds that the constant of proportionality is larger for stable conditions $[\overline{T}(h_1) < \overline{T}(h_2)]$ than for inversion conditions $[\overline{T}(h_1) > \overline{T}(h_2)]$. Even under an inversion condition typical of nighttime, the near-Earth turbulence is dominant. Thus, there is good reason to look for a correlation between stellar image motion and the mean temperature gradient, with less image motion to be expected under inversion conditions. In our experiments at Mt. Hopkins, we found fairly significant correlations between image-motion conditions and temperature-difference measurements made in the vicinity of the observation site.

Recently, a more complete method to compute $C_T^2(h)$ in the boundary layer has been reported by Wyngaard, Izumi, and Collins (1971). Starting with equation (18), they are able to show on a semiempirical basis, for conditions of a flat unobstructed plain, that

$$C_T^2(h) = h^{4/3} \left[\frac{\partial\overline{\theta}(h)}{\partial h}\right]^2 f_3(R_i) \tag{24}$$

for the boundary layer, where R_i is the Richardson number,

$$R_i = \frac{g}{\overline{T}} \frac{[\partial\overline{\theta}(h)/\partial h]}{[\partial\overline{U}(h)/\partial h]^2} \quad , \tag{25}$$

a widely used measure of stability, and f_3 is a dimensionless temperature-structure parameter, which is empirically determined by R_i alone, g is the acceleration of gravity, and $\overline{T}$ is the mean temperature.

Values of R_i near 0.25 are considered necessary for turbulence onset, while values up to 1.0 are permissible for ongoing turbulence. While small R_i numbers are necessary, they are not sufficient for the development of turbulence. The most useful role of R_i is as an indicator of the presence of turbulence. The function $f_3(R_i)$ was computed by Wyngaard et al. (1971) from their own data on boundary-layer turbulence over a flat Kansas plain. Their result is dependent only on ambient temperature, on temperature gradient, and on R_i, the measure of stability. A graph of $f_3(R_i)$ as a function of R_i is included in Figure 2. There is no explicit dependence on local parameters like surface roughness and wind speed, for these are all suppressed

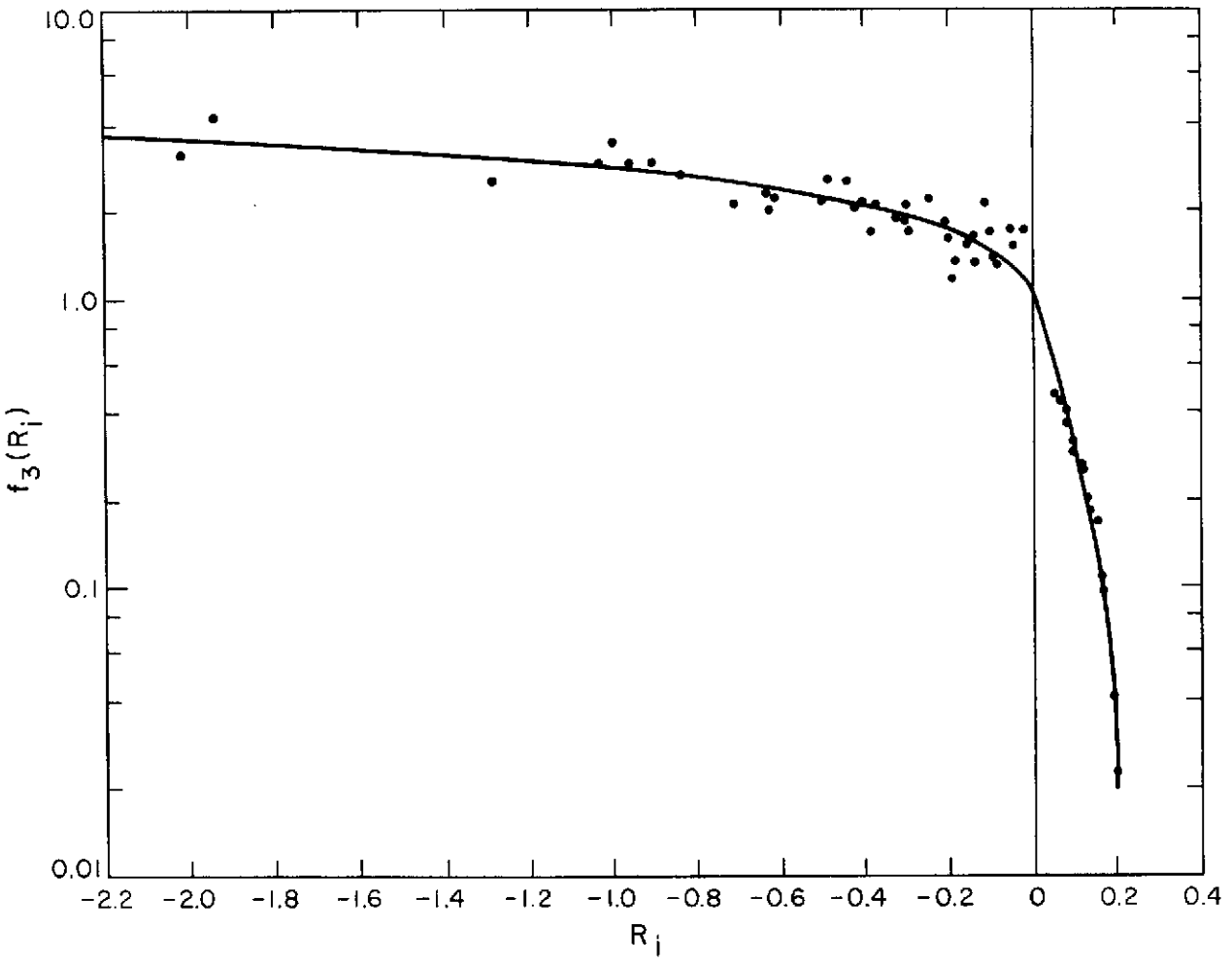

Figure 2. The dimensionless temperature-structure parameter f_3 (R_i) versus the Richardson number R_i (Wyngaard et al., 1971).

in the formation of $f_3(R_i)$. This method holds promise for a more accurate determination of $C_T^2(h)$ than does the technique relying on temperature gradient only; however, it requires the additional measurement of wind shear, $(\partial\overline{U}/\partial h)$, for calculation of R_i. Accurate wind-shear measurements are difficult to obtain because of uncertainties associated with the spacing and resolution of wind sensors.

We used equation (18) to estimate $C_T^2(h)$ values in the lowermost region along the propagation. Temperature profiles were measured with radiosonde flights. Wind speeds as a function of altitude were estimated from radiosonde-balloon positions. Even with wind speed determined in this fairly crude manner, modest correlation coefficients between the integral of $C_T(h)$ over the lowest 1000 m and σ_m were found.

Upper altitude turbulence can also often be identified by small R_i numbers. The availability of wind shear seems to be the controlling factor for this region. Typically high wind-shear values when squared in the denominator of the R_i number dominate the weaker influence of the temperature lapse rates. In fact, high turbulence has been found to associate with thin, stable, or even inverted temperature lapse-rate layers. As Scorer (1969) and Roach (1970) have pointed out, thin stable layers are especially suited for the development of turbulence when mechanisms exist to tilt them. Suitable mechanisms could include pressure fronts, gravity waves, and mountain or lee waves. At observatories located in mountainous regions, the mountain or lee wave mechanism should almost always be present. It is also at these wave boundaries or interfaces between air masses that the higher values of wind shear are found. Although stable or inverted layers may be found at all altitudes, the tropopause is especially suitable because of its large region of temperature stability. Once the stable layers are tilted and the condition $R_i \leq 0.25$ is reached, the tilts develop into Kelvin-Helmholtz rolls or billows, as illustrated by Roach (1970). Smaller, secondary instabilities are formed, and the now well-developed turbulence feeds on available wind shear to grow in extent. Turbulent energy cascades into smaller and smaller eddy sizes, becoming more isotropic until it is lost in viscous dissipation at the inner scale. Layer thickness may be only a few tens of meters, but horizontal extent is usually on the order of kilometers. Thus, the same series of turbulence layers or sheets should affect astronomical viewing at many different azimuths during the same time period.

Because the upper altitude turbulence layers, though well developed, do not have the strength of boundary-layer turbulence, optical-phase effects should have little additional contribution from these layers. Scintillation effects, however, are strongly weighted by altitude and thus should exhibit strong correlation with upper altitude turbulence layers. In lieu of direct measurement, useful tracers or estimators for the presence and strength of upper altitude turbulence should be the wind-shear squared profile, inflections in the temperature lapse rate, and the presence and sharpness of the tropopause region.

3. EXPERIMENT APPARATUS AND SITE LOCATION

3.1 Stellar-Image Monitor System

Image motion and scintillation were measured with a Stellar-Image Monitor (SIM) developed and built at GSFC during 1968. It was patterned directly on a technique described by Lindberg (1954) and a design published by Ramsay and Kobler (1962). Ramsay performed some experimental work with starlight. Later, Coulman (1969) used the device extensively for studies of horizontal optical propagation. The hardware of the Ramsay SIM produces three analog voltage signals containing information on image intensity, size, and motion. These voltages can be analyzed for the desired statistics on the stellar image. The heart of the device is an MTF measurement performed by square-wave modulating or chopping the incoming light in the telescope focal plane. Chopping is performed at a selected, but variable, spatial frequency. Operation at various spatial frequencies, detection of the chopped light, and electronic processing yield various points for an MTF that contains accessible information on image blurring. Image intensity is monitored by low-pass filtering of the chopped signal. Image-motion information is derived from electronic phase comparison of signals generated in chopping the stellar image and a reference light source. The Goddard device differs from the original Ramsay design in the way spatial frequency is varied, in electronic processing, and in data collection and reduction.

Starlight is collected by an 0.152-m-diameter doublet lens system of 1.22-m focal length. Figure 3 indicates the optical system components. A microscope objective serves as relay optics to focus an enlarged image of a star on a rotating glass disk. An eyepiece and mirror assembly mounted in a sliding tube are used to check visually the image quality and to ensure proper alignment of the image on the glass disk. The disk is composed of alternately clear and opaque pie-shaped sectors, each subtending 0.°5. The disk is belt-driven from a dc motor servosystem at a constant rate of 500 rpm. Speed regulation is better than 0.5%. Light passing through the disk is square-wave-modulated with a frequency of 3.0 kHz determined by the motor speed

304-045

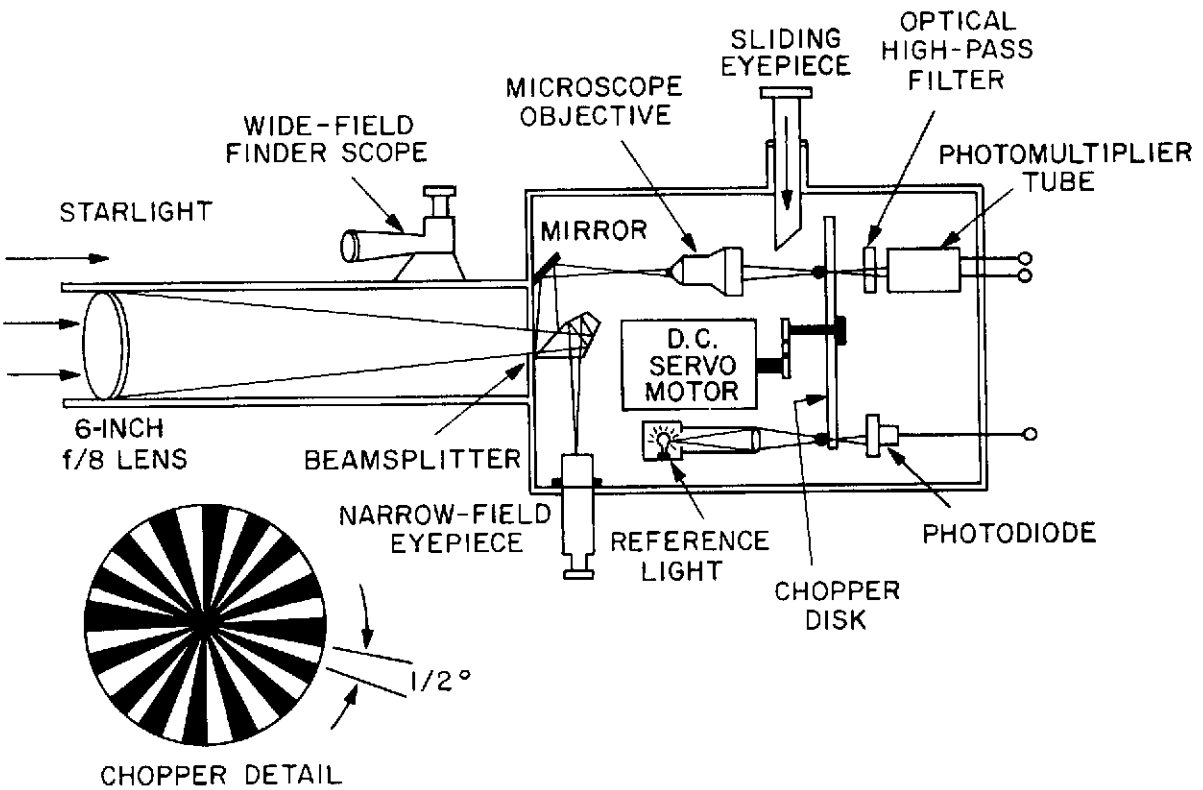

Figure 3. Optical system and detector package for the stellar-image monitor.

and the number of sectors on the disk. The spatial frequency of chopping is inversely proportional to the distance from the center of the disk and is determined by the sector width at a given distance. Starlight is brought to a focus 1 in. from the center of the disk. For unity power-relay optics, the spatial frequency of chopping is 2.26 cycles/mm or 0.0134 cycle/arcsec. Higher powers effectively increase the spatial frequency by enlarging the image on the disk. Light transmitted by the disk passes through an optical filter and is received by a photomultiplier tube (PMT), an EMI Model 9558B with S-20 response. The filter is a Corning glass filter number CS3-71. Light from a small dc-powered light bulb is also focused on the disk to act as a phase reference source. A thin glass plate in the converging light from the bulb can be tilted to adjust the position of this image on the disk. Chopped light is received by a photodiode.

Electronic signals from the starlight and reference light detectors are fed into an analog preprocessing system. In this device, a voltage proportional to image intensity is obtained by low-pass filtering of the PMT output with a 200-Hz (3-db) bandwidth. Statistical analysis of the signal gives the desired information on intensity fluctuations (scintillation). The PMT output is also sent through a bandpass filter centered at the chopping frequency. The ratio of bandpass to low-pass signals is proportional to the modulation index of the PMT data. The modulation index or percent modulation can be calibrated in terms of the modulus of the optical transfer function (OTF). Since a star is a point source, the OTF and image-intensity profile are a Fourier-transform pair. Image size in terms of width or variance follows directly from the profile derived from the OTF. The image-size determinations are averaged over a time corresponding to the reciprocal of the filter bandwidth, approximately 0.01 sec. This is effectively a measure of short-exposure image size, with essentially all effects of motion frozen out.

Motion of the image center of gravity is determined separately by phase comparison of signals at the chopping frequency (3.0 kHz) from the two detectors. As the stellar image moves on the chopping disk, it produces a waveform shifted in phase with respect to that from the phase reference source with its stationary image. The relative phase of the two signals is the relative position of the two images on the disk, along with a direction perpendicular to a disk radius. Thus, the third output becomes a voltage proportional to one-dimensional motion of the stellar-image center of gravity.

To preserve the output of the electronic preprocessing system in a form suitable for data analysis, recordings were made directly on an instrumentation tape recorder (Ampex FR-1300). The three outputs of the electronic preprocessing system have bandwidths from dc to 200 Hz. The dc requirement means a frequency modulation (FM) recording scheme must be used. Binary time signals were also recorded in order properly to characterize and identify the data. These were recorded in the direct (AM) mode. The FM and AM record bandwidths were from dc to 2.5 kHz and from 50 to 38 kHz, respectively, for the 7.5-ips tape speed used. Specifications for the signal-to-noise ratio were better than 40 db for the tape-recorder data tracks at the given tape speed. The collection and reduction of the SIM data are discussed in detail in Appendix A.

3.2 Temperature-Fluctuation Measurement System

A system to estimate the presence and strength of thermal fluctuations in the first few tens of meters above ground level was supplied by NASA through JPL. The instrument automatically records the average value of peak temperature fluctuations at several locations along a 100-ft tower. The instrument was originally designed to be used in pairs for intersite comparison of the thermal environment at an astronomical observatory. At Mt. Hopkins, one tower was installed on the top of knoll 2, and another at the summit. The locations of these towers and of the other instrumentation are discussed in Section 3.5. The base of the tower at knoll 2 was about 40 ft above and about 120 ft north of the SIM telescope. Data from the sensors on both towers were compared with SIM image-motion data to test the applicability of the sensors as indicators of seeing conditions and as tools for site evaluation.

The sensing device on each tower location was a small bead thermistor with an 0.05-sec time constant. Each sensor was followed by a biasing network and amplifier of bandpass 0.5 to 5 Hz. The major contributions to image motion were expected to be in this low-frequency range, as discussed in the theoretical section of this report. Each amplifier was followed by a peak reading and averaging circuit with a 3-min time constant. The averaged result in terms of peak fluctuations in degrees centigrade was recorded as a dc voltage on separate recorders (Rustrack) for each sensor. Ultimate system sensitivity was about 0.02°C. Thermistors were placed on each tower at 25, 50, 75, and 100 ft. Data from the device on knoll 2 were available for the

second half of Phase I and all of Phase II. The data from the peak were available only for the second half of Phase I.

3.3 Temperature-Difference Measurement System

In Phase II, concentrated studies were conducted of the correlation between SIM results and local temperature measurements. In addition to the measurements described above, data on local temperature differences were provided by a temperature recording system (Weathermeasure model T622R). It included six platinum-wire temperature sensors for remote locations and one for a reference. The instrument measured the temperature difference (ΔT) between the remote sensors and the reference.

The remote and the reference sensors form two legs of a Wheatstone bridge. A change in ambient temperature causes an unbalanced condition in the regulated, dc-powered bridge circuit. The resulting error signal is converted to ac by a chopper and then amplified. The amplifier output causes a balance motor to drive both a recording pen and a slide wire (precision potentiometer) to rebalance the bridge. The corresponding pen movement is calibrated in degrees centigrade and indicates temperature difference to a maximum of $\pm$ 10°C. Resolution is about 0.2°C. The recorder system switches input sensor channels sequentially every 5 sec and uses a multicolor-ink dotting system to distinguish the ΔT record of each sensor.

The reference sensor was located in a weather box on the roof of the Environmental Sciences Building (ESB) on knoll 2 with the SIM. The six remote sensors were at the following sites: the 50- and 100-ft levels of the JPL tower on knoll 2, the telescope level in the SIM dome, two weather boxes downhill east and west of knoll 2, and the 50-ft level of the JPL tower on the summit.

3.4 Radiosonde

Vertical profiles of temperature, relative humidity, and barometric pressure were measured during the Phase II program. Balloons were launched from the vicinity of the SIM telescope on knoll 2. The balloons, radiosonde payloads, the receiver, and

data reduction were provided by NASA–Wallops Island. Data were taken for each significant level between the surface and the altitude of signal loss (in excess of 10 km for most flights).

In addition to the standard radiosonde package, each balloon carried a small flashing light to facilitate optical tracking. The velocity and direction of winds aloft were computed from the recorded azimuth and zenith angles from the optical tracking. Angle data were recorded every 30 sec. The radiosonde balloon was tracked by a Questar telescope mounted at the site. All time-reference measurements were made with the clock from the SIM data system. Additional data on temperature, humidity, pressure, and winds aloft were available from a standard weather-service launch every 12 hr (00:00 and 12:00 GMT) at Tucson International Airport 40 mi to the north.

3.5 Mt. Hopkins Observatory Site and Location of Experiment Equipment

The SAO Mt. Hopkins Observatory is located approximately 40 mi south of Tucson, Arizona, in the Santa Rita mountain range of the Coronado National Forest. The area, about 4744 acres, includes the summit region of Mt. Hopkins, with several acres of usable space above 8000 ft and the ridge area at 7600 ft, site of the present observatory. The region around the summit is slated for development and will become a major observatory site in the future. The ridge has been the site for major instruments since early 1968 and will continue to play an important role in astrophysical and geophysical research even after the summit is developed. The ridge, the peak, and the access road are shown in Figure 4.

Figure 5 shows knoll 2, and Figure 6 is a detailed diagram of the ridge area. The ridge has four knolls, three of which are actively used. The seeing tests were performed on knoll 2. The SIM was operated inside the dome, 12 ft in diameter, on the roof of the ESB on the south side and approximately 80 ft below the top of the knoll. The instrument was placed on a concrete pier, 12 ft high, which was isolated from the building.

The tower containing the four JPL temperature sensors and temperature-difference sensors 1 and 3 was approximately 120 ft NNE of the SIM site; its base was about 40 ft

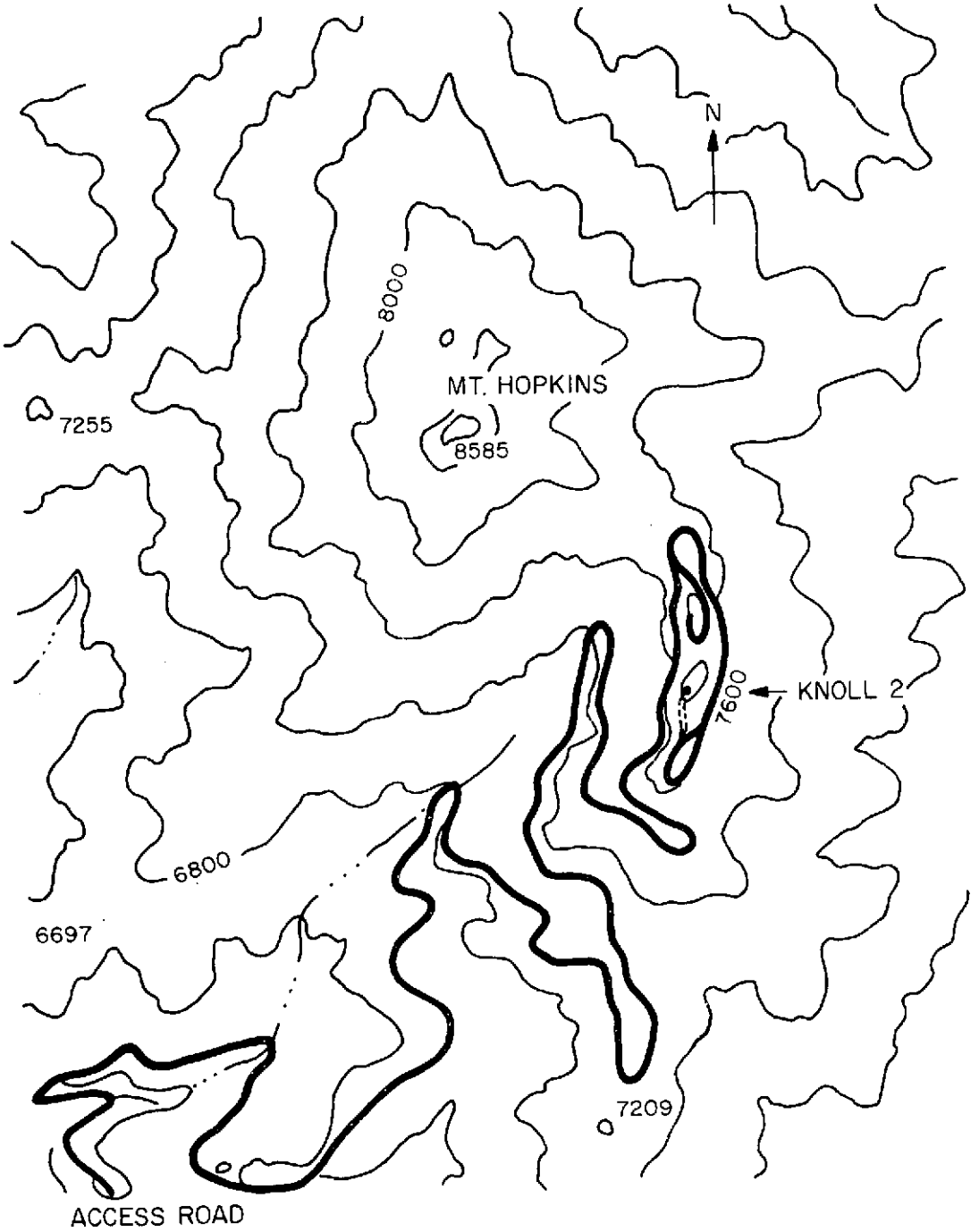

Figure 4. Mt. Hopkins ridge and peak areas shown with access road.

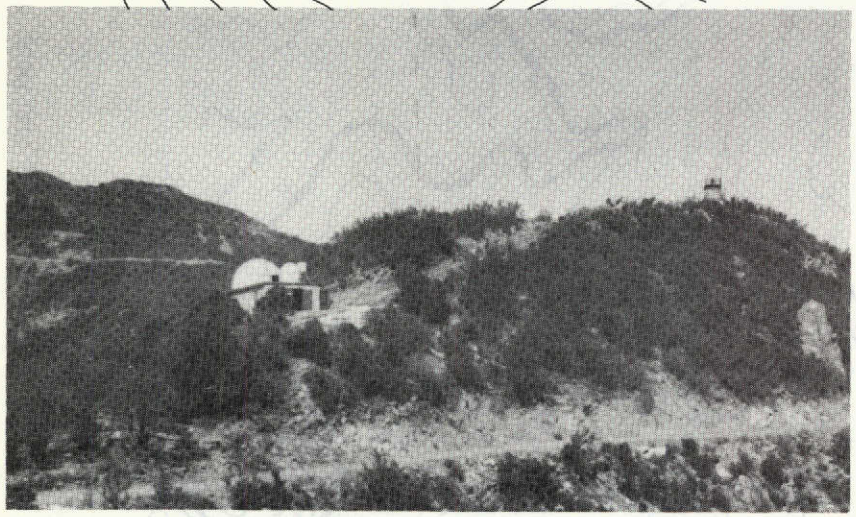

Figure 5. View of knoll 2 from the south.

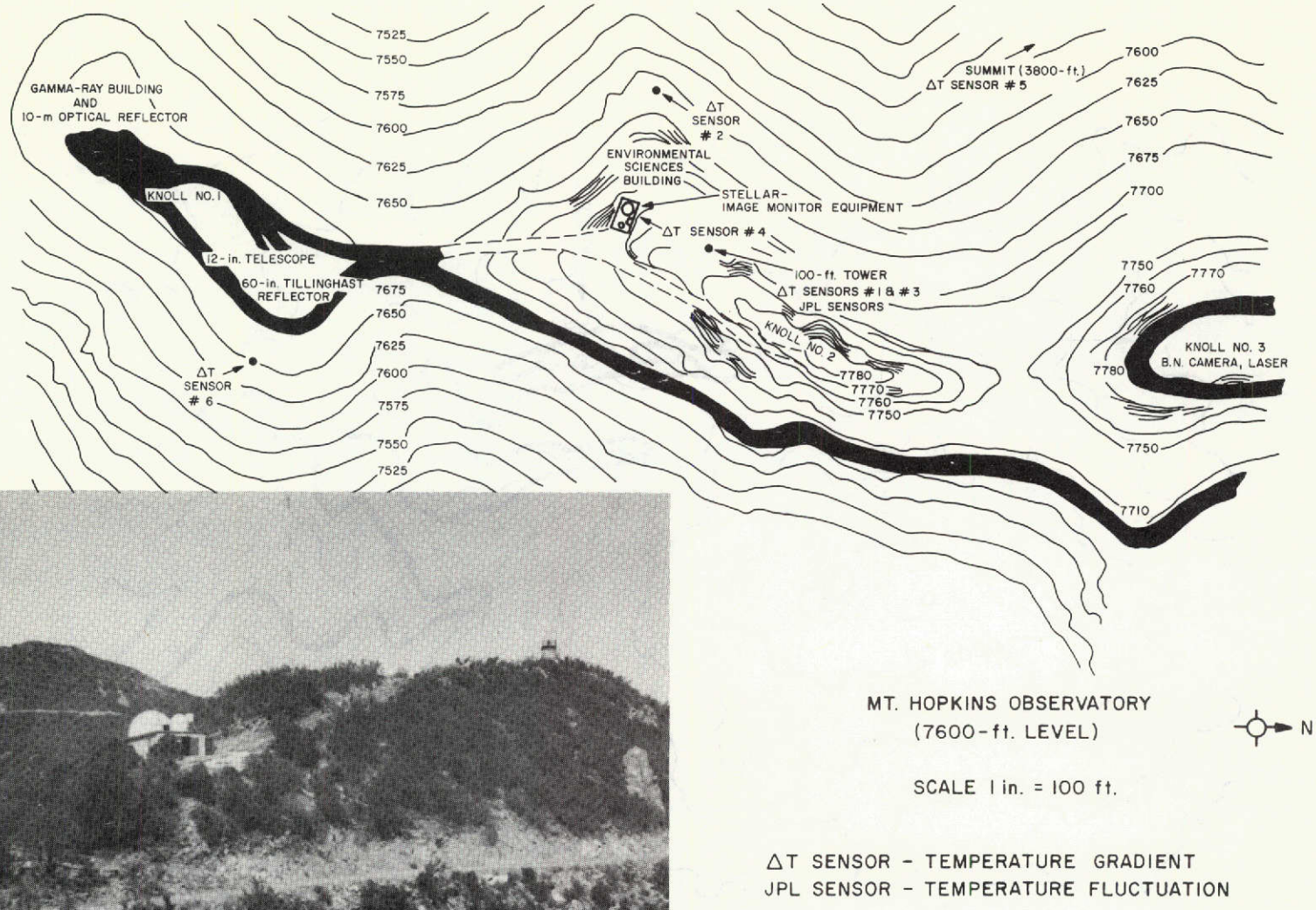

Figure 6. Detailed diagram of the ridge area showing the location of the equipment.

above the SIM telescope. JPL temperature-fluctuation sensors 1, 2, 3, and 4 were placed at heights of 25, 50, 75, and 100 ft on the tower. Temperature-difference (ΔT) sensors 1 and 3 were located at heights of 50 and 100 ft, respectively. The ΔT sensor 2 was placed about 120 ft to the east and 50 ft below the SIM. Sensor 6 was located about 400 ft SSE and 100 ft below the SIM. Sensor 4 was placed at the telescope dome, and the reference sensor in the weather box on the roof of the ESB. Weather instruments for temperature, pressure, relative humidity, and wind speed were also located at or near this box.

Another tower with four additional JPL-type sensors was located at the summit approximately 4000 ft NNW and 1000 ft above the ESB. JPL sensors 5, 6, 7, and 8 were located at the 25-, 50-, 75-, and 100-ft levels of this tower. The ΔT sensor 5 was located at the 50-ft level of the tower.

4. IMAGE-QUALITY MEASUREMENTS

4.1 Introduction

Image-quality measurements made during Phase I (June 1969 to April 1970) emphasized the observation of a variety of stars at different zenith angles and times. This was an attempt to obtain a reasonable sample of seeing conditions during the year. A typical night of observation included three data runs of 1- to 3-min duration each on two stars several hours before midnight, three stars at midnight, and two stars several hours after midnight. The three data runs on each star were made at the spatial frequencies 0.047, 0.063, 0.102 cycle/arcsec of the stellar-image monitor. The original intent was to compute an MTF for each star. It was quickly found that the observed MTFs at Mt. Hopkins were almost identical to the system MTFs measured in the laboratory. Hence, the effects of image blurring were small at the 0.152-m aperture used. The upper bound on image resolution was estimated to be the diffraction limit, and subsequent observations were limited to scintillation and image motion (see Section 2). During data reduction, 20-sec intervals were selected from the runs and processed for the pertinent statistics of scintillation and image motion.

In Phase II (September 1970 to January 1971), the emphasis was placed on longer data runs and more concentrated observation periods. A typical night of observation included one or two observation periods that lasted 1 to 2 hr. During each period, a single star of first magnitude or brighter and at a zenith angle of 45° or less was observed. Image-motion and scintillation data were recorded continuously for the entire observation period. The recording of stellar data was accompanied by operation of the thermal gradient and JPL microthermal devices, measurement with surface meteorological sensors, and, in most cases, a radiosonde balloon flight. Statistics of the stellar data were computed on a running average basis, with the averging time varied from 30 sec to 2 min. The total data set of both image-motion and scintillation measurements for Phases I and II appears in Appendix B.

4.2 Image Motion

Table 1 summarizes one-dimensional image-motion statistics from Phase I. The two-dimensional image-motion statistics can be obtained by multiplying these values by 2. These data represent observations at different zenith angles, azimuth angles, months of the year, and times of night. These different parameters sample a variety of turbulence conditions, and a large scatter of data is expected. All image-motion rms values, σ_m, were first corrected to what would be observed at zenith with the $\sec^{1/2}(\theta)$ zenith-angle dependence of equation (13). This dependence has been verified experimentally (Tatarski, 1961, see Figure 6) and is used here to eliminate much of the data scatter associated with look angle through the turbulence structure. The remaining scatter is due primarily to changes (nonstationarity) of the turbulence structure itself. The listed σ_m indicate average one-dimensional values of about 0.5 to 0.7 arcsec throughout the year, with occasional excursions to values less than 0.3 or greater than 1.0 arcsec. The data indicate what could be a slight seasonal trend, with values somewhat lower in the winter than during spring and fall.

Table 1. Summary of rms one-dimensional image-motion statistics in Phase I.

Month	Number of observing nights	Number of observations	Mean σ_m	Standard deviation of σ_m	Minimum σ_m	Maximum σ_m
1969						
June	4	19	0.67	0.27	0.43	1.40
September	5	13	0.61	0.20	0.17	0.94
October	17	66	0.67	0.16	0.27	1.09
November	5	20	0.58	0.16	0.38	1.07
December	2	7	0.49	0.06	0.37	0.57
1970						
February	4	18	0.49	0.14	0.29	0.83
March	11	29	0.73	0.22	0.27	1.09
April	5	20	0.71	0.20	0.43	1.08

Cumulative probability distributions of all the σ_m values and of a nightly average of σ_m values are shown in Figures 7 and 8, respectively. It is apparent from these figures that σ_m values fall between 0.5 and 1.0 arcsec about 70% of the time. If all the σ_m are considered separately, 94% of the values lie below 1.0 arcsec and 20% below 0.5 arcsec. For the nightly averages, 90% of the nights had image motion below 1.0 arcsec, while only 10% had image motion below 0.5 arcsec. As is indicated by the similarity between Figures 7 and 8 and borne out by the data themselves, most of the observed variation in σ_m occurred from night to night rather than from observation to observation within a particular night. It is interesting to note that conditions of greater than 1.0-arcsec rms image motion did occur at least once during more than half the months in which data were taken; however, these conditions were confined to a small number of evenings. When poor conditions existed, they tended to remain throughout the entire night, and thus it was possible to judge "bad seeing" quite early in the evening. It should also be noted that all data were collected on observing nights close to ideal, characterized by little or no cloud cover or haze and low surface winds. It is quite possible that the inclusion of more marginal nights might alter the distribution of σ_m values. The data of Phase I were essentially spot checks of image motion. To validate nightly averages or longer term averages formed from these data, it is necessary to know how representative each σ_m value is. Longer term data from Phase II show that, on the average, short-term spot-check data are good indicators of the general seeing conditions.

From the results of Phase II, a succession of σ_m values averaged over 30 sec to 1 min are available for periods of up to 1 hr. Typical short-term variations in σ_m recorded on three separate nights are plotted in Figure 9). Note that a spot check, as conducted in Phase I of σ_m in case #3, would have given an excellent indication of the average of σ_m for that time period. Data from the other two nights, however, do show wider variations from minute to minute and the differences between spot check and average values could have been as large as 0.2 arcsec. The variations are characterized by brief intervals of relatively low σ_m separated by broad peaks of σ_m for several minutes. Even under "bad seeing" conditions, it may be possible to use selectively these brief periods of low σ_m for photographic or optical communication applications; however, a close monitoring of seeing conditions would be essential to choose the proper period. Longer term trends over periods of tens of minutes were

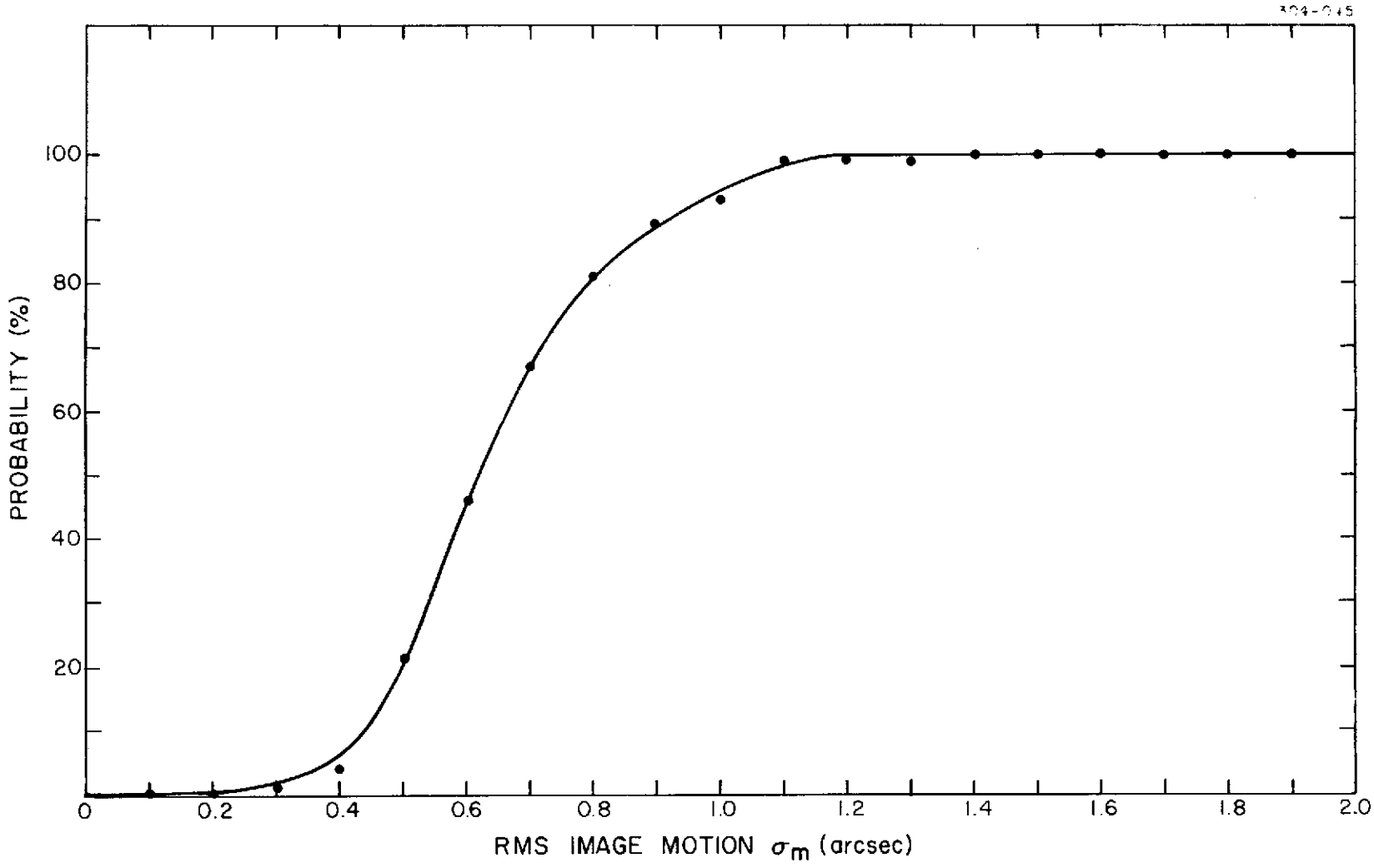

Figure 7. Cumulative probability distribution of one-dimensional image motion for short-term averages during Phase I. The values have been corrected to zenith.

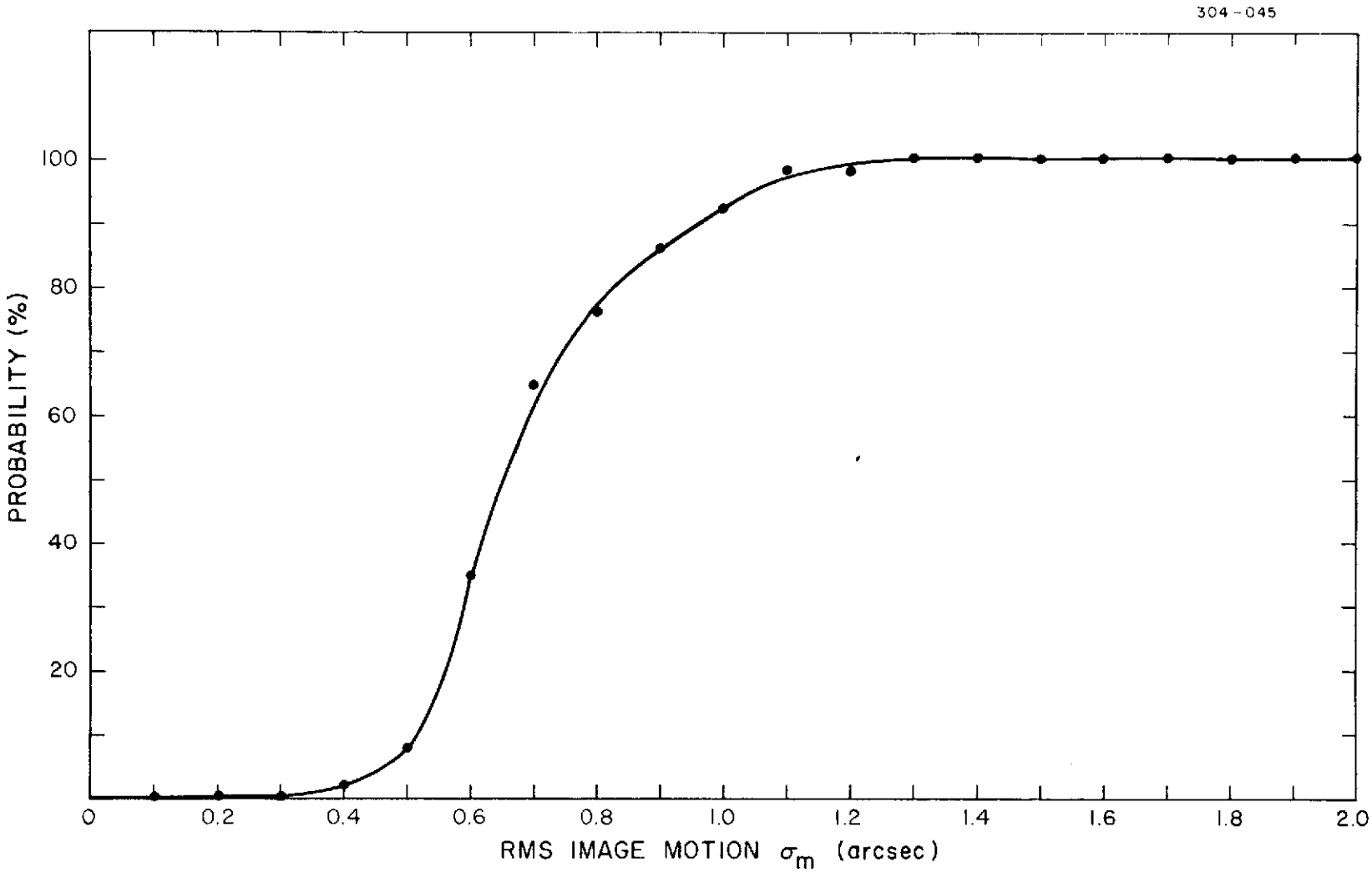

Figure 8. Cumulative probability distribution of one-dimensional image motion for nightly averages during Phase I. The values have been corrected to zenith.

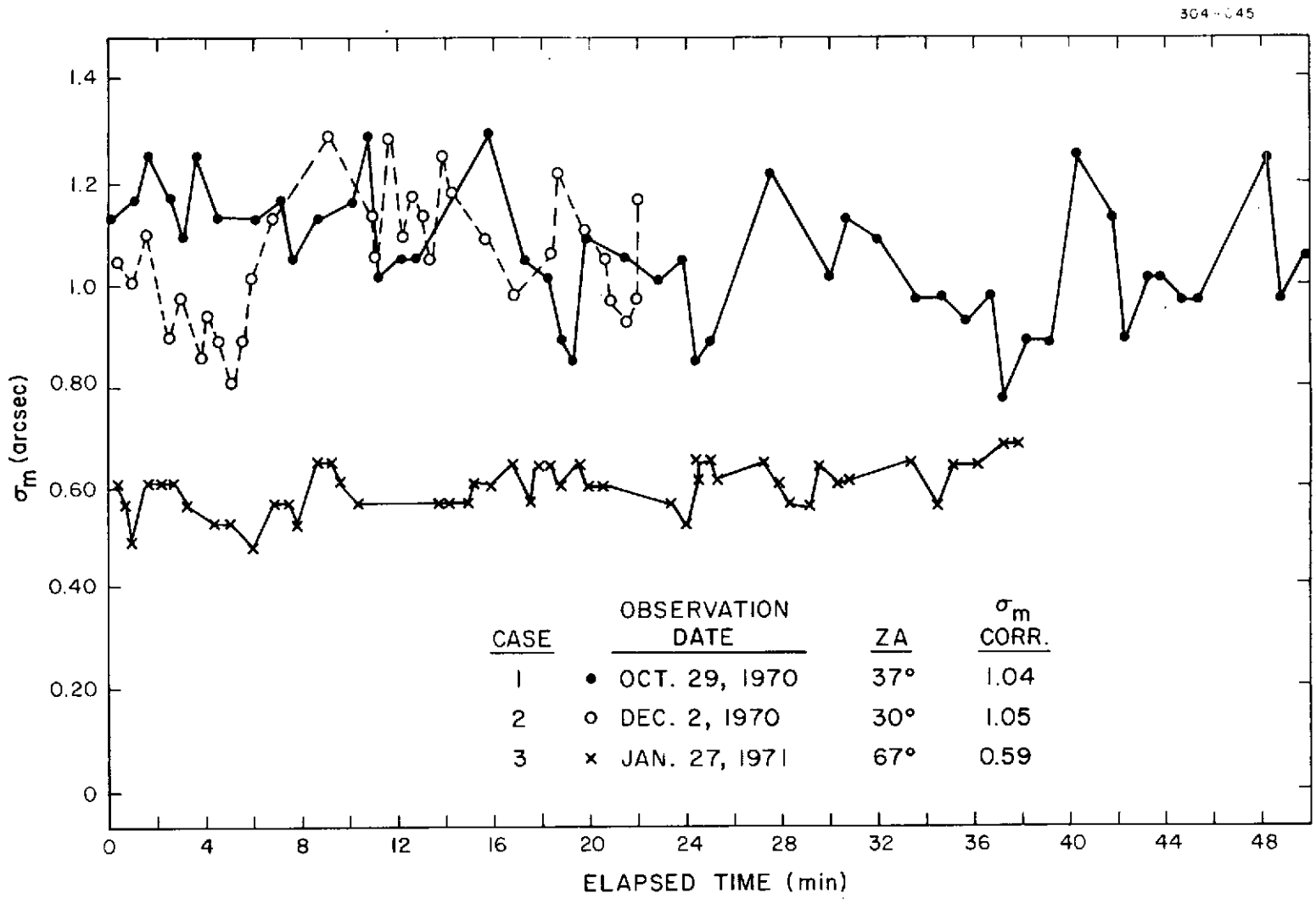

Figure 9. Three examples of short-term variations in σ_m from Phase II data corrected to zenith.

present in the data, in addition to the short-term variations. These trends are noticeable as roughly linear changes with time of average σ_m values in Figure 9.

A summary of rms image-motion results of Phase II, averaged over the total observation periods of up to 1 hr and over 30- to 60-sec intervals selected within the observation period, is in Table 2. The differences between the mean σ_m values calculated by these two averaging methods are small; they arise from the fact that some observation periods were longer than others and were sampled more times. For the short-interval runs, standard deviations and the maximum and minimum excursions of σ_m are larger than those of the long-interval averages. This indicates that the minute-by-minute excursions are larger than the variations observed from day to day. The monthly means of the long-term averages fell in the narrow range of 0.7 to 0.9 arcsec and showed no seasonal trends, but they were about 20% larger than values for the corresponding months of Phase I. The σ_m values observed during Phase II ranged from 0.54 arcsec to as large as 1.29 arcsec. This total range was considerably smaller than that observed during the same 4 months (October to January) of Phase I and was probably due to the smaller number of observation periods in Phase II. The small sample of data days during October 1970 and January 1971 and the short duration of Phase II made it impossible to test adequately the seasonal trend noted in Phase I data.

Cumulative probability distributions averaged over all the data runs and over observation-period mean values for Phase II are plotted in Figures 10 and 11, respectively. About 88% of the σ_m values in both groups fell below 1 arcsec. This percentage is quite consistent with Phase I results. Essentially all σ_m values were larger than 0.5 arcsec, which may be a result of the fewer observing nights (smaller sample) in Phase II.

Data from Phase II were also used to check the theoretical $\sec^{1/2}(\theta)$ zenith-angle dependence for σ_m. Figure 12 contains the σ_m values for the short-interval data runs plotted against zenith angle in log-log form. The data points have considerable scatter, due mainly to the night-to-night and even hour-by-hour variations in turbulence structure. However, a general trend (slope) that appears to agree well with the theoretical relation is evident. A least-squares fit to the more than 1000 short-interval measurements from Phase II over 17 nights gave an exponent of 0.52. The data from

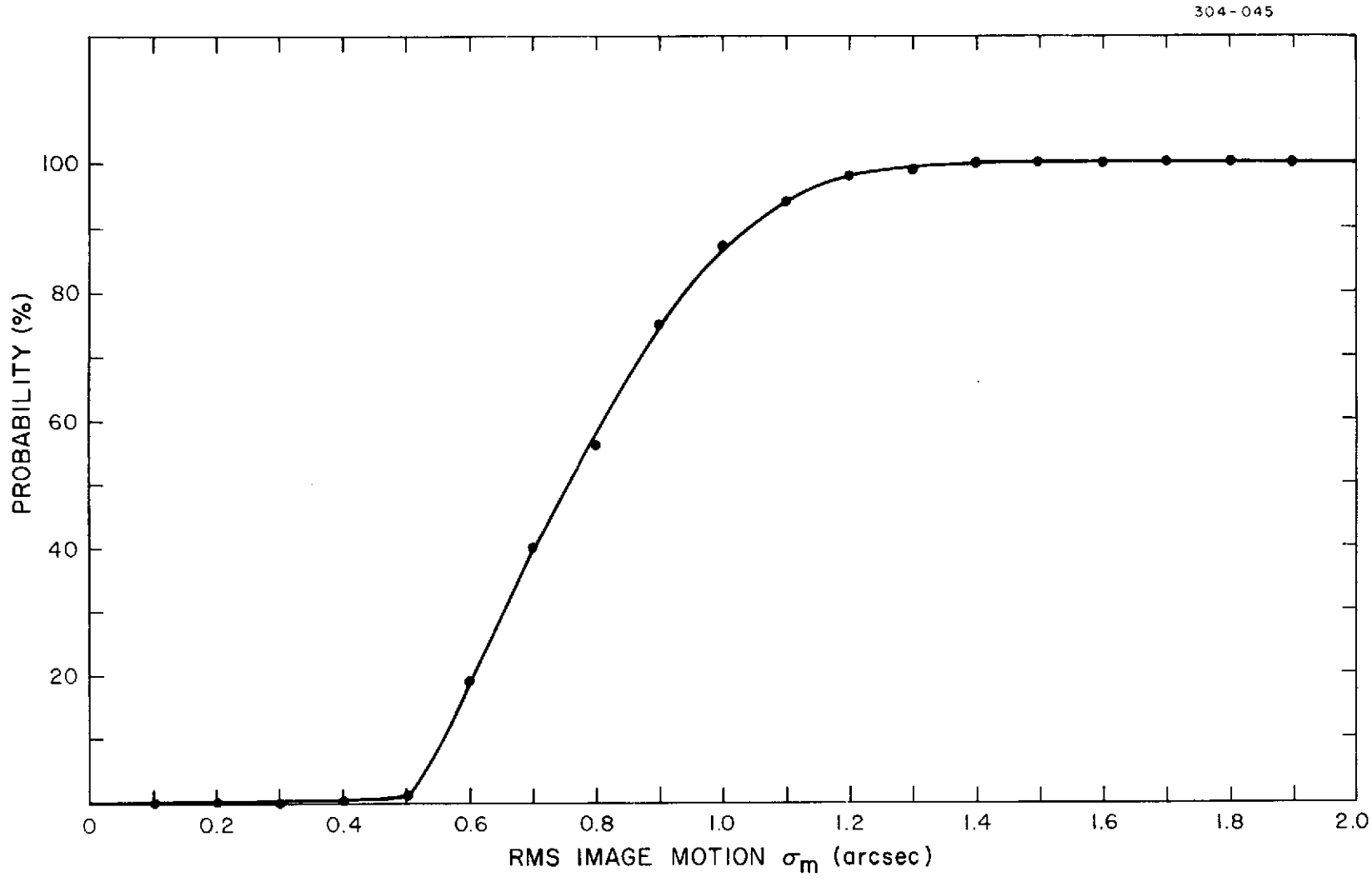

Figure 10. Cumulative probability distribution of one-dimensional image motion for short-term averages during Phase II. The values have been corrected to zenith.

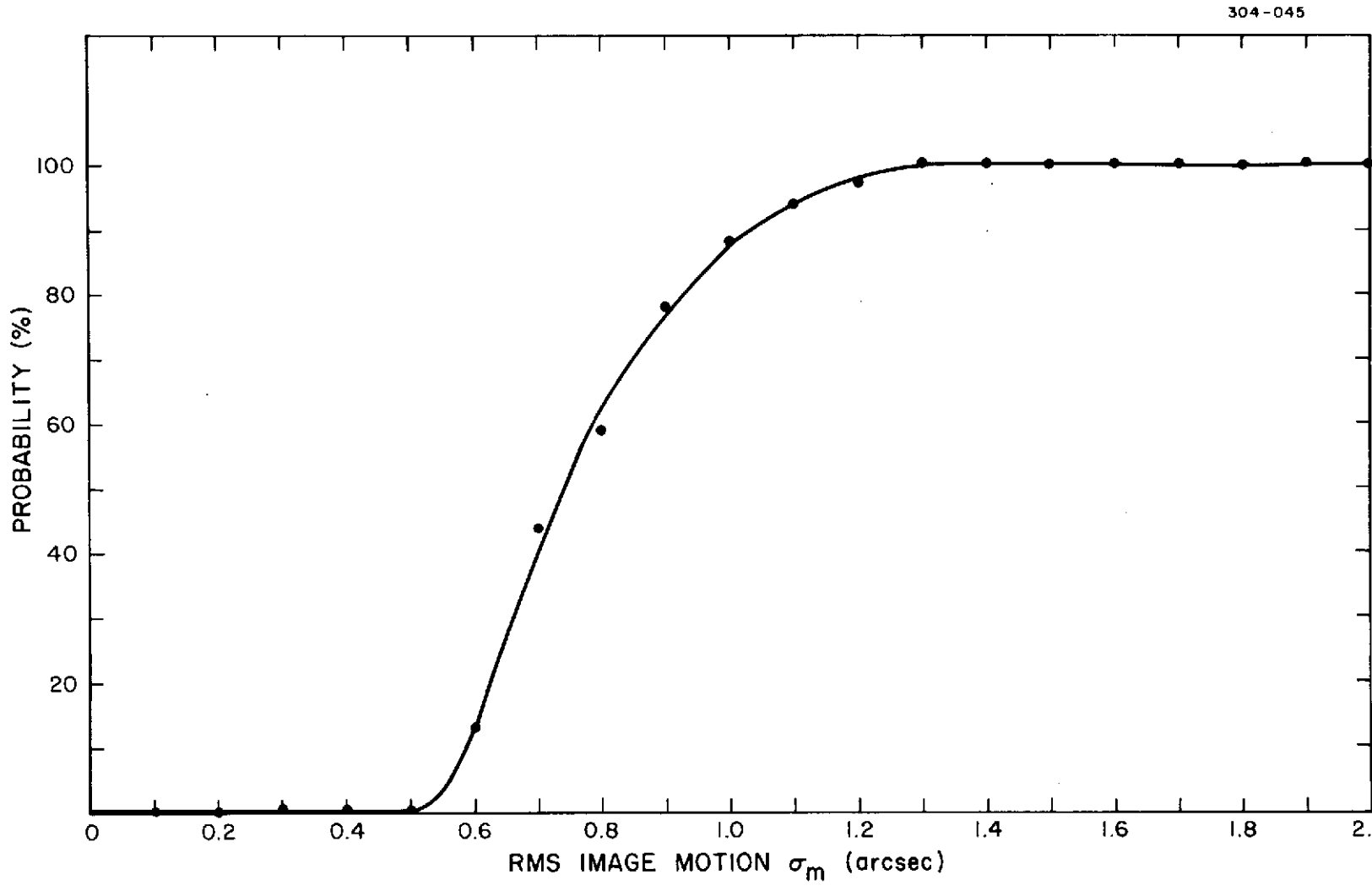

Figure 11. Cumulative probability distribution of one-dimensional image motion for long-term averages during Phase II. The values have been corrected to zenith.

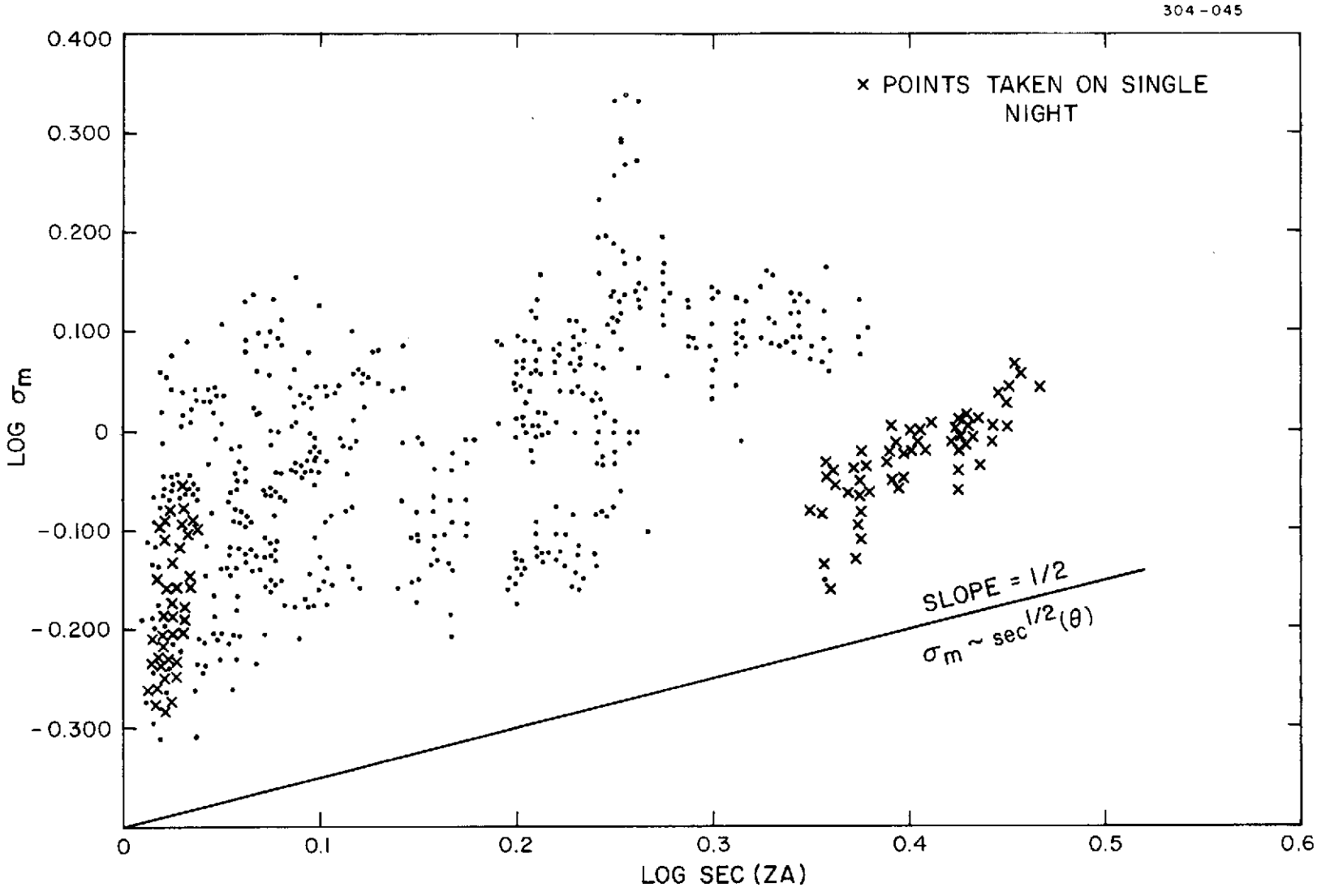

Figure 12. Experimental dependence of T_m on zenith angle. The $\sec^{1/2}(\theta)$ line is intended to show the anticipated trend. Its intercept was chosen for convenience only.

a single night's observations (denoted in Figure 12), although restricted in zenith-angle coverage, have considerably less scatter. A least-squares fit to these data gave an exponent of 0.39.

Table 2. Summary of rms one-dimensional image-motion statistics in Phase II.

Month	Number of observing nights	Number of observations	Mean σ_m	Standard deviation of σ_m	Minimum σ_m	Maximum σ_m
Averaged over observation periods of up to 1-hr duration						
1970 October	1	2	0.91	0".14	0".77	1".04
November	8	14	0.74	0.14	0.54	0.97
December	6	8	0.90	0.22	0.61	1.29
1971 January	2	8	0.71	0.12	0.59	0.93
Averaged over data runs of 30-sec to 1-min duration						
1970 October	1	101	0.90	0".17	0".62	1".29
November	8	432	0.75	0.15	0.47	1.18
December	6	192	0.86	0.22	0.48	1.63
1971 January	2	244	0.78	0.19	0.48	1.22

The normalized spectral density was computed for one or two data runs of 45 to 60 sec in each of the Phase II observation periods. A typical result is plotted in Figure 13. The spectra, all similar in shape, fall off very rapidly with increasing frequency to a half-power point near 1 to 2 Hz and a 0.10-power point near 3 to 5 Hz. The power spectra were all near zero beyond 15 to 20 Hz, although the integrated effect of components in this region and at higher frequencies may not be negligible. The local maximum, which appeared at around 8 Hz in each curve and is shown in

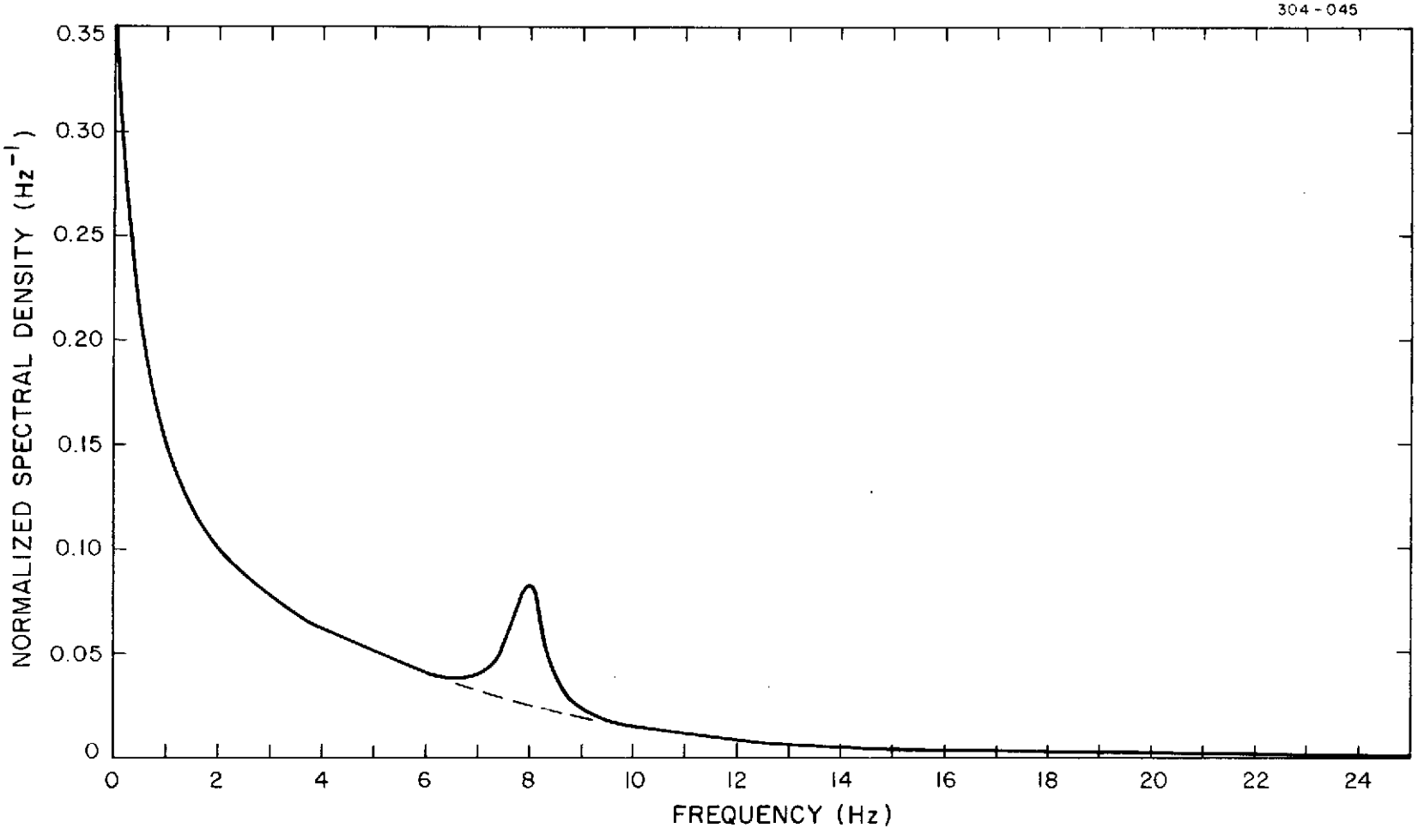

Figure 13. Typical image-motion spectral density with 8-Hz noise component introduced by the SIM equipment.

Figure 13, was due to the small residual eccentricity in the mounting of the SIM chopping wheel. The error component of the instrument is present to approximately the same degree in each data run. Thus, the measured σ_m values may be too large by about 5 to 10%, but the errors are comparable from observation to observation.

4.3 Scintillation

The summary of Phase I scintillation statistics in terms of CIV is given in Table 3. The scintillation data were acquired simultaneously with image motion and thus represent the results of observations at many different azimuth angles, zenith angles, and nights during the year with the 15.4-cm-diameter telescope aperture. CIV values were extrapolated to zenith with the $\sec^{1.2}(\theta)$ dependence of equation (12). The average monthly CIV values fell in the range 0.12 to 0.17, giving an atmospherically induced modulation on the incoming stellar irradiance of 12 to 17%. CIV values greater than 35% and smaller than 5% were observed during some periods. Seasonal trends were not evident in the monthly totals. The cumulative probability distributions of the CIV values averaged over all (short-term) data runs and over total observing nights of Phase I appear in Figures 14 and 15, respectively. The short-term data results, although based on a relatively small sample during some months, indicate that CIV values for a 15-cm aperture are equal to or below 0.13 and 0.22 for about 50% and 90% of the time, respectively. The cumulative probabilities for CIV values averaged over the entire observation periods were quite similar. Once again, it should be emphasized that these data were acquired on clear nights and that the inclusion of data from more marginal nights could alter the cumulative probability distributions.

As with image motion, the CIV data of Phase I were essentially spot checks of the actual atmospheric propagation effects. Longer period observations made in Phase II indicate that the short-interval spot-check CIV would be fairly representative of the mean CIV conditions, with errors of less than 20% to be expected in even the worst cases.

In Phase II, values for individual data runs were computed for integration times of 30 sec to 1 min, and continuous data were available for observation periods of up to 1 hr. Averages of these data over the total observation periods do not truly reflect the

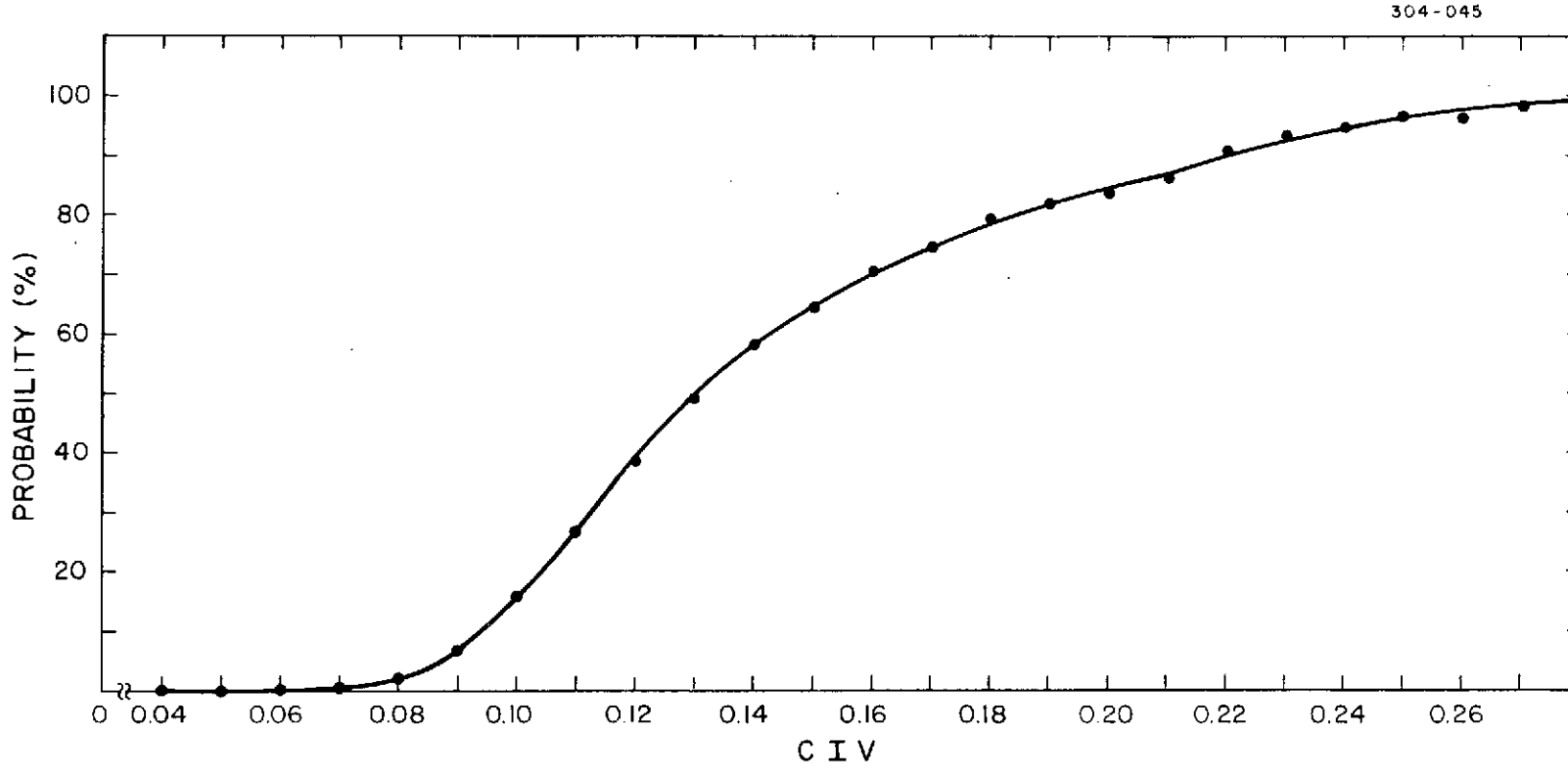

Figure 14. Cumulative probability distribution of CIV for short-term averages during Phase I. The values have been corrected to zenith.

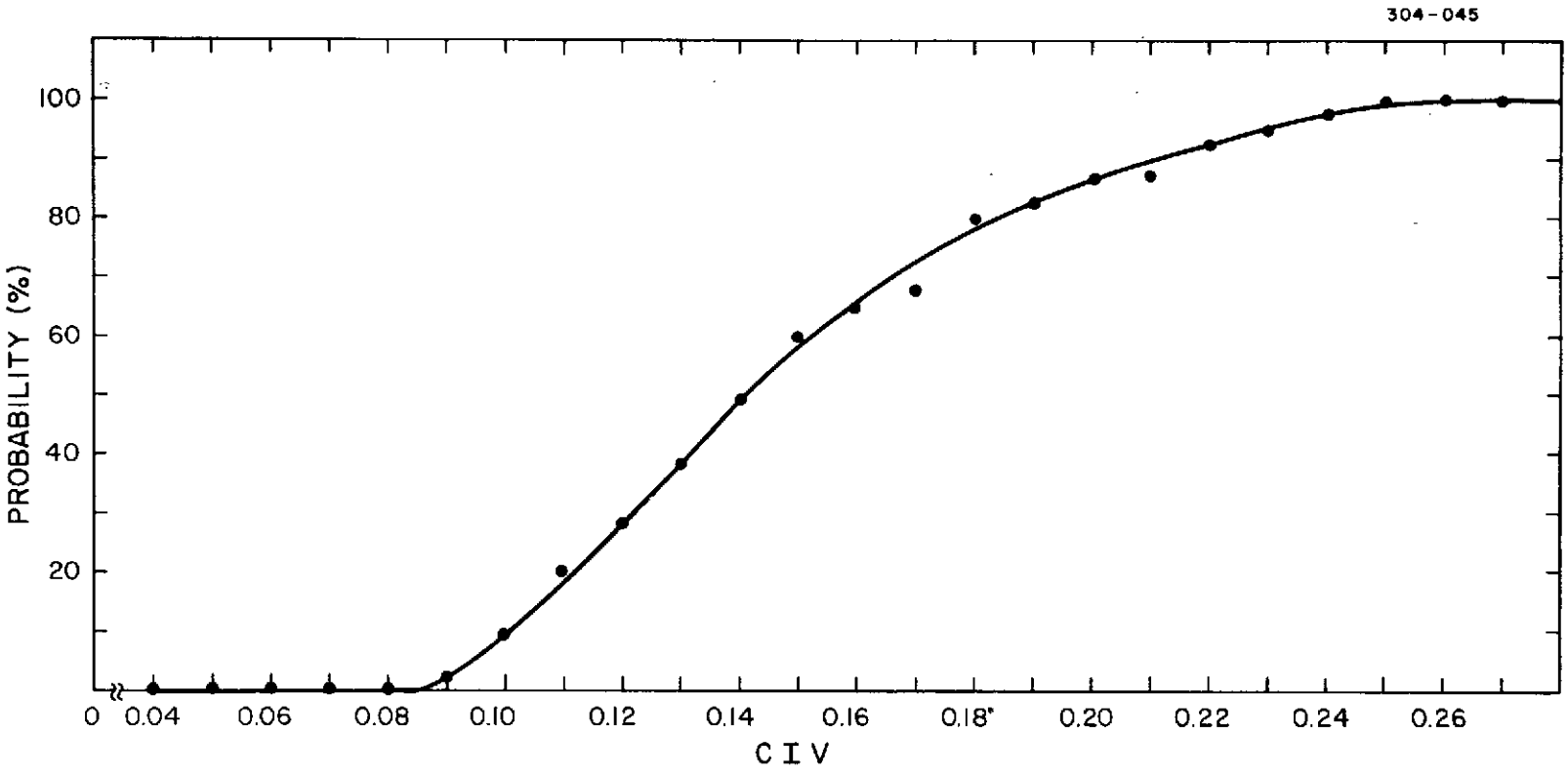

Figure 15. Cumulative probability distribution of CIV for long-term averages during Phase I. The values have been corrected to zenith.

shorter term fluctuations, and CIV data obtained during Phase II were examined for short-term effects. Time plots of CIV for Phase II, two examples of which are given in Figure 16, reveal a statistical spread of as much as 0.05 in CIV during some observation periods. No correlation was noticed between the amount of statistical spread and the average CIV level for the period. Slight trends were visible in the data during individual observation periods, but the effects were close to the noise level of the system.

Table 3. Summary of scintillation statistics for Phase I.

Month	Number of observing nights	Number of observations	Mean CIV	Standard deviation of CIV	Minimum CIV	Maximum CIV
1969						
June	4	19	0.126	0.044	0.052	0.240
September	5	13	0.131	0.048	0.065	0.221
October	17	66	0.155	0.042	0.100	0.303
November	5	20	0.124	0.025	0.088	0.189
December	2	7	0.121	0.019	0.104	0.161
1970						
February	4	18	0.173	0.066	0.097	0.319
March	11	29	0.155	0.050	0.058	0.288
April	5	20	0.157	0.072	0.087	0.377

Significant changes in CIV required at least several hours and often days to occur. This is to be expected, since the upper altitude turbulence structure most responsible for scintillation is heavily dependent on the upper altitude wind regime, which in turn varies with time constants on the order of hours. The fairly abrupt discontinuity in the data in Figure 16 is followed by a pronounced peak in CIV of about 2 min. This may reflect a change in upper altitude turbulence structure; however, detailed wind data are not available to check possible correlations.

Table 4 summarizes the scintillation statistics of Phase II. Averages are given on a monthly basis for all the short data runs, as well as averages for the longer

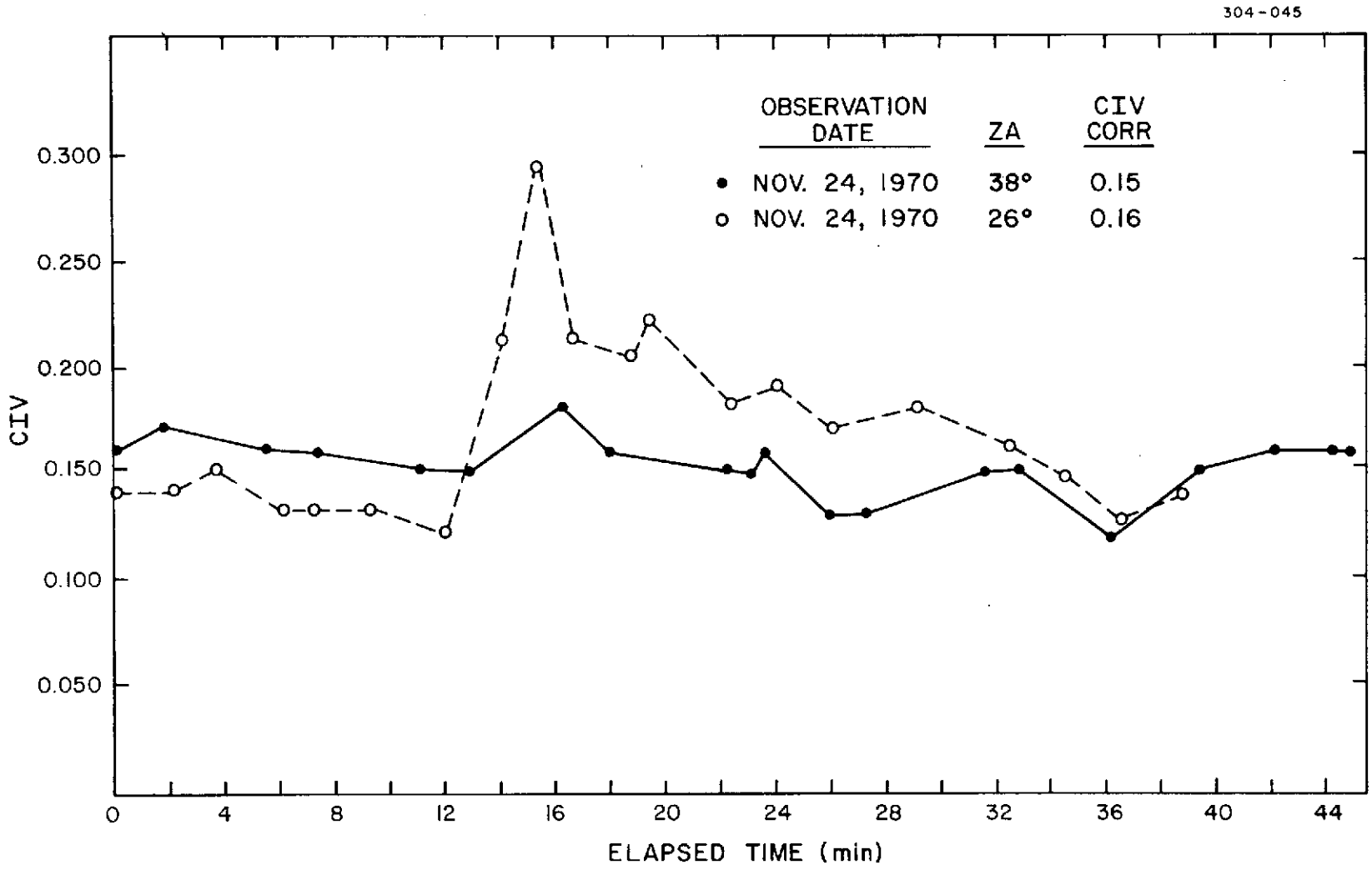

Figure 16. Two examples of short-term variations in CIV. The values have been corrected to zenith.

observation periods. The difference between the results of the two averages is again a reflection of slight differences in the length of observation intervals. The CIV values of Phase II were, on the average, similar to those observed during the same period of the previous year. Monthly averages were in the range 0.10 to 0.13, with excursions for individual observations to 0.05 and 0.29. The cumulative probability distributions for both averaging schemes are plotted in Figures 17 and 18. For data averaged over both the short and the long observation periods, CIV was less than 0.12 and 0.15 for about 50% and 90% of the time, respectively. That fewer large values of CIV (above 0.20) were observed in Phase II than in Phase I gives a steeper rise to the probability density curves. This difference is not significant at the 50% probability level; however, the difference becomes considerable at the 90% cumulative probability level, where the Phase I value is 0.21 and that of Phase II is about 0.15. This difference is most likely a reflection of the limited distribution in time of the observations in Phase II and probably does not indicate any seasonal variation.

Table 4. Summary of scintillation statistics for Phase II.

Month	Number of observing nights	Number of observations	Mean CIV	Standard deviation of CIV	Minimum CIV	Maximum CIV
Averaged over observation periods of up to 1-hr duration						
1970 November	8	13	0.126	0.025	0.090	0.160
December	6	8	0.105	0.021	0.060	0.130
1971 January	2	4	0.105	0.027	0.070	0.140
Averaged over data runs of 30-sec to 1-min duration						
1970 November	8	184	0.130	0.030	0.076	0.290
December	6	87	0.106	0.021	0.049	0.143
1971 January	2	74	0.108	0.030	0.065	0.184

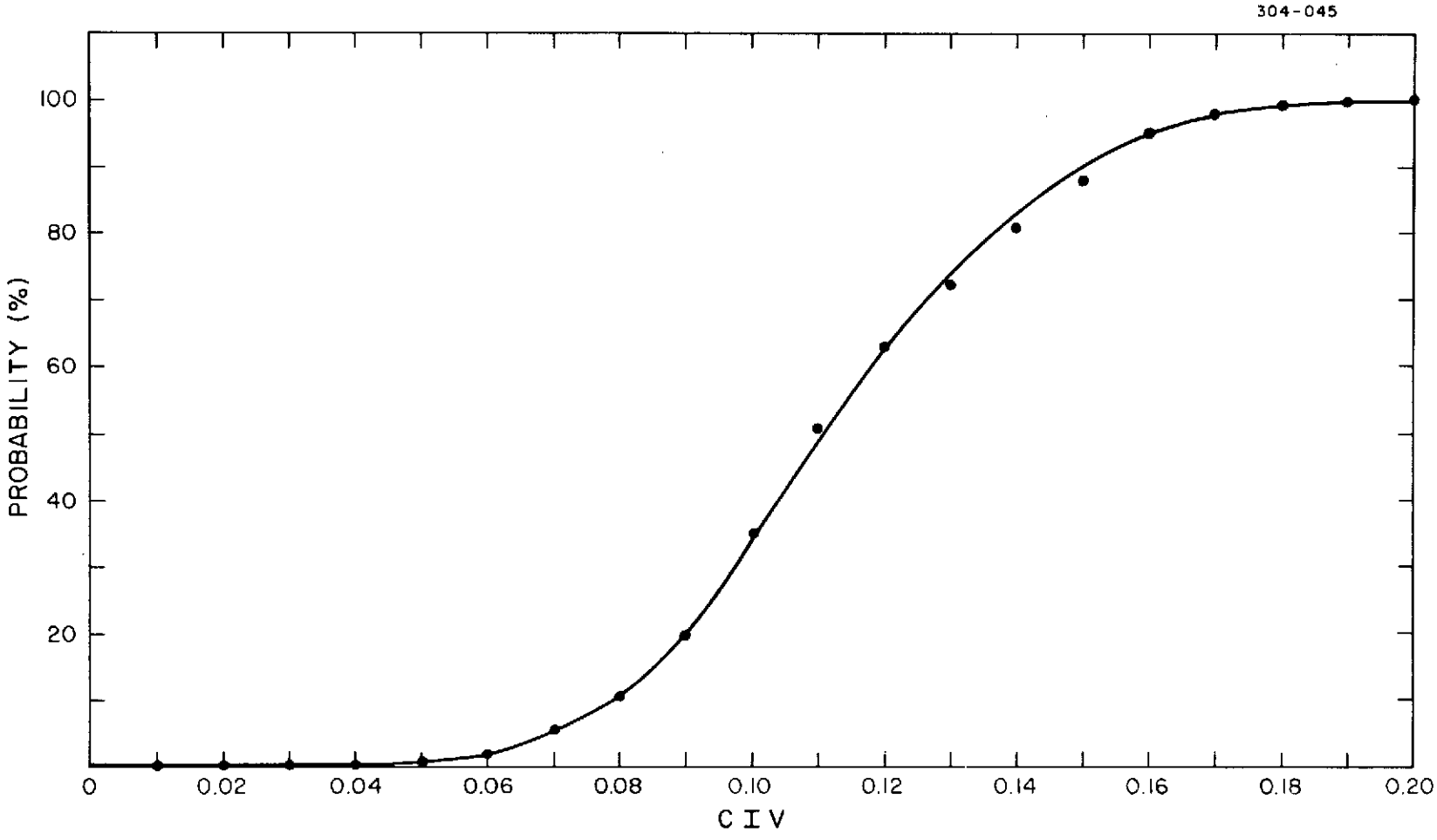

Figure 17. Cumulative probability distribution of CIV for short-term averages during Phase II. The values have been corrected to zenith.

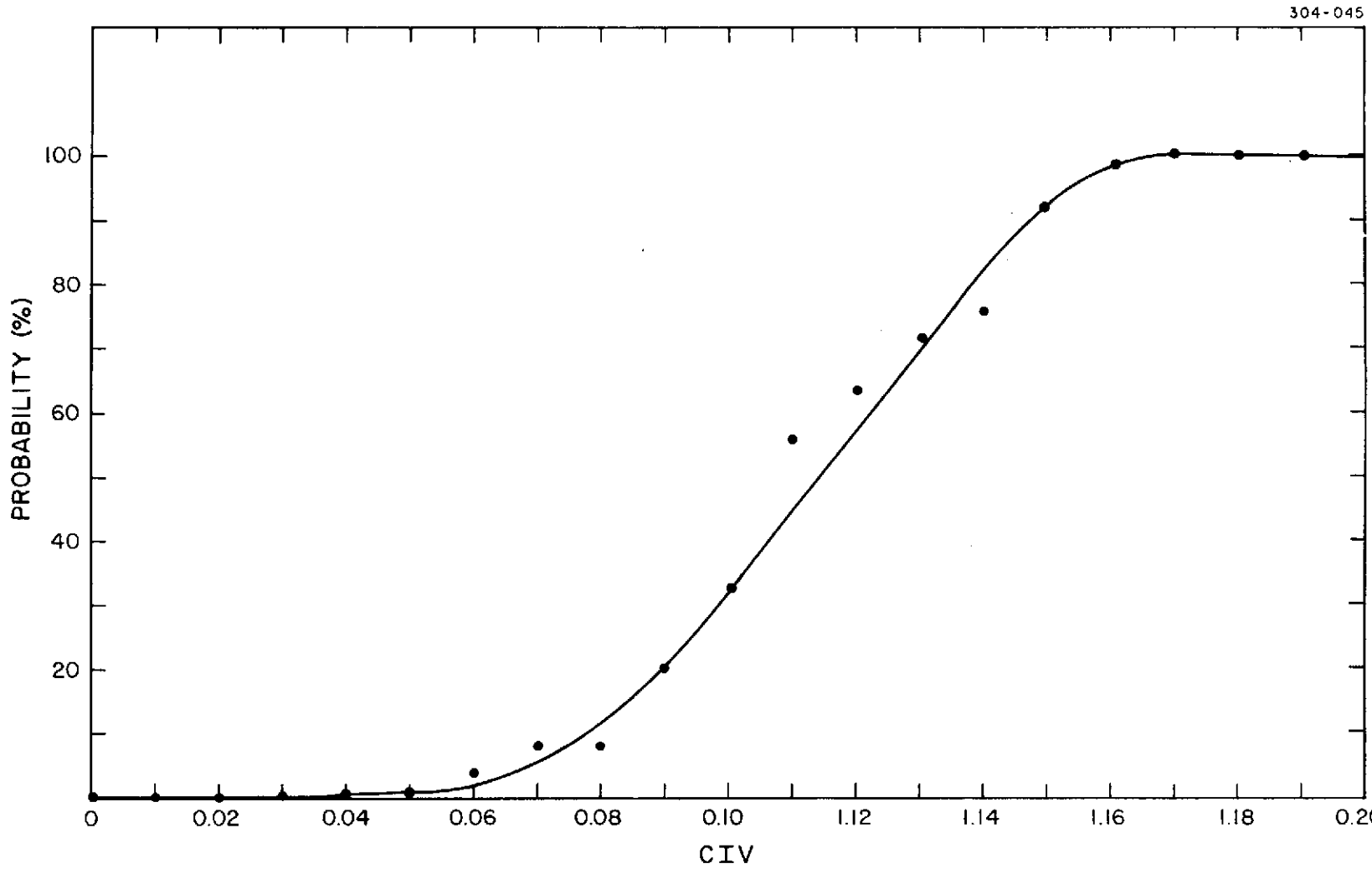

Figure 18. Cumulative probability distribution of CIV for long-term averages during Phase II. The values have been corrected to zenith.

The CIV data were examined for zenith-angle dependence by using the short-interval observations. The results, plotted in log-log form in Figure 19, show a large amount of scatter, which results primarily from the night-by-night fluctuations in the structure of the high-altitude turbulence. However, a zenith-angle dependence is clearly displayed by the data. A least-squares fit to the 345 data points for the short-interval measurements of scintillation for Phase II gives an exponent of 1.1. In spite of the large scatter in the data, log CIV and log (θ) were found to have a correlation coefficient of 0.75, leading us to place confidence in a linear relation with a slope near that computed. Data from a single night, denoted on Figure 18, show considerably reduced scatter, indicating that the high-altitude turbulence structure is fairly stable over a period of several hours. Although these data are limited in zenith-angle coverage, they clearly show a zenith-angle dependence. A least-squares fit to these data gave an exponent of 1.4.

Spectral densities of scintillation were determined from 30-sec samples of data from both Phases I and II. Typical results are given in Figure 20. For most of the data runs, the half-power point fell in the range 20 to 50 Hz, but individual runs with values as low as 4 Hz and as high as 88 Hz were observed. Components of scintillation are observed out to several hundred Hertz. A small contribution from 60-Hz noise was evident on some spectral-density curves; however, the influence was negligible in terms of total effect.

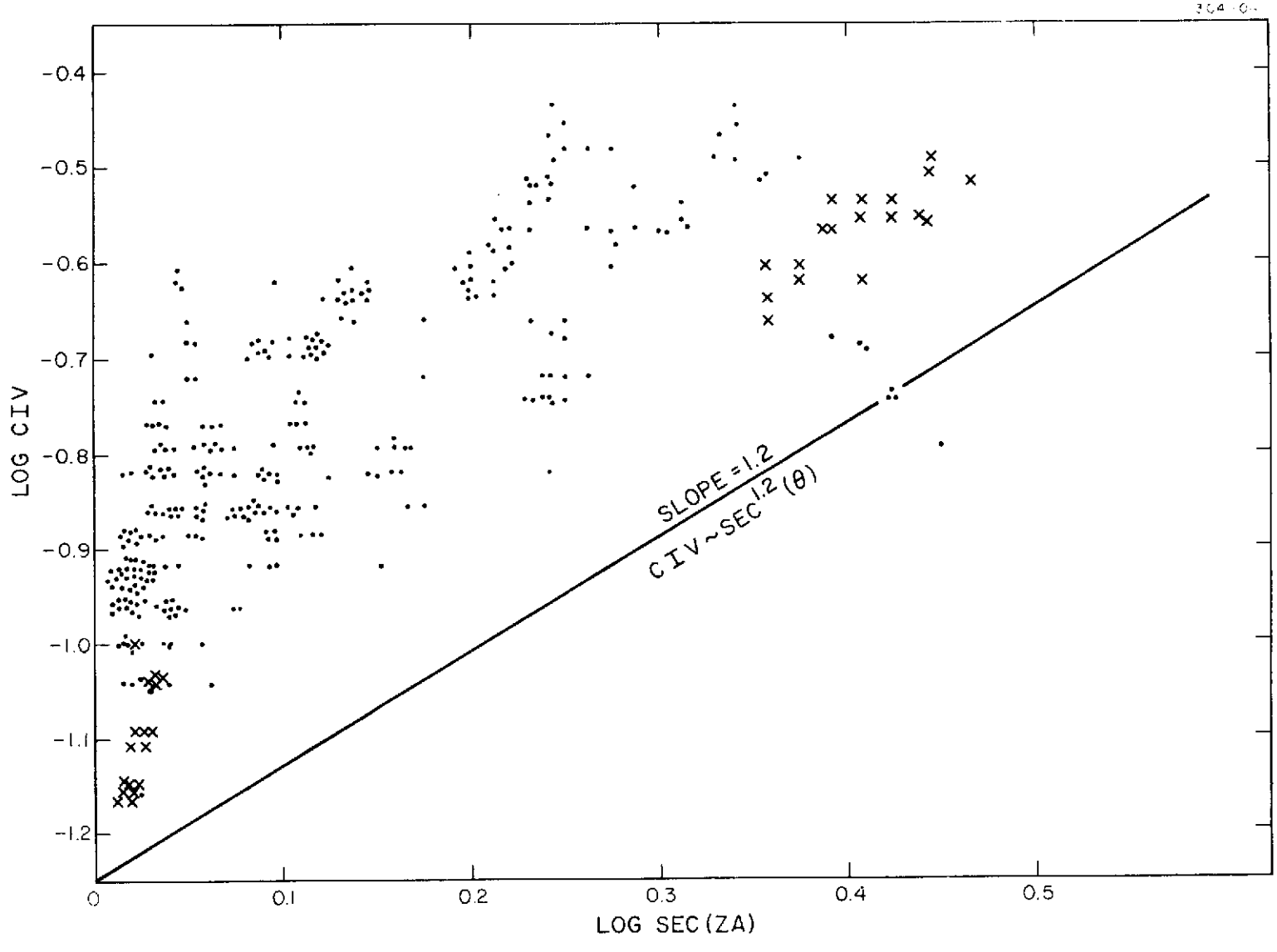

Figure 19. Experimental dependence of CIV on zenith angle. The $\sec^{1.2}(\theta)$ line is intended to show the anticipated trend. Its intercept was chosen for convenience only.

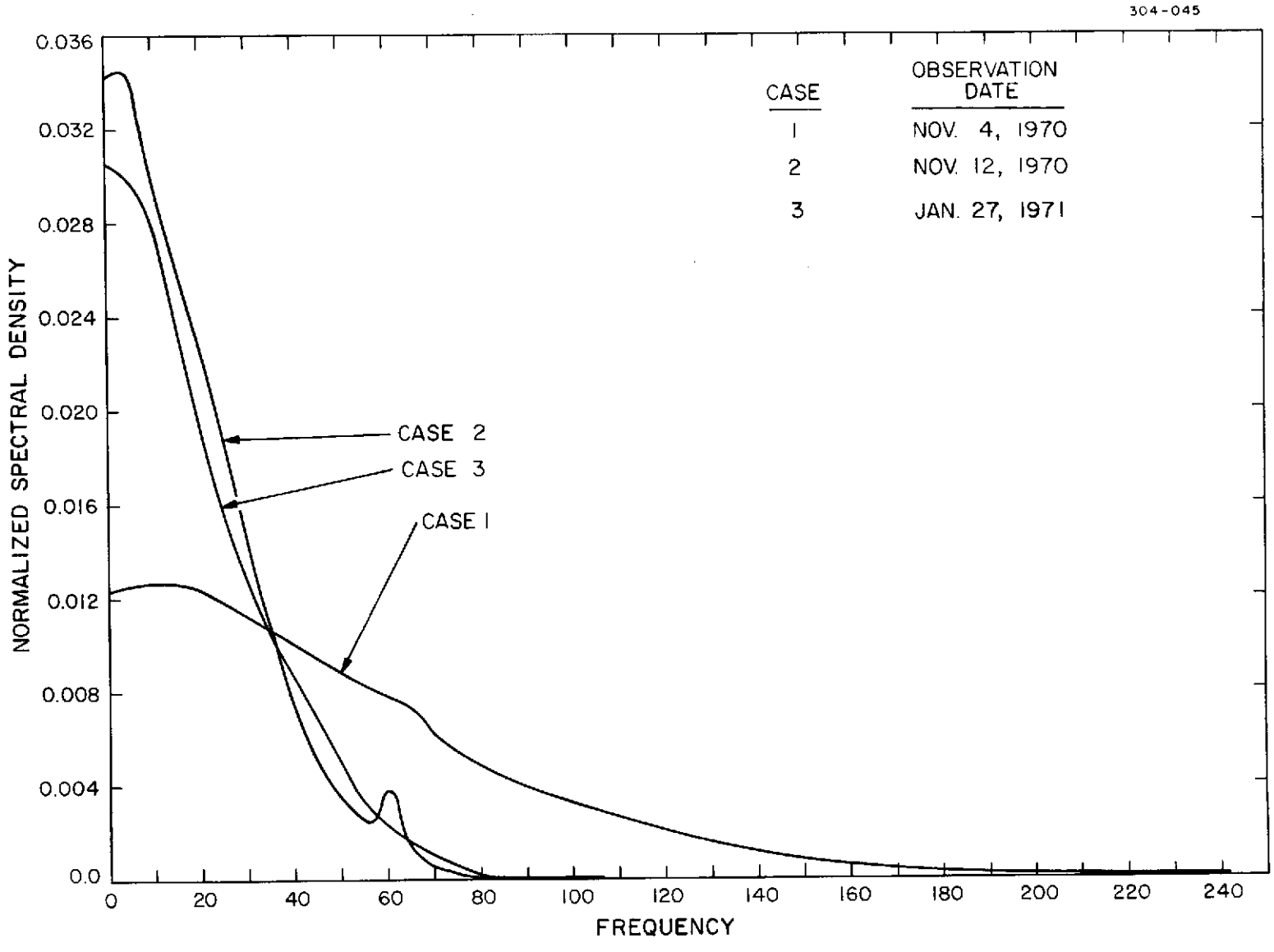

Figure 20. Three examples of the normalized spectral density for CIV showing noise contribution at 8 Hz from the SIM equipment.

5. CORRELATION OF IMAGE QUALITY WITH METEOROLOGICAL PARAMETERS

5.1 Image Quality vs. Local Meteorological Conditions

The data were examined for correlations between image quality (image motion and scintillation) and local meteorological conditions. These conditions should, in a sense, be one of the prime influences on seeing conditions; however, the actual dependence and the interaction with the terrain may be so complicated that simple functional dependencies are not evident.

In the long-period observations of image motion from Phase II, a very slight correlation with temperature of -0.44 (27 samples) was observed. The points that provided the major strength to the correlation were at the temperature extremes, with the worst seeing conditions prevailing at the lowest temperatures. Very slight correlations in σ_m were noticed with wind direction, changes in barometric pressure, and absolute humidity, but the correlation coefficients were very weak and may well not have been significant.

The data from Phase I showed even less correlation with meteorological conditions. This would be anticipated since the observation periods were very short and may not have been indicative of average conditions.

5.2 Image Motion vs. Temperature Fluctuations

The image-motion results of both Phases I and II expressed in terms of σ_m were compared with simultaneously acquired temperature-fluctuation data. The temperature data in the form of average values of peak fluctuations were supplied by the JPL-instrumented towers. These data are not the mean-square temperature measurements required to compute $C_T^2(h)$, however, they are a measure of the turbulence strength and should enjoy a direct correlation with $C_T^2(h)$. It was noted in Section 2 that the large near-ground $C_T^2(h)$ values should be most responsible for image motion. The connection was first made with $C_N^2(h)$ in equation (2) and then with σ_m in equation (13). Thus, there should be correlation between the JPL temperature data and σ_m.

The averaged long-period image-motion data taken during Phase II (integration times of 30 min to 1 hr) showed stronger correlation with the JPL temperature data than did the shorter interval measurements during Phase I. In Figure 21, the Phase II σ_m results averaged over each observation period are plotted along with the sum of the data from all four sensors located on the knoll 2 tower. Data from each sensor were first averaged over the same time period as the stellar observation period; then the sum of all four sensors was computed. For a significant portion of the available data, there appears to be a reasonably strong correlation between σ_m and the local temperature fluctuations. Many of the same peak and valley features appear in both data sets. Phase II correlation coefficients between σ_m and the outputs of the individual sensors, as well as between σ_m and the sum of the sensor outputs, are listed in Table 5. For comparison, it is noted that a coefficient of 0.47 has an 0.01 probability of being exceeded for a data sample of this size if σ_m and the temperature data are independent. A correlation coefficient of 0.58 has a probability of about 0.001. These values were computed by using a standard statistical reference (see Appendix C). Thus, the observed coefficients were all significant to at least the 0.01 probability level except for that associated with sensor 2.

Table 5. Correlation of rms image motion with average peak temperature fluctuation in Phase II.

JPL sensor	Height above surface (m)	Correlation coefficient	Number of data points	Probability* of random occurrence
1	7.5	0.58	29	0.001
2	15	0.35	29	0.06
3	23	0.52	29	0.005
4	30	0.60	29	<0.001
1+2+3+4	–	0.61	29	<0.001

*This is the probability that a correlation of this size or greater would be achieved with a data set of this size with two independent variables.

It is interesting to note that the correlation is quite high (0.58) for the lowest sensor, is minimum (0.35) for sensor 2, and then increases to the highest value (0.60)

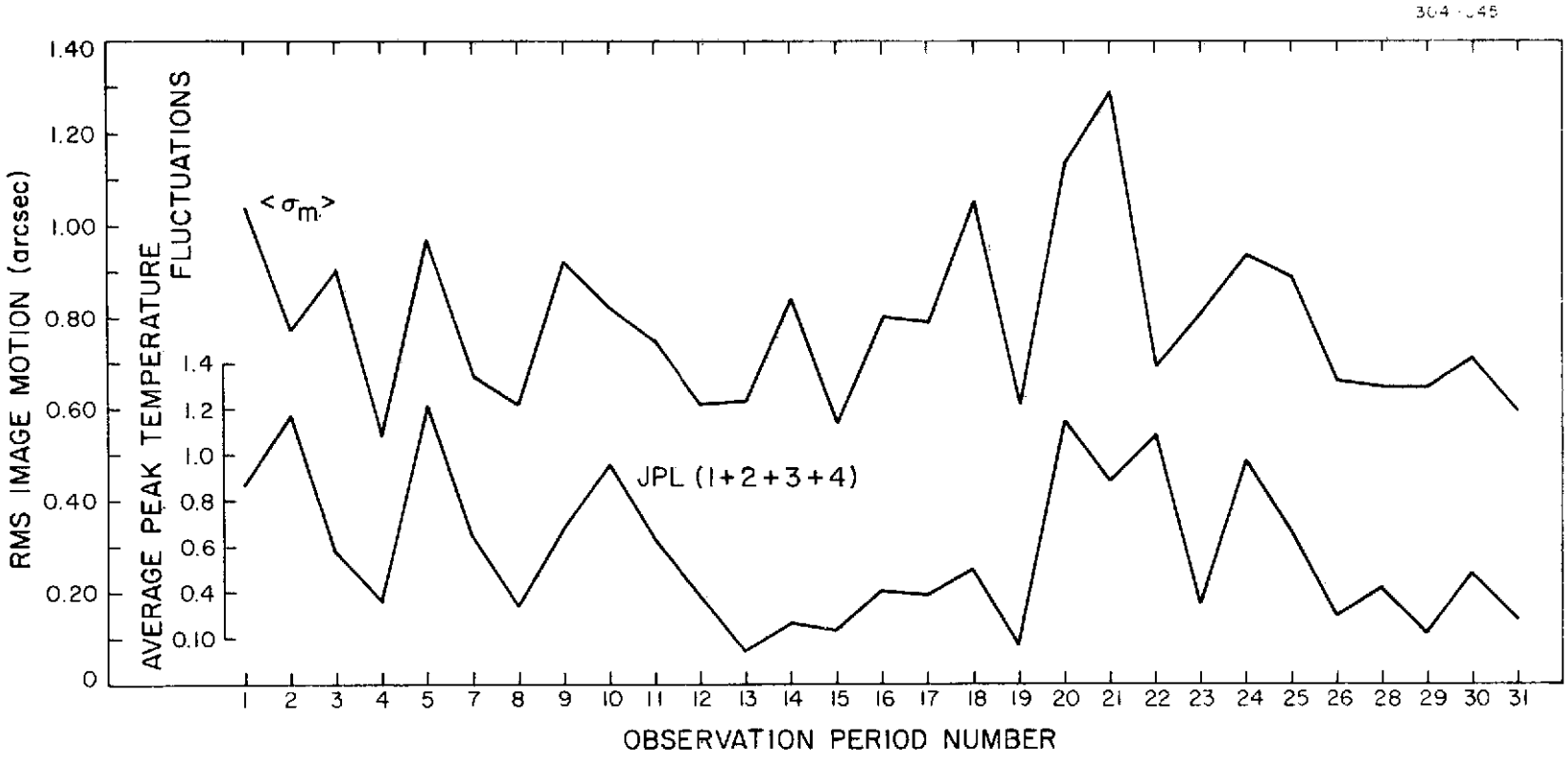

Figure 21. Long-term-averaged image-motion and peak temperature fluctuation as a function of observation period during Phase II. The data from observation periods 6 and 27 were not available owing to equipment failure.

for the sensor highest above ground level. The increase in correlation with sensor height could be associated with the predicted linear growth with altitude of the turbulence outer scale length. Since the stellar-image monitor and the JPL temperature tower were separated horizontally by ~ 100 m, it seems reasonable to assume that both instruments would be affected by more and more of a common turbulence structure as altitude and, hence, turbulence scale length are increased. Unfortunately, because of terrain factors and the difficulty of moving either tower or telescope, it was not possible to test for the horizontal separation that would yield the greatest correlation coefficients. Better correlation would presumably occur for direct side-by-side operation of the two instruments.

Within each stellar observation period, there were occasional significant short-term variations in σ_m with periods as short as 1 min. A more detailed look at the JPL temperature data that took into account these minute-by-minute fluctuations may have shown similar variations. The intent here, however, was to look for techniques to estimate average rather than instantaneous seeing conditions. With this in mind, the JPL equipment was built with a 3-min time constant.

With the correlation coefficient values 0.50 to 0.60 obtained for the long-term averages, the temperature-fluctuation data appear to be a useful tool to predict trends in σ_m. Improved results would be anticipated with better placement of the instruments.

5.3 Image Motion vs. Temperature Gradient

It is shown in equation (23) that under appropriate assumptions $C_T^2(h)$ is proportional to the temperature difference between two altitudes in the Earth's boundary layer. Thus, the optical strength of turbulence near the ground (measured here by σ_m) should enjoy some relationship with temperature difference (ΔT) between two points near the σ_m measurement. During Phase II, temperature-difference measurements (ΔT) were made between points in the region of knoll 2 (see Section 3.5) and a reference thermometer in a weather box on the roof of the Environmental Sciences Building, in close proximity to the SIM. As in the case of the JPL temperature-fluctuation measurements, the ΔT and σ_m data were first averaged over the stellar observation periods and then plotted (Figure 22) vs. σ_m. The ΔT data were available during Phase II only.

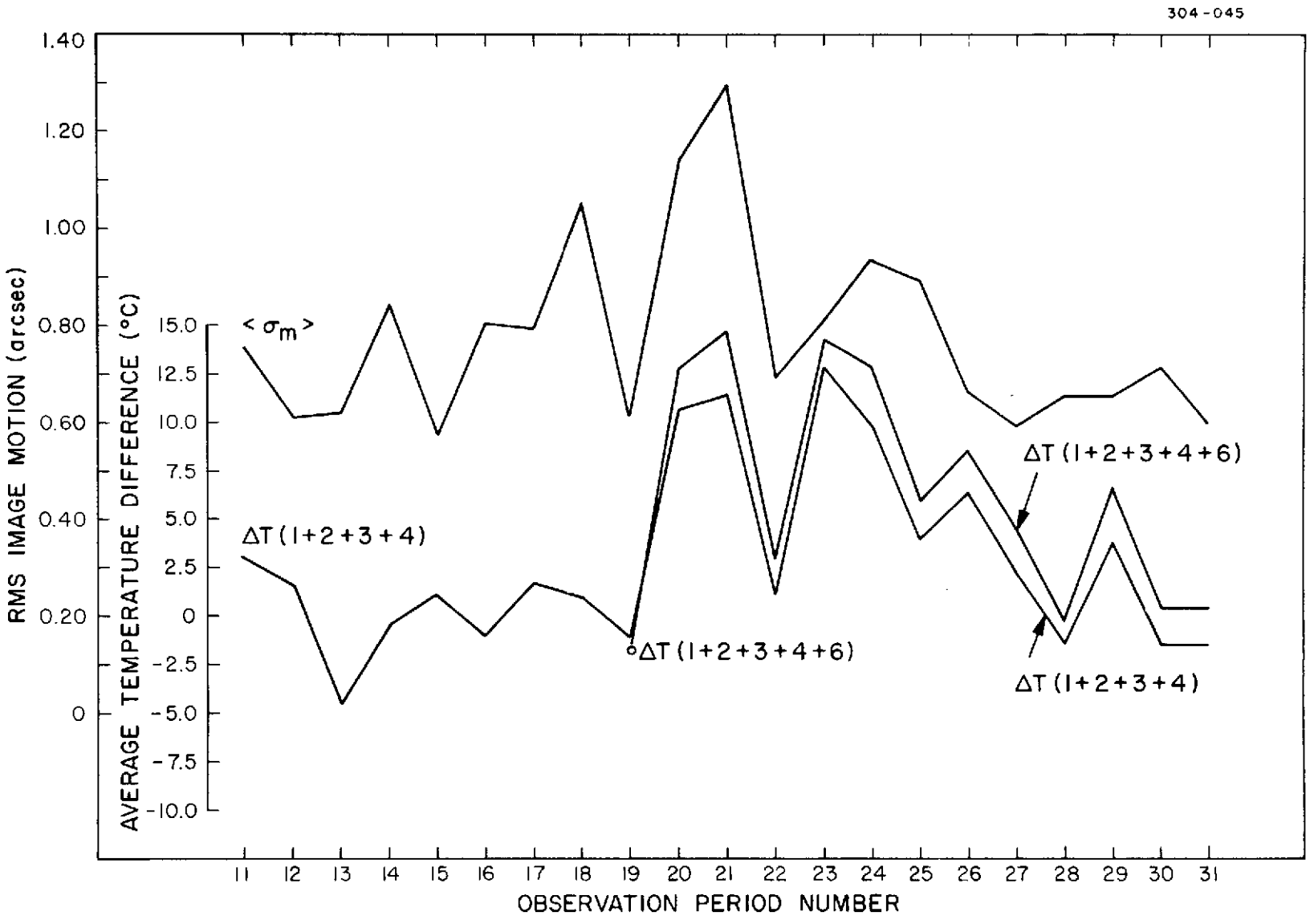

Figure 22. Long-term-averaged image-motion and temperature differences as a function of observation period during Phase II.

In Figure 22, two combinations of ΔT data from the sensor probes in the neighborhood of knoll 2 are plotted vs. σ_m. These two combinations are simple sums of the ΔT contribution by each of the probes included. Once again, a reasonably good correlation is achieved, and it should be quite possible to predict the trend of σ_m from ΔT data alone. Correlation coefficients between σ_m and various combinations of the ΔT data were computed; they appear in Table 6. There are 21 sets of observations with data from sensors 1, 2, 3, and 4 and the combination (sum). Only the ΔT data from sensor 2, the weather box downhill, are significant at an 0.01 probability level; however, data from sensor 4, on the telescope dome, are significant at the 0.02 level. These two sensors were probably monitoring the local temperature differences associated with the flow of air over the knoll and in the immediate vicinity of the telescope. In particular, the correlation observed with the dome sensor indicates that the dome environment is contributing somewhat to the σ_m values, possibly through residual thermal radiation and interaction with local winds. The best correlation results (0.62) are seen in the combination sum of the data from the four sensors. This value is significant at a probability level of considerably better than 0.01.

There are 13 sets of observations with data from sensors 5 and 6. The data from these individual sensors are not significant even at a 10% probability level. The smallest correlation coefficient was associated with ΔT from sensor 5, located on the summit tower. The slant range separation of over 1 km between the summit and the knoll 2 telescope and the differences in local terrain at these sites make a lack of data correlation quite understandable. It is possible that placement of the summit sensor at the top of the 32-m tower on the summit or use of an even taller tower would result in a slightly enhanced correlation due to the increase in turbulence scale with altitude. The weak correlation with the ΔT data from sensor 6 indicates that it too is not in a position where it is sensitive to the local activities that produce the turbulence structure through which the SIM observations were taken.

It is quite apparent from Table 6 that combining data from several sensors improves the correlation coefficient. Both combinations (1+2+3+4) and (1+2+3+4+6) are significant at probability levels of 0.003. The combining of data averages out local fluctuations and results in a more synoptic view of the ΔT conditions that is probably more indicative of the average seeing conditions. The array of ΔT sensors

Table 6. Correlation of rms image motion with temperature difference (ΔT) in Phase II.

Sensor	Sensor location	Correlation coefficients	Number of data points	Probability of random occurrence *
1	30-m level of knoll 2 tower	0.47	21	0.04
2	West weather box downhill	0.60	21	0.005
3	15-m level of knoll 2 tower	0.42	21	0.06
4	Telescope level in dome	0.52	21	0.02
5	15-m level of summit tower	0.34	13	>0.10
6	East weather box downhill	0.48	13	0.10
1+2+3+4	–	0.62	21	0.003
1+2+3+4+6	–	0.76	13	0.003

*This is the probability that a correlation of this size or greater would be achieved with a data set of this size with two independent variables.

used in this experiment appears to be an indicator of seeing conditions, particularly when the data are combined. The marked variation in correlation coefficients achieved by different sensors suggests, however, that a better array of sensor locations could be found that would give even better correlations.

5.4 Scintillation Spectral Density vs. High-Altitude Winds

The correlation between the scintillation spectrum and the high-altitude wind structure was investigated with data from both phases of the experiment. The normalized spectral densities for scintillation observations were available from data reduction in both phases. The high-altitude wind speed and direction were determined from regular rawinsonde flights from Tucson International Airport. All stellar observations were made within 6 hr of a rawinsonde flight. Because of the relative stationarity of upper altitude winds, the time differences of 6 hr or less were not considered significant. Wind data obtained from the Tucson flights were corrected to velocities normal to the propagation path from star to telescope by using equation (9) before the correlations were computed.

There are several ways to characterize scintillation bandwidth from the spectral-density data. Correlations with high-altitude winds were investigated by using the frequency value at which the spectral density fell to half the value at 0 Hz. In some cases, the scintillation spectral density was not maximum at 0 Hz but rather in the vicinity of 10 Hz. However, the difference in amplitudes was small, and using the maximum amplitude instead of that at 0 Hz made little difference. Correlation coefficients between these scintillation "half widths" and the ratio of the normal wind component to irradiance correlation distance (equation 10) are presented in Table 7 for Phase II. Coefficients were calculated for all data points and for data restricted to zenith angles above 45°. The former correlation coefficients were significant for probability levels of 0.001 or better; the latter, to 0.002 to 0.007. Similar data were computed for Phase I; however, the results were generally not so good. This was most likely due to the longer integration times (1 min vs. 20 sec) used for spectral-density determinations in Phase II, which gave a better picture of the averaged conditions. In the Phase II data, slightly stronger correlations were obtained with winds at the 200-mb and the 100-mb pressure levels than at the altitudes of maximum

wind speeds, which are for the most part below 200 mb. The differences are, however, quite small and are probably not significant.

Table 7. Correlation of scintillation half-width frequency with wind speed/correlation distance ratio (Phase II).

Altitude	Correlation coefficient*	
	All data	Data with $\theta \leq 45°$
Maximum wind speed	0.50 (0.001)	0.53 (0.007)
200-mb pressure level	0.53 (0.001)	0.59 (0.002)
100-mb pressure level	0.53 (0.001)	0.59 (0.002)
Number of points in the data set	43	24

*The probability that a correlation of this size or greater would be achieved with a data set of this size with two independent variables is shown in parentheses.

Restricting the data set to 3 hr within launch did not improve the results, supporting the assumption of stationarity of the upper altitude winds. Other representations of spectral width including 1/e and 1/10 power points were investigated, but the correlation coefficients were considerably worse than those in Table 7.

Another technique used to characterize the scintillation spectral widths was to express them in terms of normalized spectral amplitudes. The spectral amplitudes were measured at 50, 100, and 150 Hz, and normalized to the 10-Hz level. These normalized quantities were used to calculate correlation coefficients for the normal component of wind velocity at the height of maximum wind speed, at the 200-mb level, and at the 100-mb level. The results are given in Table 8.

The 50 Hz/10 Hz representations gave the best results for both the total data set and the set restricted to zenith angles of less than 45°. This is not surprising when the shape of the scintillation spectral density is considered (see Figure 20). The amplitude at 50 Hz is sizable and appears to be quite sensitive to spectral shape. On the other hand, the amplitudes at 100 and 150 Hz are considerably smaller and far less sensitive to spectral shape; in many cases, the 150-Hz component is not even measurable.

Table 8. Scintillation: Power spectrum components vs. high-altitude winds.

Component	Altitude	Correlation coefficient* All data	Correlation coefficient* $\theta \leq 45°$
50 Hz/10 Hz	Maximum wind	0.54 (<0.001)	0.60 (0.002)
	200 mb	0.53 (<0.001)	0.61 (0.001)
	100 mb	0.50 (<0.001)	0.44 (0.03)
100 Hz/10 Hz	Maximum wind	0.49 (<0.001)	0.48 (0.02)
	200 mb	0.48 (0.001)	0.51 (0.01)
	100 mb	0.40 (0.007)	0.31 (>0.10)
150 Hz/10 Hz	Maximum wind	0.42 (0.005)	0.41 (0.05)
	200 mb	0.37 (0.01)	0.38 (0.06)
	100 mb	0.29 (0.1)	0.15 (>0.10)

*The probability that a correlation of this size or greater would be achieved with a data set of this size with two independent variables is shown in parentheses.

In the case of this type of representation, the winds at the height of maximum speed, usually below 200 mb, and those at the 200-mb level gave higher correlations than did the data from the 100-mb level for all three spectrum-amplitude ratios used. The difference appears to be quite significant and may indicate that at least the higher frequency components (50 Hz and above) are associated with activity at the lower altitudes (200 mb or below) as indicated in equation (10).

The correlation coefficients between the 50 Hz/10 Hz component and the wind data (at 200 mb and at the altitude of maximum speed) for both sets of data are significant to a random probability level of 0.001. As in the previous calculation with the half-width data, the full data set gave better results than the data set with zenith angle restricted to 45° or less.

5.5 Image Motion vs. Temperature and Wind Profiles

The radiosonde temperature-profile data were examined for correlations with σ_m, but no significant dependences were found. In these analyses, computed lapse rates for the lowest radiosonde significance level and averaged lapse rates for the

first 2 km above the surface were used. Although the data included a wide range of both negative and positive lapse rates over the lowest few kilometers of path length, there was no indication that seeing conditions were related to the sign of the lapse rate. In particular, image-motion quality σ_m was not noticeably better under conditions of temperature inversion. This should, of course, not be too surprising, since this mountain-top terrain is considerably different from the type of site location assumed by Tatarski (1961). In addition, the path of the radiosonde balloons showed quite clearly that the wind direction changes significantly as a function of height above the surface and that the wind-shear pattern and the turbulence structure can be quite complicated in some cases.

The low-altitude wind data were examined for correlations with σ_m. Wind speed and direction at altitudes as low as a few hundred meters were computed from balloon azimuth and altitude readings measured by optical tracking.

Some correlation was found between σ_m^2 and the wind direction at levels close to the surface. A correlation coefficient of 0.51 (random probability of about 0.02) was found between σ_m and the difference in directions between the wind at 300 m above the site and at the site itself. The larger values of σ_m corresponded to the cases where the winds were blowing in opposite directions. This is just the case where the largest turbulence by induced wind shear is expected. The correlation between σ_m^2 and the winds at the 700-m level was not significant. The simplest conclusion is that wind-direction measurements at points fairly close to the ground, at altitudes of 50 to 100 m, are likely to be the most useful indications of image-motion quality. No significant correlations were found between image-motion conditions and the magnitude of the vector difference of wind velocity at various altitudes and at the ground.

Tatarski's equation (22) (1961), relating C_T^2 with the outer scale of the turbulence and the temperature profile, was also tested for a simple model, but without success. The outer scale was chosen as the altitude above the site for altitudes below 1 km, and as equal to 1 km above that. The quantity $C_T^2(h)$ was then integrated over the first few kilometers. Only very weak correlation coefficients were found between σ_m^2 and the integrated value of $C_T^2(h)$, and they were considered not to be significant.

6. COMMENTS AND APPLICATIONS

6.1 Comments on the Seeing Conditions at the Mt. Hopkins Site

The image-quality measurements taken at Mt. Hopkins in this experiment extended over a period of about a year and a half. The measurements were taken with a 6-in. telescope. Estimates for instruments of larger diameters can be extrapolated through relations developed by Tatarski and others (see Section 2).

With the 6-in. telescope, the one-dimensional image-motion σ_m corrected to zenith was approximately 0.7 arcsec for a yearly average. Excursions as high as 1.6 and as low as 0.2 arcsec were observed. For two-dimensional image-motion σ values, these quantities would be multiplied by $\sqrt{2}$.

The scintillation conditions at the site are characterized by an average coefficient of irradiance variance corrected to zenith of about 0.13, with excursions as high as 0.38 and as low as 0.05. Since scintillation is caused by turbulent conditions in the upper atmosphere, these CIV values would be indicative of the general area rather than just the Mt. Hopkins site.

Definitive measurements of image-blurring conditions at the site could not be made with the SIM apparatus; however, an upper limit on the size of the blur circle is estimated to about 0.9 arcsec. The MTF values measured in the field fell very close to the actual system MTF determined in the laboratory. The blur circle then appears to be smaller than the minimum spot size (full width, half power) of the apparatus, which is 0.9 arcsec, but a larger telescope would be required to determine its size. This spot size was determined from equation 15 by using the laboratory-measured MTF.

The total image size as seen in the telescope is the result of image blurring and image motion. The variances add to give essentially the variance of the long-term image size. From the upper bound for the variance of the blurring component and

$\sigma_m^2 = (0.7\sqrt{2})^2$ for the average two-dimensional image motion, the upper bound for the average long-term image size for a 6-in. telescope is calculated to be approximately 1.3 arcsec.

The results obtained from the measurements in this experiment can be extrapolated to telescopes with larger apertures. From the $D^{-1/3}$ relation for image motion (equation 13) and the results found experimentally, the average one-dimensional image-motion σ_m extrapolated for a 60-in. telescope would be about 0.3 arcsec. From the $D^{-7/3}$ relation for $(CIV)^2$ (see Section 2.2), the average scintillation conditions (CIV) at the Mt. Hopkins site extrapolated for a 60-in. telescope would be down by more than an order of magnitude to values of the order of 0.01. In a large telescope, the atmospheric influence appears primarily as blurring; the image-motion component is negligible. The blurring component would be approximately equal to the long-term image size, which for this site has an average value whose upper bound is about 1.3 arcsec.

At Mt. Hopkins, we observed several interesting correlations between seeing conditions and local meteorological measurements that could form a basis for selecting a new site and for monitoring seeing conditions at an established site. Image motion was found to be correlated with the average peak temperature fluctuations above the site and with temperature differences measured between points in the vicinity of the site. In many cases, correlations of 0.50 to 0.60 with random probabilities of occurrence of less than 0.01 were found.

Correlations were observed between image-motion quality and the wind activity at levels just above the site. The wind-direction measurements were made by tracking radiosonde balloons from the ground site. Correlations of 0.5 were found between σ_m^2 and the wind direction at levels a few hundred meters above the surface. The connection here is through the turbulence structure induced by wind shear near the ground. The largest values of σ_m were found when the winds above the surface and those at the ground were blowing in opposite directions.

Correlation coefficients between scintillation spectral width and high-altitude wind activity above the site were found to be as large as 0.5 and 0.6, with a random

probability of less than 0.001 in some cases. These correlations were found to exist even though the high-altitude winds were measured at Tucson Airport, which is approximately 50 mi north of the Mt. Hopkins site, and at times as much as 5 or 6 hr before the scintillation measurement was made. Wind speed in the vicinity of 200-mb altitude was found to be a reasonably good indicator of the character of the higher frequency components of scintillation activity.

Many other points about seeing conditions and correlations with meteorological conditions are discussed in detail in the earlier sections of this report. However, one item that is worth mentioning here is the frequent occurrence of temperature inversions above the mountain, and yet the apparent lack of any correlation between temperature profile above the site and image-motion conditions. In approximately half the runs in Phase II, the radiosonde measured temperature inversions in the first few thousand meters above the mountain. For some cases (see Section 2), inversions are characteristic of stable atmospheric conditions and of low values of C_T^2 and hence low values of σ_m. In this series of measurements, however, no systematic improvement in seeing conditions was noticed for those cases where temperature inversions were present.

6.2 Comments on Site Testing

The stellar-image monitor is an excellent tool to measure image-quality conditions at a site. It provides a direct and continuous reading of image motion and scintillation and their respective spectral densities. The instrument can also provide information on image blurring; however, the limitation here is at about the 1-arcsec level for the present instrument.

The spectral-density functions for image motion show clearly that high-frequency components must be included in the measurement to obtain accurate values. For image motion, significant contributions are apparent at 10 and even 15 Hz in some cases. More than half the area under the spectral-density curve is at frequencies above 3 Hz. It appears that bandwidths of at least 10 Hz (or sampling rates of 20/sec) are required to make measurements with an accuracy of 10%. It should be noted that the shape of the spectral-density function changes appreciably from run to

run, with half-power points varying from one to several cycles. Observations at a bandwidth of 1 or 2 cycles do not measure a constant fraction of the total image motion, and measurements or comparisons made with such techniques are open to serious question.

The scintillation spectral-density functions have significant components out to 100 and in some cases 150 Hz. Measurements of scintillation must be made with bandwidths of at least 150 Hz to obtain an accurate value.

The connection between image-quality conditions and meteorological and other ground-based measurements offers a basis for site selection, but even more important, it offers potential techniques for monitoring conditions at a site for the selection of particular observing conditions.

The measurements of peak temperature fluctuation made with the JPL-instrumented tower gave a good indication of the image-motion conditions. The variation in the correlation coefficient from one sensor to the next indicates strongly that other instrumentation configurations would probably have been better and have given even better results. Had terrain permitted, the JPL-instrumented tower should have been placed in much closer proximity to the SIM so that it would have sampled a greater portion of the turbulent structure through which the optical observations were being made. The system is, in general, quite easy to use, and very little effort along the lines of data reduction is required. It appears that this technique can monitor (predict) image-motion quality with a correlation coefficient of at least 0.60, and possibly higher with a better placement of the tower.

The temperature-difference measurements with the weather apparatus also gave an indication of the image-motion conditions. Here again, the differences in the correlation coefficients indicate that a better placed network of sensors would have been more effective. Sensors placed several feet above ground level in the vicinity of the observation site and on the dome appear to add the greatest strength to the correlation. These sensors are probably sampling the local structure created by the local wind and temperature conditions. In future work of this kind, it would probably be advisable to place additional sensors near the surface and closer to the observing

site. It does not appear that measurements of temperature gradient above the site add very much strength to the correlation. It seems that this temperature-difference technique can monitor (predict) image-motion quality with a correlation of at least 0.60 and probably somewhat better with a more strategic placement of the sensors on the ground.

The connection between image motion and wind activity just above the site offers another potential technique to monitor conditions. The largest correlations seen were between image-motion quality and the difference between the wind direction at 300-m altitude and that at the ground. The wind direction at 700-m altitude showed essentially no correlation with image motion. Wind-direction measurements at levels of 100 or 50 m or even lower would probably give better indications of seeing conditions. Such measurements could easily be taken from a tower.

The high-altitude winds are a good indicator of the width of the scintillation spectral density. With the stationarity of the high-altitude winds, rawinsonde data from a location 50 or more miles away appear to be sufficient to indicate conditions for at least 6 to 12 hr. Correlation coefficients as large as 0.6 with a random probability of less than 0.001 were found in spite of the fact that the measurements of high-altitude wind and scintillation in this experiment were separated by about 50 mi and by as much as 5 or 6 hr in time.

6.3 Direct Detection of Pulsed Laser Radiation

The advent of practical optical communication systems is one of the most attractive applications of recent progress in laser technology. For civilian and military space applications, one of the most important optical communication system links would consist of a spaceborne laser transmitter and a ground-based receiver. This communication link could inherently provide information at a very high data rate (near 1 GHz) from space to ground. The successful performance of the link depends on the optical effects of turbulence in the intervening atmosphere, to much the same extent as does the success of stellar observations. Thus, the measured scintillation and image-motion effects reported here have direct and immediate application to the prediction of a laser communication link. One type of laser link with a high data rate that is

under active consideration employs pulsed transmission of visible or near-infrared laser radiation from a satellite platform to a telescope system of very large aperture and convential photoelectric detection at ground level. This technique is discussed below, with special emphasis given to its applications under conditions similar to those at Mt. Hopkins.

The ground receiver in this link would consist of a single, large-aperture telescope or of an array of smaller telescopes. The main intent would be to collect all possible incident laser radiation in order to determine accurately the presence or absence of a laser pulse. This is called the "photon bucket" receiver mode. The pertinent propagation statistic is scintillation, since only the fluctuations in total irradiance sampled by the aperture affect the detection of pulses. Because of the pulse transmission, the link is digital in character, and an appropriate specification of receiver performance is through a probability-of-error calculation (for incorrect interpretation of an individual bit). A recent analysis by Titterton and Speck (1973) has determined probability of error P_E expected in a typical binary communication channel in the presence of log-normally distributed fluctuations in total irradiance (signal). Results produced by numerical integration are plotted in Figure 23 for the following channel parameters:

A. Equal a priori probability exists for transmitting a zero (nothing) or a one (pulse).

B. Average number of noise photoelectrons per bit equals 1.

C. Modulator extinction ratio equals 31.6 (30 db).

D. S_x is the average number of signal photoelectrons received per bit in the absence of turbulence.

E. S is the number of signal photoelectrons per bit under the presence of turbulence.

F. S_0 is the average of S.

G. The probability of error must be less than or equal to 10^{-6}.

Scintillation strength and thus turbulence strength are specified in Figure 23 in terms of log-amplitude variance σ_ℓ^2. The connection with data reported here in terms of CIV was given in equation (8). The CIV results of Phase I of Section 4 indicate that

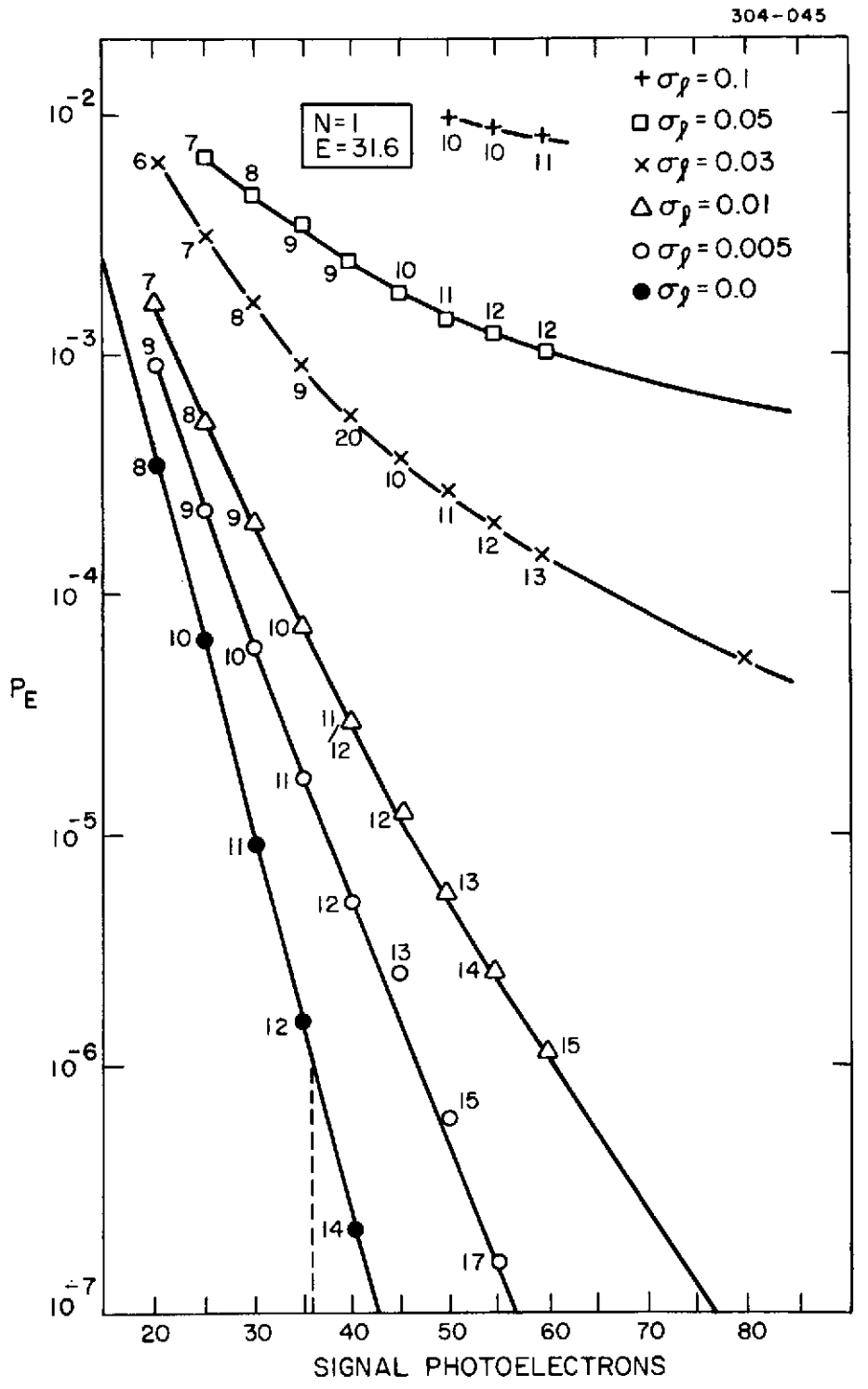

Figure 23. Probability of error in the presence of log-normal fading (Titterton and Speck, 1973).

90% of the time, CIV was below 0.25. In terms of σ_ℓ^2, this is 0.015. From Figure 23, it is seen that for $P_E = 10^{-6}$ and $\sigma_\ell^2 = 0$, the average number of signal photoelectrons S_x is approximately 36 for this choice of link parameters. The intersection of the curve for $\sigma_\ell^2 = 0.015$ with the line for $P_E = 10^{-6}$ yields a value for S_0 of approximately 86. This means that 86 photoelectrons must be received per bit to ensure a probability of error of less than 10^{-6}. Because of the assumed log-normal distribution for S, the probability $P\{S < S_x\}$ that S falls below threshold S_x is given by

$$P\left\{\frac{(1/2)\ell n\,(S_x/S_0) + \sigma_\ell^2}{\sqrt{\sigma_\ell^2}}\right\} \quad ,$$

where the probability function is the normal probability or error-function integral. The result, $P\{S < S_x\} = 0.0003$, yields the percentage of time, 0.03%, that P_E would exceed 10^{-6} for these system parameters. This is called the "link-outage" approach to P_E calculation. This number is contingent on use of a 0.152-m aperture. With a larger aperture, the irradiance fluctuation would be reduced through aperture averaging. An increase by a factor of 10 in telescope diameter would reduce σ_ℓ^2 by more than 2 orders of magnitude. Thus, we expect σ_ℓ^2 to be less than 0.00015 about 90% of the time. The P_E curve for this value is so close to that for $\sigma_\ell^2 = 0.0$ that there is little difference in the average number of signal photoelectrons required in the presence of no turbulence. An S value of 36 photoelectrons would then be sufficient to maintain the link under these conditions.

6.4 Heterodyne Detection of Continuous-Wave Laser Radiation

An alternative approach to space-to-ground communications is to use continuous-wave radiation and a ground-based heterodyne receiver. This technique is discussed below, once again with special emphasis given to conditions similar to those at Mt. Hopkins.

The ground-based optical heterodyne receiver in this link would employ a telescope with aperture diameter chosen for best performance in the presence of turbulence-induced optical effects. Although both scintillation and imaging effects will cause degradation of heterodyne performance, the wavefront degradation and phase changes

associated with image motion and blur are the most serious. Fried (1967) has shown that the average signal-to-noise ratio is a function of receiver diameter D and that there is an optimum diameter $D = r_0$ for which the signal-to-noise ratio is a maximum. Fried's calculation plus the theory of Tatarski (1961) and Hufnagel (1966a) for image motion can be combined to yield

$$r_0 = 1.19\, D^{-1/5}\, (2\pi/\lambda)^{-6/5}\, \sigma_m^{-6/5} \quad ,$$

where σ_m is the rms of the image motion, and r_0 is thus nearly inversely proportional to σ_m; and D is the aperture diameter for which the σ_m data were obtained.

The image motion σ_m for both phases of the Mt. Hopkins experiment averaged about 0.7 arcsec. For a wavelength of $\lambda = 0.5$ μm, this implies an aperture size of about $r_0 = 0.01$ m. A practical optical heterodyne system would probably employ a wavelength of 10.6 μm. For this wavelength and the measured value of σ_m, an aperture size of $r_0 = 0.35$ m is indicated.

7. ACKNOWLEDGMENTS

The authors wish to acknowledge the guidance and assistance received from a number of individuals on this project:

Mr. Michael Shumate from the Jet Propulsion Laboratory for his recommendation of the instrumented tower for the temperature-fluctuation measurements and for his preparation of the equipment and his assistance in the setup at the site;

Dr. C. E. Coulman of the Commonwealth Scientific and Industrial Research Organization in Sydney, Australia, for his guidance and foresight in the initial planning of the experiment;

Mr. Sol H. Genatt of Goddard Space Flight Center for his help in setting up the SIM and other equipment at the site;

NASA/Wallops Station for its loan of the radiosonde equipment, for assistance in setting up the equipment at the site, and for help in reducing the radiosonde data;

Dr. John Wyngaard of Air Force Cambridge Research Laboratory for his thoughts and guidance on particular aspects of the experiment; and

Mrs. Diane Hills and Miss Barbara Welther for their programing support.

8. REFERENCES

BROOKNER, E.

1971. Improved model for the structure constant variations with altitude. Appl. Opt., vol. 10, no. 8, pp. 1960-1970.

BUFTON, J. L., and GENATT, S. H.

1971. Simultaneous observations of atmospheric turbulence effects on stellar irradiance and phase. Astron. Journ., vol. 76, no. 4, pp. 378-386.

BUFTON, J. L., MINOTT, P. O., FITZMAURICE, M. W., and TITTERTON, P. J.

1972. Measurements of turbulence profiles in the troposphere. Journ. Opt. Soc. Amer., vol. 62, no. 9, pp. 1068-1070.

COULMAN, C. E.

1965. Optical image quality in a turbulent atmosphere. Journ. Opt. Soc. Amer., vol. 55, no. 7, pp. 806-812.

1969. A quantitative treatment of solar seeing. Solar Phys., vol. 7, no. 8, pp. 123-143.

FRIED, D. L.

1967. Optical heterodyne detection of an atmospherically distorted signal wavefront. Proc. IEEE, vol. 55, no. 1, p. 57.

HARDY, K. R., and KATZ, I.

1969. Probing the clear atmosphere with high resolution radars. Proc. IEEE, vol. 57, no. 4, pp. 468-480.

HUFNAGEL, R. E.

1966a. Optical propagation study. Tech. Rep. (RADC-TR-65-511, ASTIA No. AD 476244), Perkin-Elmer Corp., January.

1966b. An improved model turbulent atmosphere. Appendix 3 in Restoration of Atmospherically Degraded Images, vol. 2, Woods Hole Summer Study.

1966c. On the mean short term blur. Appendix 4 in Restoration of Atmospherically Degraded Images, vol. 2, Woods Hole Summer Study.

HUFNAGEL, R. E., and STANLEY, N. R.

1964. Modulation transfer function associated with image transmission through a turbulent media. Journ. Opt. Soc. Amer., vol. 54, no. 1, pp. 52-61.

HULETT, H. R.

1967. Turbulence limitations in photographic resolution of planet surfaces. Journ. Opt. Soc. Amer., vol. 57, no. 11, pp. 1335-1338.

KOLCHINSKII, I. G.

1969. Optical instability of the earth's atmosphere according to stellar observations. Tech. Transl. (ACIC-TC-1395, ASTIA No. AD 682665), Academy of Sciences of the Ukrainian SSR, Main Astronomical Observatory, February.

LAWRENCE, R. S., OCHS, G. R., and CLIFFORD, S. F.

1970. Measurements of atmospheric turbulence relevant to optical propagation. Journ. Opt. Soc. Amer., vol. 60, pp. 826-830.

LINDBERG, P. J.

1954. Measurement of contrast transmission characteristics in optical image formation. Optica Acta, vol. 2, pp. 80-89.

OBUKHOV, A. M.

1941. On the distribution of energy in the spectrum of turbulent flow. Doklady Akad. Nauk SSSR, vol. 32, no. 1, pp. 19-21.

OCHS, G. R.

1967. A resistance thermometer for measurement of rapid air temperature fluctuations. Tech. Rep. (IER 47-ITSA 46), Environmental Science Services Administration, October.

PROTHEROE, W. M.

1954. Preliminary report on stellar scintillation. Sci. Rep. No. 4 (AF 19(604)-41, ASTIA No. AD 56040), Physics and Astronomy Dept., Ohio State Univ., November.

RAMSAY, J. V., and KOBLER, H.

1962. A stellar image monitor. Observatory, vol. 82, pp. 107-111.

REIGER, S. H.

1963. Starlight scintillation and atmospheric turbulence. Astron. Journ., vol. 68, no. 6, pp. 395-406.

ROACH, W. T.

1970. On the influence of synoptic development on the production of high level turbulence. Quart. Journ. Roy. Meteorol. Soc., vol. 96, no. 2, pp. 413-429.

SCORER, R. S.

1969. Billow mechanics. Radio Sci., vol. 4, no. 12, pp. 1299-1308.

TATARSKI, V. I.

1961. Wave Propagation in a Turbulent Medium. Translated by R. A. Silverman, McGraw-Hill, New York, 285 pp.

1971. The Effects of the Turbulent Atmosphere on Wave Propagation. Translated by the Israel Program for Scientific Translations, No. 5319, National Science Foundation, Washington, D.C., Chapter 4, U.S. Dept. of Commerce, Springfield, Virginia.

TITTERTON, P. J., and SPECK, J. P.

1973. Probability of bit error for an optical binary communication link in the presence of atmospheric scintillation: Poisson case. Appl. Opt., vol. 12, no. 2, pp. 425-427.

TOPPING, J.

1960. Errors of Observation and Their Treatment. Reinhold Publ. Corp., New York, Chapter 3.

TSVANG, L. R.

1969. Microstructure of temperature fields in the free atmosphere. Radio Sci., vol. 4, no. 12, pp. 1175-1178.

U.S. AIR FORCE CAMBRIDGE RESEARCH CENTER, GEOPHYSICS RESEARCH DIRECTORATE

1960. Handbook of Geophysics. Macmillan Co., New York.

WYNGAARD, J. C., IZUMI, Y., and COLLINS, S. A.

1971. Behavior of the refractive index structure parameter near the ground. Journ. Opt. Soc. Amer., vol. 61, no. 12, pp. 1646-1650.

YOUNG, A. T.

1969. Photometric error analysis. VIII. The temporal power spectrum of scintillation. Appl. Opt., vol. 8, no. 5, pp. 869-891.

APPENDIX A

COLLECTION AND REDUCTION OF SIM DATA

APPENDIX A

COLLECTION AND REDUCTION OF SIM DATA

Observations during Phase I (June 1969–May 1970) were intended to reveal the variations in seeing conditions at the Mt. Hopkins site and, if possible, to relate these to local meteorological measurements. Emphasis was placed on equipment checkout, observing procedures, quantitative results on seeing, and determination of the appropriate meteorological variables to measure. During Phase II (October 1970–February 1971), increased use was made of meteorological instrumentation, including means to measure the thermal and wind-velocity structure near the telescope and on vertical paths above it. Observations were taken over periods of 30 min to 1 hr each night, and conditions averaged over these periods were used to characterize the site and to seek correlations with the meteorological parameters.

The stellar data from Phase I were reduced by digital computer. This had the advantage of automatic data handling and provided a variety of statistics for each data record. Data-acquisition procedures were tailored closely to the demands of data reduction. Calibration voltages, star identification codes, and background runs were recorded on magnetic tape, along with the data, time, and reference signals. A voice-edge track was used to note experiment parameters. The observer periodically pointed the telescope so that the star was just beyond the field of view. Thus, all the effects of stray light, sky background noise, and electronic offset were routinely recorded. Data from the three SIM signal outputs were recorded simultaneously in each data run, along with a continuous reading of time and reference signals. The three data outputs were voltage signals that represented optical fluctuations in the stellar image being monitored. The signal levels had large dynamic ranges and had periods as short as several milliseconds.

The data were recorded on magnetic tape and subsequently processed through an analog-to-digital (A/D) conversion at a rate of 4 kHz. The data tracks were sampled sequentially, each every millisecond. By the fundamental sampling theorem, data

components up to 500 Hz were available for analysis. A 36-bit time code was also digitized; it was used primarily as a bookkeeping device. The digital tapes were processed on a large-scale digital computer through programs written in the Fortran IV language. Statistics of image-quality signals were calculated and scaled by the appropriate conversion factors. Image motion and modulation index were calibrated by prior laboratory measurements. Image-intensity data required no calibration, since the important statistics were nondimensional.

Computer output reported the following statistics: average, variance, probability density, cumulative probability, autocorrelation, and spectral density. All statistics were reported for each data run of 10-sec to 1-min duration. Nominal data-run length was chosen as 20 sec for the best compromise between the opposing factors of statistical accuracy and data nonstationarity. Errors due to these sources and to instrument effects are discussed by Bufton and Genatt (1971). The computer also calculated stellar zenith and azimuth angles for each run.

Although methods of statistical analysis apply in general to all data from the SIM, each data track must be handled in a particular way. The image-intensity track represents aperture-averaged irradiance fluctuations of starlight. Voltage produced by the monitor is directly proportional to irradiance I, the optical power per unit area at the receiver. Before the connection can be made, the effect of optical and electronic background must be removed from voltage statistics. The primary effect of background is the introduction of an unwanted dc offset into the data. Computer measurement of background data taken at the end of each data run allowed the dc offset to be subtracted before calculations were made. The output signal is a direct measure of the incoming stellar irradiance, and its coefficient of irradiance variation is the parameter defined in equation (7).

The image-motion data can be handled directly in terms of voltage statistics, since optical phase, image motion, and output voltage of the electronic phase comparator enjoy a linear relationship. Image motion in the telescope focal plane is the result of random deviations in the angle-of-arrival of various parts of the incoming wavefront; these tilts are actually optical-phase differences that follow a gaussian distribution. Stellar image motion is measured with respect to a fixed reference light.

The electronic phase difference between the stellar and the reference image detectors is the direct measure of image motion. Laboratory calibrations were used to develop a conversion factor in arc seconds per volt for each spatial frequency. A linear drift attributable to telescope tracking errors was observed in the image-motion data. It was removed by a computer-generated least-squares fit of the observed trend in the data. Note that the conversion of average image position is meaningless in the data reduction, since it is important only to know precisely how the image fluctuates with respect to a fixed point, not where it is. The important parameter is image-motion variance.

We estimate that the quoted values of σ_m^2 are in error by 5 to 15% as a result of imperfect centering of the chopper pattern on the rotating shaft. The resultant wobble causes a cyclic noise component (frequency determined by motor rpm) to be present in all the data. This effect is noticeable in some of the data and will result in a slight increase in the measured σ_m^2 values and in increased data scatter.

Despite the flexibility and sophistication provided by computer analysis, it was found that large quantities of data from which only simple statistics were required were more suited to analog data reduction. The primary problem was the large core storage and the long processing times required to handle large quantities of stellar data. In the second series of observations, analog techniques were used almost exclusively in the basic reduction to variance statistics and the autocorrelation function. This greatly simplified the initial data handling and provided the capability to examine larger data records. Checks between the two methods of data reduction revealed a consistency within 5%.

Analog data reduction of Phase II observations resulted in CIV and σ_m^2 values to characterize image intensity and motion, respectively. CIV was determined by a B & K model 215 rms voltmeter. This meter is capable of measuring true rms and the average value of random analog waveforms over a 70-db dynamic range and a variable averaging time. An averaging time of 10 or 30 sec was used in this experiment. The average background level was subtracted from the data to yield the true average value. The meter was used to obtain the rms values by first passing the raw data through an 0.05-Hz high-pass filter and then into the meter itself. The filter served to remove the

average value for irradiance data and any slow tracking drifts for the image-motion data. The rms meter output was squared to obtain σ_m^2.

An autocorrelation function for both image-motion and irradiance data was obtained by passing each signal in turn through a Hewlett Packard model 3721A signal analyzer/correlator. This instrument provided a 100-point autocorrelation function of variable length of input data. A discrete Fourier transform was then taken of each correlated output to obtain a spectral-density function. Typical data-run lengths used in this analysis ranged from 30 sec to 2 min.

APPENDIX B

DATA

APPENDIX B

DATA

The short-term measured values of σ_m and CIV are tabulated here for both Phases I and II. The corresponding values corrected for zenith are also included.

In Phase I, the σ_m and CIV values were averages for periods of 1 to 3 min. Both quantities were determined from simultaneously collected data and are accordingly tabulated together.

In Phase II, the σ_m and CIV values were averages for periods of 30 sec to 2 min selected arbitrarily from raw data extending over 1 hr or more. No effort was made to choose simultaneous short averaging periods for the two quantities, although in all cases the raw data for each were accumulated over the same interval of 1 to 2 hr. In Phase II, we have identified run numbers: 80–108 correspond to specific radiosonde flights, 16–19 denote runs made without radiosonde flights.

In both phases, the stars were identified by the catalog numbers below. An asterisk denotes the stars used in Phase II.

Number	Star
21	SCHEDIR
74	HAMAL
193*	CAPELLA
194	RIGEL
224	BETELGEUSE
257*	SIRIUS
291	PROCYON
295	POLLUX
380	REGULUS
417	DUBHE
483	URSAE MAJORIS
526	ARCTURUS
699*	VEGA
745	ALTAIR
777*	ARIDED

Phase I Data

DATE TIME	ZA	AZ	STAR	SIG/UNC	SIG/COR	CIV/UNC	CIV/COR
6906262314	19.00	62.00	699	1.44	1.40	.195	.182
6906262345	38.00	120.00	745	1.45	1.28	.235	.177
6906262356	61.00	201.00	616	1.52	1.06	.438	.184
6906272131	21.00	238.00	526	.46	.44	.110	.101
6906272205	32.00	66.00	699	.73	.67	.146	.120
6906272214	42.00	321.00	483	.54	.46	.200	.140
6906272222	54.00	104.00	745	.72	.55	.297	.157
6906272230	27.00	66.00	699	.73	.69	.115	.100
6906272236	51.00	106.00	745	.75	.60	.229	.131
6906272315	18.00	62.00	699	.53	.52	.111	.105
6906272331	45.00	266.00	526	.66	.56	.163	.108
6906272345	13.00	53.00	699	.58	.58	.108	.105
6906272351	36.00	55.00	777	.73	.65	.309	.240
6906272400	62.00	203.00	616	.79	.54	.238	.096
6906280104	9.00	324.00	699	.45	.44	.090	.089
6906280135	78.00	137.00	867	.96	.44	.344	.052
6906280143	73.00	283.00	526	.79	.43	.347	.079
6906280159	16.00	299.00	699	.78	.76	.095	.089
6906302030	38.00	64.00	699	.81	.72	.198	.149
6909232109	29.00	294.00	699	.57	.54	.145	.123
6909232129	ND	ND	745	.17	ND	.149	ND
6909240015	41.00	304.00	777	.61	.53	.162	.116
6909240038	69.00	303.00	699	.69	.41	.302	.088
6909240331	27.00	49.00	193	.49	.46	.099	.086
6909240349	51.00	134.00	224	.61	.48	.114	.065
6909242133	34.00	294.00	699	.91	.83	.129	.103
6909242158	36.00	236.00	745	.80	.72	.285	.221
6909250019	66.00	302.00	699	ND	ND	.271	.092
6909250034	45.00	304.00	777	ND	ND	ND	ND
6909250356	56.00	137.00	224	.82	.66	ND	ND
6909292021	24.00	295.00	699	.76	.73	.134	.120
6909292054	29.00	220.00	745	.62	.58	.223	.190
6909300126	44.00	55.00	193	1.01	.86	.199	.134
6909300358	47.00	143.00	224	1.14	.94	.344	.217
6910022308	36.00	94.00	74	.98	.88	.332	.257
6910032202	47.00	296.00	699	1.10	.91	.354	.224
6910062009	27.00	294.00	699	1.16	1.09	.133	.116
6910062039	30.00	226.00	745	1.11	1.04	.173	.146
6910070043	13.00	127.00	74	.89	.88	.241	.234
6910070104	43.00	55.00	193	.87	.74	.160	.110
6910070326	20.00	39.00	193	1.00	.97	.135	.125
6910070346	45.00	147.00	224	.94	.79	.168	.111
6910082051	37.00	294.00	699	.59	.53	.214	.163
6910082107	36.00	238.00	745	.73	.66	.199	.154
6910090015	51.00	305.00	777	.66	.53	.348	.200
6910090045	45.00	55.00	193	.88	.74	.329	.217
6910090311	21.00	41.00	193	.57	.55	.156	.144
6910090326	46.00	144.00	224	.89	.74	.254	.164
6910092026	33.00	294.00	699	.62	.57	.194	.157
6910092040	32.00	230.00	745	.88	.81	.260	.213

DATE TIME	ZA	AZ	STAR	SIG/UNC	SIG/COR	CIV/UNC	CIV/COR
6910092345	46.00	304.00	777	.89	.75	.320	.207
6910100018	49.00	54.00	193	.92	.74	.290	.175
6910100315	20.00	39.00	193	.91	.88	.146	.135
6910132129	48.00	296.00	699	.85	.69	.162	.100
6910132157	50.00	253.00	745	.67	.54	.214	.126
6910140115	9.00	201.00	74	.73	.72	.132	.130
6910140359	41.00	161.00	224	.93	.81	.158	.113
6910140418	40.00	164.00	194	.77	.68	.165	.120
6910142114	46.00	295.00	699	.61	.51	.337	.218
6910142134	27.00	309.00	777	.65	.61	.265	.231
6910150012	55.00	306.00	777	.86	.65	.433	.222
6910150047	62.00	122.00	194	.97	.67	.419	.169
6910150313	44.00	147.00	224	.90	.76	.208	.140
6910150331	57.00	144.00	257	.93	.68	.366	.177
6910152126	49.00	296.00	699	.81	.65	.388	.234
6910152144	29.00	307.00	777	.77	.72	.356	.303
6910160034	59.00	307.00	777	.69	.50	.381	.172
6910160052	37.00	105.00	168	.70	.63	.227	.173
6910160108	57.00	126.00	194	.98	.73	.331	.160
6910232020	42.00	295.00	699	.68	.58	.251	.176
6910232041	43.00	246.00	745	.49	.42	.206	.142
6910232105	51.00	297.00	699	.63	.50	.264	.151
6910232132	56.00	298.00	699	1.02	.77	ND	ND
6910240020	39.00	55.00	193	.54	.47	.191	.141
6910240046	62.00	120.00	224	.74	.51	.262	.106
6910240054	55.00	130.00	194	.74	.56	.279	.143
6910240130	70.00	126.00	257	.77	.45	.411	.113
6910242041	25.00	311.00	777	.87	.83	.112	.100
6910250003	63.00	121.00	194	.69	.47	.341	.132
6910250024	36.00	107.00	168	.57	.52	.141	.109
6910250043	31.00	330.00	21	.62	.57	.175	.145
6910250321	53.00	151.00	257	.66	.51	.237	.129
6910250341	15.00	351.00	193	.59	.58	.125	.120
6910282102	54.00	298.00	699	1.23	.94	.281	.149
6910282119	26.00	23.00	21	.95	.89	.180	.155
6910282243	49.00	305.00	777	.82	.66	.210	.127
6910282301	25.00	352.00	21	.73	.69	.180	.160
6910290002	29.00	335.00	21	.68	.63	.206	.175
6910290016	9.00	201.00	74	.79	.79	.147	.145
6910290032	55.00	130.00	194	.69	.52	.209	.107
6910290133	39.00	322.00	21	.53	.47	.182	.134
6910290148	22.00	42.00	193	.66	.63	.129	.118
6910290204	47.00	142.00	224	.66	.55	.163	.103
6910290251	55.00	148.00	257	.85	.64	.281	.144
6910290308	ND	ND	193	.27	ND	ND	ND
6910292205	43.00	304.00	777	.91	.77	.189	.130
6910292220	25.00	4.00	21	.82	.79	.191	.170
6910300010	30.00	333.00	21	.84	.78	.170	.143
6910300025	10.00	217.00	74	.68	.67	ND	ND
6910300030	11.00	222.00	74	ND	ND	.137	.134

DATE TIME	ZA	AZ	STAR	SIG/UNC	SIG/COR	CIV/UNC	CIV/COR
6910300040	ND	ND	168	.47	ND	.152	ND
6910300247	15.00	14.00	193	.60	.59	.115	.110
6910300303	53.00	152.00	257	.87	.68	.234	.127
6911022122	36.00	304.00	777	.68	.60	.147	.110
6911022137	26.00	13.00	21	.69	.65	.136	.120
6911030035	35.00	326.00	21	.70	.63	.153	.120
6911030050	27.00	50.00	193	.72	.68	.113	.098
6911030105	ND	ND	194	1.07	ND	.158	ND
6911030245	14.00	4.00	193	.62	.61	.091	.088
6911030302	52.00	156.00	257	.60	.47	.170	.095
6911032112	37.00	305.00	777	.52	.46	.155	.118
6911032125	ND	ND	777	.38	ND	.155	ND
6911040010	33.00	53.00	193	.55	.50	.155	.125
6911040024	26.00	117.00	168	.94	.88	.130	.112
6911040038	56.00	127.00	224	.64	.48	.186	.093
6911040250	53.00	154.00	257	.69	.53	.204	.111
6911040306	15.00	347.00	193	.52	.51	.121	.116
6911042203	25.00	2.00	21	.47	.45	.135	.120
6911042218	52.00	54.00	193	.66	.52	.206	.115
6911050043	27.00	50.00	193	.66	.62	.159	.138
6911050056	22.00	131.00	168	.65	.62	.137	.125
6911150149	41.00	156.00	224	.52	.45	.230	.164
6911150131	49.00	113.00	291	.64	.52	.314	.189
6912112303	62.00	135.00	257	.83	.57	.340	.137
6912112329	17.00	30.00	193	.53	.52	.124	.118
6912120051	50.00	162.00	257	.46	.37	.273	.161
6912120117	39.00	188.00	224	.57	.50	.160	.118
6912120142	22.00	317.00	193	.52	.50	.114	.104
6912120308	52.00	205.00	257	.60	.47	.186	.104
6912120323	10.00	275.00	287	.54	.53	.109	.107
7002172223	51.00	200.00	257	.56	.44	.235	.135
7002172237	27.00	194.00	291	.51	.48	.144	.125
7002180043	44.00	241.00	291	.48	.41	.206	.139
7002180106	20.00	198.00	380	.30	.29	.141	.131
7002180132	30.00	1.00	417	.47	.44	.147	.124
7002180315	34.00	339.00	417	.52	.47	.164	.131
7002180355	17.00	133.00	526	.37	.37	.102	.097
7002182034	42.00	199.00	194	ND	ND	.184	.129
7002182059	20.00	320.00	193	ND	ND	.119	.110
7002182345	46.00	306.00	193	.48	.39	.301	.186
7002190000	37.00	231.00	291	.69	.62	.277	.211
7002190014	20.00	164.00	380	.60	.58	.344	.319
7002190227	32.00	239.00	380	.90	.83	.148	.121
7002190242	34.00	345.00	417	.41	.38	.185	.152
7002240028	20.00	188.00	380	.39	.38	.220	.204
7002240051	30.00	5.00	417	.58	.54	.326	.274
7002240305	35.00	337.00	417	.74	.67	.340	.268
7002240321	19.00	127.00	526	.62	.61	.283	.265
7003032129	37.00	114.00	380	1.03	.92	.217	.166
7003032148	27.00	197.00	291	.77	.73	.150	.131

DATE TIME	ZA	AZ	STAR	SIG/UNC	SIG/COR	CIV/UNC	CIV/COR
7003040122	30.00	234.00	380	.57	.53	.138	.116
7003040142	34.00	346.00	417	.63	.58	.143	.117
7003040155	29.00	108.00	526	.65	.61	.121	.103
7003040315	15.00	143.00	526	.64	.63	.085	.082
7003040332	41.00	331.00	417	.57	.50	.133	.095
7003042115	26.00	181.00	291	.79	.75	.109	.096
7003042125	37.00	114.00	380	1.17	1.04	.201	.153
7003092052	50.00	197.00	257	.91	.73	.282	.166
7003092112	27.00	190.00	291	ND	ND	.173	.151
7003100258	14.00	148.00	526	.73	.72	.224	.216
7003202113	56.00	214.00	257	.79	.59	.307	.153
7003222253	36.00	275.00	295	ND	ND	.231	.179
7003230047	60.00	286.00	295	.71	.50	.314	.137
7003230106	64.00	288.00	526	.41	.27	.155	.058
7003230203	15.00	146.00	417	1.04	1.02	.225	.216
7003230312	47.00	327.00	417	1.15	.95	.239	.151
7003230336	18.00	230.00	526	.33	.32	.188	.177
7003242150	21.00	157.00	380	1.13	1.09	.256	.236
7003242216	30.00	272.00	295	1.16	1.08	.342	.288
7003250033	56.00	286.00	295	1.06	.77	.392	.183
7003250101	35.00	339.00	417	.84	.76	.264	.208
7003250141	17.00	135.00	526	.98	.96	.238	.226
7003252351	51.00	282.00	295	.71	.56	.238	.137
7003260042	33.00	341.00	417	.93	.85	.177	.143
7003260307	48.00	327.00	417	.75	.62	.259	.160
7003260329	19.00	233.00	526	.66	.65	.137	.128
7003302150	42.00	238.00	291	1.08	.93	.167	.117
7004012059	48.00	306.00	193	1.28	1.04	.170	.105
7004012124	25.00	269.00	295	1.13	1.08	.424	.377
7004020035	35.00	338.00	417	.77	.70	.148	.116
7004020055	47.00	256.00	380	.99	.82	.199	.126
7004020149	13.00	169.00	526	ND	ND	.104	.101
7004020202	12.00	183.00	526	.49	.48	.108	.105
7004020233	15.00	215.00	526	.62	.61	.112	.107
7004022115	38.00	232.00	291	.91	.81	.116	.087
7004030034	66.00	289.00	295	.67	.43	.447	.152
7004030057	37.00	334.00	417	.63	.57	.134	.102
7004030115	15.00	142.00	526	.80	.79	.104	.100
7004030324	24.00	244.00	526	.53	.51	.100	.090
7004030343	32.00	66.00	699	.73	.68	.149	.122
7004062250	48.00	281.00	295	1.26	1.03	.424	.262
7004062307	31.00	351.00	417	.75	.70	.283	.235
7004070121	41.00	330.00	417	.69	.60	.244	.174
7004070136	12.00	177.00	526	.49	.48	.208	.203
7004070154	50.00	64.00	699	.69	.55	.332	.195
7004070330	31.00	66.00	699	1.05	.97	.193	.160
7004070350	32.00	255.00	526	.60	.55	.265	.217

Phase II Data

DATE	TIME	ZA	AZ	STAR	CIV/UNC	CIV/CCR	RUN	
7011	4 626	40.67	54.68	193	.15	.11	82	Period 3
7011	4 627	40.45	54.67	193	.14	.10	82	
7011	4 628	40.19	54.64	193	.13	.09	82	
7011	4 631	39.71	54.60	193	.13	.09	82	
7011	4 633	39.32	54.56	193	.16	.12	82	
7011	4 636	38.88	54.51	193	.13	.10	82	
7011	4 638	38.58	54.47	193	.14	.10	82	
7011	4 639	38.32	54.43	193	.14	.10	82	
7011	4 641	38.02	54.39	193	.14	.11	82	
7011	4 646	37.19	54.24	193	.13	.10	82	
7011	4 648	36.72	54.15	193	.13	.10	82	
7011	4 650	36.42	54.08	193	.12	.09	82	
7011	4 653	35.98	53.99	193	.12	.09	82	
7011	4 927	54.74	148.13	257	.15	.08	83	Period 4
7011	4 929	54.57	148.52	257	.19	.10	83	
7011	4 930	54.46	148.78	257	.18	.09	83	
7011	4 931	54.30	149.18	257	.18	.09	83	
7011	4 932	54.24	149.31	257	.22	.12	83	
7011	5 422	39.65	304.15	777	.20	.15	84	Period 5
7011	5 423	39.83	304.14	777	.20	.15	84	
7011	5 424	40.14	304.12	777	.20	.14	84	
7011	5 426	40.36	304.11	777	.21	.15	84	
7011	5 427	40.67	304.10	777	.21	.15	84	
7011	5 429	40.98	304.08	777	.20	.14	84	
7011	5 430	41.15	304.08	777	.21	.15	84	
7011	5 434	41.80	304.07	777	.24	.17	84	
7011	5 435	41.99	304.06	777	.22	.15	84	
7011	5 436	42.21	304.06	777	.23	.16	84	
7011	5 438	42.54	304.06	777	.23	.16	84	
7011	5 439	42.65	304.07	777	.22	.15	84	
7011	5 442	43.21	304.08	777	.23	.16	84	
7011	5 443	43.45	304.08	777	.25	.17	84	
7011	5 445	43.71	304.09	777	.23	.16	84	
7011	5 445	43.86	304.10	777	.23	.16	84	
7011	5 447	44.13	304.11	777	.23	.15	84	
7011	5 448	44.24	304.11	777	.24	.16	84	
7011	5 932	53.77	150.48	257	.29	.15	85	Period 6
7011	5 937	53.25	151.83	257	.27	.15	85	
7011	5 943	52.71	153.34	257	.27	.15	85	
7011	5 946	52.43	154.18	257	.28	.15	85	
7011	5 952	51.89	155.87	257	.26	.15	85	
7011	5 956	51.55	157.01	257	.24	.14	85	
7011	510 0	51.22	158.17	257	.23	.13	85	
7011	510 3	50.99	159.05	257	.23	.13	85	
7011	510 4	50.89	159.44	257	.24	.14	85	
7011	510 9	50.52	160.97	257	.26	.15	85	
7011	51011	50.41	161.41	257	.25	.15	85	
701110	643	33.65	53.30	193	.12	.10	86	Period 7
701110	645	33.31	53.18	193	.11	.09	86	
701110	647	32.97	53.05	193	.14	.11	86	

DATE TIME	ZA	AZ	STAR	CIV/UNC	CIV/CCR	RUN	
701110 655	31.61	52.47	193	.11	.09	86	
701110 7 1	30.47	51.89	193	.09	.08	86	
701110 710	29.09	51.06	193	.10	.09	86	
701112 251	50.74	296.46	699	.25	.14	87	Period 8
701112 253	51.12	296.57	699	.24	.14	87	
701112 254	51.41	296.66	699	.23	.13	87	
701112 256	51.84	296.78	699	.23	.13	87	
701112 258	52.08	296.85	699	.26	.14	87	
701112 3 2	52.90	297.10	699	.25	.14	87	
701112 3 4	53.22	297.20	699	.26	.14	87	
701112 3 5	53.41	297.26	699	.25	.13	87	
701112 3 7	53.79	297.38	699	.27	.14	87	
701112 3 9	54.16	297.50	699	.30	.16	87	
701112 312	54.73	297.68	699	.37	.19	87	
701112 315	55.30	297.86	699	.34	.17	87	
701112 317	55.67	297.99	699	.35	.18	87	
701112 319	56.11	298.14	699	.33	.16	87	
701112 322	56.61	298.31	699	.33	.16	87	
701112 858	54.88	147.81	257	.32	.16	88	Period 9
701112 859	54.79	148.01	257	.30	.15	88	
701112 9 0	54.65	148.33	257	.31	.16	88	
701112 9 2	54.51	148.66	257	.29	.15	88	
701112 9 3	54.40	148.92	257	.31	.16	88	
701112 9 4	54.21	149.38	257	.30	.16	88	
701117 656	26.79	49.30	193	.13	.11	89	Period 10
701117 7 2	25.91	48.46	193	.11	.10	89	
701117 7 3	25.75	48.30	193	.10	.09	89	
701117 7 4	25.51	48.05	193	.12	.11	89	
701117 7 7	25.12	47.63	193	.11	.10	89	
701117 7 8	24.96	47.45	193	.11	.10	89	
701117 7 9	24.72	47.18	193	.11	.10	89	
701117 712	24.26	46.61	193	.11	.10	89	
701117 713	24.06	46.37	193	.09	.08	89	
701117 714	23.95	46.22	193	.11	.10	89	
701117 716	23.67	45.84	193	.12	.11	89	
701117 718	23.41	45.49	193	.13	.12	89	
701117 718	23.33	45.39	193	.12	.11	89	
701117 720	23.11	45.06	193	.11	.10	89	
701117 722	22.73	44.49	193	.11	.10	89	
701117 724	22.51	44.14	193	.10	.09	89	
701117 726	22.21	43.66	193	.11	.10	89	
701117 727	22.07	43.41	193	.09	.08	89	
701118 252	32.92	305.47	777	.14	.11	90	Period 11
701118 253	33.09	305.41	777	.14	.11	90	
701118 255	33.35	305.33	777	.14	.11	90	
701118 256	33.57	305.26	777	.14	.11	90	
701118 257	33.79	305.19	777	.14	.11	90	
701118 259	34.05	305.12	777	.14	.11	90	
701118 3 0	34.22	305.07	777	.14	.11	90	
701118 3 1	34.48	305.00	777	.14	.11	90	

DATE TIME	ZA	AZ	STAR	CIV/UNC	CIV/CCR	RUN	
701118 3 2	34.66	304.95	777	.14	.11	90	
701118 3 4	34.92	304.88	777	.14	.11	90	
701118 3 5	35.10	304.84	777	.14	.11	90	
701118 3 6	35.33	304.79	777	.15	.12	90	
701118 3 7	35.53	304.74	777	.15	.12	90	
701118 3 9	35.80	304.68	777	.13	.10	90	
701118 312	36.41	304.56	777	.14	.11	90	
701118 314	36.76	304.50	777	.14	.11	90	
701118 315	36.94	304.47	777	.15	.11	90	
701118 317	37.20	304.43	777	.15	.11	90	
701118 916	15.15	342.46	193	.11	.11	91	Period 12
701118 917	15.25	341.53	193	.11	.11	91	
701118 919	15.35	340.62	193	.12	.11	91	
701118 922	15.57	338.85	193	.10	.10	91	
701118 924	15.73	337.70	193	.10	.10	91	
701118 928	16.07	335.48	193	.12	.11	91	
701118 930	16.25	334.40	193	.11	.10	91	
701118 932	16.44	333.36	193	.12	.11	91	
701118 933	16.53	332.85	193	.12	.11	91	
701118 935	16.73	331.85	193	.11	.10	91	
701118 938	17.04	330.40	193	.12	.11	91	
701118 940	17.26	329.46	193	.12	.11	91	
701118 942	17.56	328.22	193	.11	.10	91	
701118 944	17.70	327.68	193	.11	.10	91	
701118 947	18.05	326.41	193	.11	.10	91	
701118 949	18.35	325.39	193	.12	.11	91	
701118 952	18.72	324.23	193	.12	.11	91	
701118 953	18.84	323.85	193	.12	.11	91	
701118 954	19.00	323.39	193	.12	.11	91	
701118 957	19.35	322.41	193	.12	.11	91	
701118 959	19.58	321.80	193	.14	.13	91	
70111810 0	19.75	321.38	193	.14	.13	91	
70111810 2	19.95	320.89	193	.13	.12	91	
70111810 4	20.22	320.25	193	.12	.11	91	
701121 255	35.41	304.77	777	.15	.12	92	Period 13
701121 259	36.11	304.62	777	.13	.10	92	
701121 3 2	36.64	304.52	777	.15	.12	92	
701121 3 4	37.08	304.45	777	.16	.12	92	
701121 3 9	37.87	304.33	777	.17	.13	92	
701121 311	38.31	304.28	777	.17	.13	92	
701121 314	38.75	304.23	777	.18	.13	92	
701121 317	39.34	304.18	777	.16	.12	92	
701121 319	39.64	304.16	777	.17	.12	92	
701121 322	40.16	304.12	777	.16	.12	92	
701121 323	40.43	304.11	777	.16	.12	92	
701124 236	34.19	305.07	777	.20	.16	93	Period 14
701124 238	34.54	304.98	777	.21	.17	93	
701124 242	35.20	304.82	777	.20	.16	93	
701124 243	35.46	304.76	777	.21	.16	93	
701124 247	36.12	304.62	777	.20	.15	93	

DATE TIME	ZA	AZ	STAR	CIV/UNC	CIV/CCR	RUN	
701124 249	36.43	304.56	777	.20	.15	93	
701124 252	37.00	304.46	777	.24	.18	93	
701124 254	37.31	304.41	777	.21	.16	93	
701124 258	38.01	304.32	777	.20	.15	93	
701124 259	38.28	304.28	777	.21	.16	93	
701124 3 1	38.63	304.25	777	.18	.13	93	
701124 3 3	38.89	304.22	777	.18	.13	93	
701124 3 7	39.60	304.16	777	.20	.15	93	
701124 3 8	39.86	304.14	777	.21	.15	93	
701124 311	40.39	304.11	777	.17	.12	93	
701124 314	40.97	304.08	777	.21	.15	93	
701124 317	41.42	304.07	777	.23	.16	93	
701124 319	41.81	304.07	777	.23	.16	93	
701124 320	41.94	304.06	777	.23	.16	93	
70112410 0	23.08	314.98	193	.15	.14	94	Period 15
70112410 2	23.42	314.49	193	.15	.14	94	
70112410 4	23.65	314.17	193	.17	.15	94	
70112410 6	24.00	313.72	193	.14	.13	94	
70112410 7	24.19	313.47	193	.14	.13	94	
70112410 9	24.50	313.09	193	.14	.13	94	
7011241012	24.97	312.54	193	.14	.12	94	
7011241014	25.32	312.15	193	.24	.21	94	
7011241016	25.52	311.93	193	.33	.29	94	
7011241017	25.73	311.71	193	.24	.21	94	
7011241019	26.12	311.33	193	.25	.22	94	
7011241022	26.52	310.95	193	.21	.18	94	
7011241024	26.80	310.69	193	.22	.19	94	
7011241026	27.16	310.39	193	.19	.17	94	
7011241028	27.58	310.04	193	.21	.18	94	
7011241032	28.11	309.63	193	.19	.16	94	
7011241034	28.44	309.39	193	.17	.15	94	
7011241036	28.77	309.16	193	.15	.13	94	
7011241038	29.10	308.93	193	.17	.14	94	
7011241039	29.39	308.74	193	.14	.12	94	
7012 1 533	31.51	52.42	193	.16	.13	95	Period 16
7012 1 534	31.34	52.34	193	.16	.13	95	
7012 1 536	31.00	52.18	193	.17	.14	95	
7012 1 537	30.71	52.02	193	.15	.13	95	
7012 1 539	30.37	51.84	193	.17	.14	95	
7012 1 541	30.16	51.72	193	.16	.13	95	
7012 1 542	29.95	51.60	193	.16	.13	95	
7012 1 546	29.33	51.22	193	.16	.14	95	
7012 1 548	29.00	51.00	193	.15	.13	95	
7012 1 550	28.67	50.77	193	.14	.12	95	
7012 1 550	28.58	50.72	193	.14	.12	95	
7012 1 552	28.34	50.54	193	.14	.12	95	
7012 1 553	28.17	50.42	193	.14	.12	95	
7012 1 556	27.68	50.04	193	.13	.11	95	
7012 1 556	27.60	49.98	193	.13	.11	95	
7012 2 151	66.53	48.31	779	.16	.05	96	Period 17

DATE	TIME	ZA	AZ	STAR	CIV/UNC	CIV/CCR	RUN	
7012	2 153	68.29	48.42	779	.18	.05	96	
7012	2 154	68.05	48.53	779	.18	.06	96	
7012	2 156	67.73	48.68	779	.18	.06	96	
7012	2 158	67.41	48.83	779	.21	.07	96	
7012	2 2 0	67.09	48.97	779	.20	.06	96	
7012	2 2 5	66.28	49.33	779	.21	.07	96	
7012	2 959	27.86	309.82	193	.16	.14	97	Period 18
7012	210 3	28.51	309.33	193	.15	.13	97	
7012	210 4	28.68	309.22	193	.14	.12	97	
7012	8 715	14.64	11.38	193	.13	.12	98	Period 19
7012	8 717	14.56	10.03	193	.10	.10	98	
7012	8 718	14.52	9.35	193	.09	.09	98	
7012	8 720	14.44	7.64	193	.09	.09	98	
7012	8 722	14.40	6.60	193	.11	.11	98	
7012	8 726	14.32	3.46	193	.10	.10	98	
7012	8 727	14.31	2.76	193	.11	.11	98	
7012	8 729	14.30	1.70	193	.11	.11	98	
7012	8 731	14.29	.29	193	.11	.11	98	
7012	8 733	14.29	358.88	193	.10	.10	98	
7012	8 736	14.32	356.41	193	.12	.12	98	
7012	8 738	14.35	355.36	193	.12	.12	98	
7012	8 738	14.35	355.01	193	.12	.12	98	
7012	8 740	14.39	353.96	193	.09	.09	98	
7012	8 741	14.42	352.92	193	.10	.10	98	
7012	8 742	14.44	352.58	193	.09	.09	98	
701211	627	17.49	31.51	193	.13	.12	99	Period 20
701211	629	17.33	30.84	193	.13	.12	99	
701211	630	17.14	30.03	193	.11	.10	99	
701211	633	16.90	28.96	193	.12	.11	99	
701211	634	16.72	28.10	193	.13	.12	99	
701211	636	16.57	27.36	193	.13	.12	99	
7012111033		54.53	211.37	257	.20	.10	100	Period 21
7012111034		54.67	211.70	257	.18	.09	100	
7012111036		54.81	212.02	257	.19	.10	100	
7012111037		55.01	212.47	257	.21	.11	100	
7012111040		55.26	213.05	257	.18	.09	100	
7012111042		55.59	213.75	257	.19	.10	100	
7012111046		55.98	214.57	257	.22	.11	100	
7012111048		56.22	215.07	257	.18	.09	100	
7012111050		56.47	215.56	257	.21	.10	100	
7012111051		56.59	215.81	257	.19	.09	100	
701217	253	48.26	54.44	193	.22	.14	103	Period 22
701217	254	48.01	54.46	193	.18	.11	103	
701217	256	47.73	54.50	193	.14	.09	103	
701217	257	47.49	54.52	193	.14	.09	103	
701217	3 0	47.10	54.56	193	.15	.09	103	
701217	3 1	46.92	54.58	193	.16	.10	103	
701217	3 3	46.58	54.61	193	.16	.10	103	
701217	3 5	46.14	54.64	193	.16	.10	103	
701217	3 6	45.97	54.66	193	.16	.10	103	

DATE TIME	ZA	AZ	STAR	CIV/UNC	CIV/CCR	RUN	
701217 3 7	45.79	54.67	193	.15	.10	103	
701217 3 9	45.47	54.69	193	.16	.10	103	
701217 310	45.27	54.70	193	.12	.08	103	
701217 312	44.88	54.72	193	.15	.10	103	
701217 315	44.36	54.74	193	.16	.11	103	
701217 317	44.05	54.75	193	.15	.10	103	
701231 5 6	17.76	32.55	193	.13	.12	104	Period 23
701231 5 8	17.53	31.67	193	.15	.14	104	
701231 510	17.37	31.00	193	.15	.14	104	
701231 512	17.15	30.08	193	.11	.10	104	
701231 514	16.94	29.14	193	.12	.11	104	
701231 515	16.84	28.65	193	.12	.11	104	
701231 518	16.50	26.99	193	.11	.10	104	
701231 519	16.39	26.39	193	.11	.10	104	
701231 522	16.12	24.81	193	.13	.12	104	
701231 525	15.90	23.44	193	.11	.10	104	
701231 528	15.65	21.74	193	.10	.10	104	
701231 529	15.52	20.72	193	.11	.11	104	
701231 532	15.35	19.39	193	.11	.11	104	
701231 534	15.21	18.17	193	.13	.12	104	
701231 536	15.09	16.93	193	.11	.11	104	
71 126 527	19.46	322.13	193	.13	.12	105	Period 24
71 126 528	19.65	321.62	193	.15	.14	105	
71 126 530	19.92	320.96	193	.17	.16	105	
71 126 533	20.26	320.16	193	.15	.14	105	
71 126 535	20.54	319.55	193	.15	.14	105	
71 126 539	21.10	318.38	193	.20	.18	105	
71 126 540	21.27	318.03	193	.17	.16	105	
71 126 542	21.52	317.56	193	.17	.16	105	
71 126 544	21.81	317.03	193	.18	.16	105	
71 126 548	22.48	315.91	193	.16	.15	105	
71 126 550	22.70	315.56	193	.18	.16	105	
71 126 553	23.15	314.88	193	.16	.14	105	
71 126 555	23.45	314.45	193	.16	.14	105	
71 126 558	23.99	313.73	193	.15	.13	105	
71 126 6 2	24.53	313.05	193	.16	.14	105	
71 126 6 4	24.92	312.59	193	.14	.12	105	
71 126 6 3	24.77	312.77	193	.15	.13	105	
71 126 6 9	25.63	311.82	193	.14	.12	105	
71 126 612	26.11	311.34	193	.14	.12	105	
71 126 913	57.11	307.38	193	.27	.13	106	Period 25
71 126 916	57.71	307.55	193	.27	.13	106	
71 126 919	58.13	307.67	193	.26	.12	106	
71 126 920	58.38	307.75	193	.25	.12	106	
71 126 924	59.06	307.96	193	.27	.12	106	
71 126 926	59.39	308.06	193	.30	.13	106	
71 126 929	59.81	308.20	193	.27	.12	106	
71 126 931	60.23	308.34	193	.27	.12	106	
71 126 934	60.65	308.48	193	.27	.11	106	
71 126 936	60.98	308.59	193	.28	.12	106	

DATE TIME	ZA	AZ	STAR	CIV/UNC	CIV/CCR	RUN	
71 126 939	61.48	308.77	193	.29	.12	106	
71 126 941	61.90	308.92	193	.32	.13	106	
71 126 944	62.31	309.07	193	.34	.14	106	
71 126 946	62.73	309.22	193	.32	.13	106	
71 126 949	63.14	309.38	193	.35	.13	106	
71 126 951	63.47	309.51	193	.36	.14	106	
71 126 954	63.96	309.70	193	.31	.12	106	
71 126 955	64.21	309.80	193	.31	.11	106	
71 126 958	64.62	309.96	193	.33	.12	106	
71 126 959	64.78	310.03	193	.32	.11	106	
71 127 251	21.61	42.59	193	.09	.08	107	Period 26
71 127 253	21.32	42.05	193	.09	.08	107	
71 127 254	21.18	41.78	193	.09	.08	107	
71 127 256	20.82	41.07	193	.09	.08	107	
71 127 259	20.41	40.17	193	.08	.07	107	
71 127 3 3	19.86	38.90	193	.08	.07	107	
71 127 3 6	19.53	38.06	193	.08	.07	107	
71 127 3 9	19.14	37.01	193	.08	.07	107	
71 127 312	18.76	35.91	193	.08	.07	107	
71 127 314	18.51	35.14	193	.07	.07	107	
71 127 317	18.15	33.95	193	.07	.07	107	
71 127 319	17.86	32.91	193	.07	.07	107	
71 127 322	17.57	31.82	193	.08	.08	107	
71 127 324	17.29	30.70	193	.07	.07	107	
71 127 326	17.13	30.01	193	.07	.07	107	
71 127 328	16.92	29.06	193	.07	.07	107	
71 127 329	16.82	28.57	193	.07	.07	107	
71 127 838	63.94	227.38	257	.22	.08	108	Period 27
71 127 840	64.34	227.89	257	.25	.09	108	
71 127 841	64.49	228.09	257	.23	.08	108	
71 127 843	64.73	228.38	257	.25	.09	108	
71 127 845	65.05	228.78	257	.24	.09	108	
71 127 850	65.86	229.76	257	.27	.09	108	
71 127 851	66.11	230.04	257	.27	.09	108	
71 127 853	66.35	230.33	257	.29	.10	108	
71 127 854	66.60	230.62	257	.29	.10	108	
71 127 856	66.93	231.00	257	.24	.08	108	
71 127 859	67.37	231.50	257	.28	.09	108	
71 127 9 1	67.68	231.84	257	.28	.09	108	
71 127 9 3	68.02	232.21	257	.29	.09	108	
71 127 9 6	68.52	232.76	257	.31	.09	108	
71 127 9 9	69.04	233.31	257	.32	.09	108	
71 127 911	69.38	233.67	257	.28	.08	108	
71 127 911	69.46	233.75	257	.27	.08	108	
71 127 913	69.72	234.02	257	.30	.08	108	

DATE	TIME	ZA	AZ	STAR	SIG/UNC	SIG/CCR	RUN	
701029	4 6	32.11	305.77	777	1.22	1.12	80	Period 1
701029	4 7	32.33	305.68	777	1.26	1.16	80	
701029	4 8	32.43	305.65	777	1.34	1.23	80	
701029	4 9	32.59	305.59	777	1.26	1.16	80	
701029	4 9	32.68	305.56	777	1.16	1.06	80	
701029	410	32.78	305.52	777	1.36	1.25	80	
701029	411	33.04	305.43	777	1.24	1.14	80	
701029	413	33.30	305.34	777	1.24	1.13	80	
701029	414	33.47	305.29	777	1.26	1.15	80	
701029	414	33.56	305.26	777	1.14	1.04	80	
701029	415	33.73	305.21	777	1.22	1.11	80	
701029	417	34.07	305.11	777	1.30	1.18	80	
701029	418	34.15	305.09	777	1.42	1.29	80	
701029	419	34.30	305.05	777	1.10	1.00	80	
701029	420	34.49	304.99	777	1.14	1.03	80	
701029	420	34.55	304.98	777	1.16	1.05	80	
701029	424	35.16	304.83	777	1.42	1.28	80	
701029	425	35.42	304.77	777	1.16	1.05	80	
701029	426	35.66	304.71	777	1.10	.99	80	
701029	427	35.77	304.69	777	.99	.89	80	
701029	427	35.85	304.67	777	.95	.86	80	
701029	428	35.98	304.65	777	1.18	1.06	80	
701029	430	36.24	304.60	777	1.14	1.02	80	
701029	432	36.56	304.54	777	1.12	1.00	80	
701029	433	36.83	304.49	777	.95	.85	80	
701029	434	36.92	304.48	777	.99	.89	80	
701029	436	37.40	304.40	777	1.34	1.19	80	
701029	439	37.93	304.33	777	1.14	1.01	80	
701029	440	38.02	304.32	777	1.26	1.12	80	
701029	442	38.32	304.28	777	1.22	1.08	80	
701029	443	38.59	304.25	777	1.10	.97	80	
701029	444	38.79	304.23	777	1.10	.97	80	
701029	445	38.97	304.21	777	1.03	.91	80	
701029	446	39.16	304.19	777	1.10	.97	80	
701029	447	39.25	304.19	777	.85	.75	80	
701029	448	39.47	304.17	777	.99	.87	80	
701029	449	39.65	304.15	777	1.03	.90	80	
701029	451	39.91	304.14	777	1.42	1.24	80	
701029	452	40.15	304.12	777	1.26	1.10	80	
701029	453	40.31	304.11	777	1.03	.90	80	
701029	454	40.44	304.11	777	1.14	.99	80	
701029	454	40.53	304.10	777	1.14	.99	80	
701029	456	40.80	304.09	777	1.10	.96	80	
701029	456	40.91	304.09	777	1.10	.96	80	
701029	459	41.47	304.07	777	1.42	1.23	80	
701029	5 0	41.55	304.07	777	1.12	.97	80	
701029	5 1	41.72	304.07	777	1.20	1.04	80	
701029	722	34.92	53.71	193	.90	.81	81	Period 2
701029	723	34.88	53.70	193	.92	.83	81	
701029	723	34.79	53.67	193	.92	.83	81	

DATE	TIME	ZA	AZ	STAR	SIG/UNC	SIG/CCR	RUN
701029	723	34.72	53.65	193	.98	.89	81
701029	725	34.45	53.57	193	1.00	.91	81
701029	726	34.34	53.53	193	1.00	.91	81
701029	727	34.15	53.47	193	.98	.89	81
701029	727	34.05	53.44	193	.77	.70	81
701029	729	33.81	53.36	193	.86	.78	81
701029	730	33.65	53.30	193	.90	.82	81
701029	730	33.54	53.26	193	.79	.72	81
701029	732	33.22	53.15	193	.92	.84	81
701029	732	33.18	53.13	193	.94	.86	81
701029	733	33.04	53.08	193	.88	.81	81
701029	735	32.83	53.00	193	.75	.69	81
701029	735	32.78	52.98	193	.81	.74	81
701029	735	32.70	52.95	193	.81	.74	81
701029	737	32.34	52.80	193	.83	.76	81
701029	738	32.23	52.75	193	.83	.76	81
701029	738	32.19	52.73	193	.86	.79	81
701029	739	32.12	52.70	193	.96	.88	81
701029	739	32.09	52.69	193	.96	.88	81
701029	740	31.93	52.62	193	.88	.81	81
701029	740	31.86	52.59	193	.83	.76	81
701029	742	31.58	52.46	193	.76	.70	81
701029	744	31.27	52.31	193	.82	.76	81
701029	744	31.21	52.28	193	.82	.76	81
701029	745	31.13	52.24	193	.80	.74	81
701029	745	31.02	52.18	193	.80	.74	81
701029	748	30.63	51.98	193	.72	.67	81
701029	748	30.49	51.90	193	.74	.69	81
701029	750	30.26	51.78	193	.67	.62	81
701029	750	30.15	51.71	193	.74	.69	81
701029	752	29.82	51.52	193	.74	.69	81
701029	753	29.73	51.47	193	.82	.76	81
701029	753	29.66	51.42	193	.78	.73	81
701029	754	29.59	51.38	193	.74	.69	81
701029	754	29.57	51.36	193	.90	.84	81
701029	755	29.45	51.30	193	.90	.84	81
701029	755	29.41	51.27	193	.76	.71	81
701029	755	29.32	51.21	193	.74	.69	81
701029	757	29.07	51.05	193	.76	.71	81
701029	757	29.00	51.00	193	.78	.73	81
701029	758	28.96	50.97	193	.82	.77	81
701029	759	28.76	50.84	193	.88	.82	81
701029	759	28.71	50.80	193	.78	.73	81
701029	759	28.65	50.76	193	.80	.75	81
701029	8 0	28.58	50.72	193	.70	.66	81
701029	8 0	28.47	50.64	193	.76	.71	81
701029	8 2	28.25	50.48	193	.86	.81	81
701029	8 2	28.21	50.45	193	.74	.69	81
701029	8 4	27.93	50.23	193	.94	.88	81
701029	8 4	27.83	50.16	193	.86	.81	81

DATE	TIME	ZA	AZ	STAR	SIG/UNC	SIG/CCR	RUN	
701029	8 5	27.79	50.13	193	.90	.85	81	
7011	4 626	40.58	54.67	193	1.06	.92	82	Period 3
7011	4 627	40.49	54.67	193	.84	.73	82	
7011	4 628	40.32	54.65	193	.92	.80	82	
7011	4 628	40.16	54.64	193	.94	.82	82	
7011	4 629	40.13	54.64	193	.92	.80	82	
7011	4 630	39.88	54.62	193	.84	.74	82	
7011	4 631	39.71	54.60	193	.90	.79	82	
7011	4 632	39.51	54.58	193	1.14	1.00	82	
7011	4 633	39.42	54.57	193	.94	.83	82	
7011	4 633	39.29	54.56	193	.92	.81	82	
7011	4 636	38.93	54.51	193	1.10	.97	82	
7011	4 636	38.87	54.51	193	1.10	.97	82	
7011	4 637	38.60	54.47	193	.88	.78	82	
7011	4 638	38.54	54.46	193	.88	.78	82	
7011	4 639	38.35	54.44	193	.94	.83	82	
7011	4 640	38.23	54.42	193	.94	.83	82	
7011	4 640	38.09	54.40	193	1.12	.99	82	
7011	4 641	37.94	54.37	193	1.21	1.07	82	
7011	4 642	37.84	54.36	193	1.00	.89	82	
7011	4 642	37.80	54.35	193	1.06	.94	82	
7011	4 643	37.63	54.32	193	1.08	.96	82	
7011	4 646	37.16	54.24	193	.94	.84	82	
7011	4 646	37.05	54.22	193	1.14	1.02	82	
7011	4 647	36.93	54.19	193	1.10	.98	82	
7011	4 648	36.79	54.16	193	1.25	1.12	82	
7011	4 648	36.70	54.15	193	1.12	1.00	82	
7011	4 649	36.67	54.14	193	1.06	.95	82	
7011	4 649	36.53	54.11	193	1.10	.99	82	
7011	4 650	36.44	54.09	193	1.10	.99	82	
7011	4 651	36.19	54.03	193	.96	.86	82	
7011	4 652	36.11	54.02	193	.90	.81	82	
7011	4 652	36.07	54.01	193	.90	.81	82	
7011	4 652	36.00	53.99	193	.90	.81	82	
7011	4 653	35.96	53.98	193	1.04	.94	82	
7011	4 654	35.81	53.94	193	1.04	.94	82	
7011	4 656	35.47	53.86	193	1.06	.96	82	
7011	4 656	35.41	53.84	193	1.08	.98	82	
7011	4 656	35.34	53.82	193	.92	.83	82	
7011	4 657	35.29	53.81	193	.94	.85	82	
7011	4 927	54.74	148.13	257	.71	.54	83	Period 4
7011	4 929	54.57	148.52	257	.73	.56	83	
7011	4 929	54.52	148.65	257	.75	.57	83	
7011	4 930	54.42	148.87	257	.69	.53	83	
7011	4 931	54.35	149.04	257	.75	.57	83	
7011	4 931	54.30	149.18	257	.61	.47	83	
7011	5 421	39.62	304.16	777	.95	.83	84	Period 5
7011	5 423	39.83	304.14	777	1.26	1.10	84	
7011	5 423	39.99	304.13	777	1.14	1.00	84	
7011	5 424	40.05	304.13	777	1.12	.98	84	

DATE	TIME	ZA	AZ	STAR	SIG/UNC	SIG/CCR	RUN	
7011	5 426	40.36	304.11	777	1.14	1.00	84	
7011	5 427	40.53	304.10	777	1.14	.99	84	
7011	5 428	40.71	304.09	777	1.14	.99	84	
7011	5 430	41.21	304.08	777	1.14	.99	84	
7011	5 433	41.68	304.07	777	1.32	1.14	84	
7011	5 436	42.12	304.06	777	1.05	.90	84	
7011	5 438	42.48	304.06	777	1.20	1.03	84	
7011	5 439	42.80	304.07	777	1.10	.94	84	
7011	5 442	43.23	304.08	777	1.38	1.18	84	
7011	5 443	43.51	304.08	777	1.10	.94	84	
7011	5 444	43.70	304.09	777	.95	.81	84	
7011	5 445	43.80	304.09	777	.97	.82	84	
7011	5 447	44.11	304.11	777	1.22	1.03	84	
7011	5 448	44.33	304.12	777	1.05	.89	84	
7011	5 449	44.51	304.13	777	.97	.82	84	
7011	5 931	53.89	150.17	257	1.26	.97	85	Period 6
7011	5 931	53.86	150.24	257	1.14	.88	85	
7011	5 931	53.83	150.33	257	1.22	.94	85	
7011	5 932	53.79	150.42	257	1.18	.91	85	
7011	5 932	53.73	150.57	257	1.18	.91	85	
7011	5 933	53.69	150.69	257	1.10	.85	85	
7011	5 934	53.53	151.09	257	1.14	.88	85	
7011	5 936	53.39	151.47	257	1.14	.88	85	
7011	5 936	53.37	151.52	257	1.22	.94	85	
7011	5 938	53.16	152.08	257	1.10	.85	85	
7011	5 939	53.05	152.38	257	1.18	.91	85	
7011	5 939	53.04	152.43	257	1.18	.92	85	
7011	5 940	52.96	152.65	257	1.01	.78	85	
7011	5 942	52.78	153.16	257	1.28	1.00	85	
7011	5 944	52.57	153.76	257	1.24	.97	85	
7011	5 944	52.55	153.83	257	1.22	.95	85	
7011	5 945	52.48	154.02	257	1.14	.89	85	
7011	5 946	52.43	154.18	257	1.14	.89	85	
7011	5 947	52.34	154.46	257	1.32	1.03	85	
7011	5 947	52.29	154.60	257	1.26	.99	85	
7011	5 947	52.27	154.67	257	1.24	.97	85	
7011	5 947	52.25	154.72	257	1.34	1.05	85	
7011	5 948	52.22	154.81	257	1.10	.86	85	
7011	5 948	52.21	154.86	257	1.28	1.00	85	
7011	5 951	51.90	155.82	257	1.05	.82	85	
7011	5 952	51.86	155.96	257	.93	.73	85	
7011	5 952	51.83	156.06	257	.99	.78	85	
7011	5 952	51.81	156.13	257	.95	.75	85	
7011	5 953	51.78	156.23	257	1.01	.79	85	
7011	5 953	51.73	156.39	257	1.05	.83	85	
7011	5 953	51.72	156.42	257	1.01	.79	85	
7011	5 954	51.67	156.58	257	.99	.78	85	
7011	5 955	51.56	156.97	257	1.20	.95	85	
7011	5 956	51.53	157.06	257	1.14	.90	85	
7011	5 956	51.51	157.16	257	1.18	.93	85	

DATE	TIME	ZA	AZ	STAR	SIG/UNC	SIG/CCR	RUN	
7011	5 957	51.45	157.37	257	1.18	.93	85	
7011	5 957	51.40	157.54	257	1.14	.90	85	
7011	5 958	51.32	157.83	257	1.24	.98	85	
7011	510 1	51.09	158.68	257	1.12	.89	85	
7011	510 2	51.04	158.85	257	1.03	.82	85	
7011	510 2	51.00	159.02	257	1.12	.89	85	
7011	510 3	50.96	159.14	257	.99	.79	85	
7011	510 3	50.93	159.27	257	1.01	.80	85	
7011	510 5	50.82	159.71	257	1.12	.89	85	
7011	510 6	50.70	160.20	257	1.01	.80	85	
7011	510 7	50.65	160.40	257	1.18	.94	85	
7011	510 8	50.57	160.74	257	1.03	.82	85	
7011	510 8	50.56	160.77	257	1.16	.92	85	
7011	510 9	50.55	160.82	257	1.24	.99	85	
7011	510 9	50.53	160.92	257	1.07	.85	85	
7011	51010	50.48	161.12	257	1.03	.82	85	
7011	51010	50.44	161.31	257	1.22	.97	85	
701110	642	33.73	53.33	193	.67	.61	86	Period 7
701110	643	33.65	53.30	193	.67	.61	86	
701110	645	33.31	53.18	193	.79	.72	86	
701110	645	33.18	53.13	193	.67	.61	86	
701110	646	33.05	53.08	193	.97	.89	86	
701110	647	32.94	53.04	193	.71	.65	86	
701110	647	32.82	53.00	193	.89	.82	86	
701110	648	32.65	52.93	193	.71	.65	86	
701110	649	32.57	52.89	193	.69	.63	86	
701110	649	32.50	52.86	193	.63	.58	86	
701110	653	31.79	52.56	193	.75	.69	86	
701110	654	31.65	52.49	193	.67	.62	86	
701110	655	31.55	52.44	193	.71	.66	86	
701110	655	31.48	52.41	193	.72	.66	86	
701110	657	31.23	52.29	193	.59	.55	86	
701110	657	31.11	52.23	193	.63	.58	86	
701110	659	30.86	52.10	193	.67	.62	86	
701110	7 0	30.71	52.02	193	.79	.73	86	
701110	7 1	30.51	51.91	193	.81	.75	86	
701110	7 4	30.09	51.68	193	.75	.70	86	
701110	7 6	29.76	51.48	193	.75	.70	86	
701110	7 7	29.56	51.36	193	.73	.68	86	
701110	7 8	29.42	51.28	193	.75	.70	86	
701110	7 9	29.22	51.14	193	.73	.68	86	
701110	710	28.97	50.98	193	.69	.65	86	
701110	713	28.47	50.64	193	.75	.70	86	
701110	714	28.40	50.59	193	.71	.67	86	
701110	714	28.29	50.51	193	.71	.67	86	
701110	715	28.22	50.46	193	.73	.69	86	
701110	715	28.18	50.43	193	.71	.67	86	
701110	716	28.10	50.37	193	.69	.65	86	
701110	717	27.81	50.15	193	.75	.71	86	
701110	718	27.77	50.11	193	.81	.76	86	

DATE TIME	ZA	AZ	STAR	SIG/UNC	SIG/CCR	RUN	
701111 250	50.73	296.46	699	.73	.58	87	Period 8
701111 251	50.79	296.48	699	.70	.56	87	
701111 251	50.85	296.50	699	.73	.58	87	
701111 252	50.98	296.53	699	.67	.53	87	
701111 252	51.06	296.55	699	.65	.52	87	
701111 252	51.11	296.57	699	.67	.53	87	
701111 253	51.25	296.61	699	.75	.59	87	
701111 254	51.31	296.63	699	.73	.58	87	
701111 254	51.38	296.65	699	.75	.59	87	
701111 254	51.46	296.67	699	.71	.56	87	
701111 256	51.87	296.79	699	.75	.59	87	
701111 257	51.98	296.82	699	.79	.62	87	
701111 258	52.11	296.86	699	.75	.59	87	
701111 259	52.27	296.91	699	.75	.59	87	
701111 259	52.31	296.92	699	.81	.63	87	
701111 259	52.38	296.94	699	.71	.55	87	
701111 259	52.43	296.96	699	.69	.54	87	
701111 3 1	52.81	297.07	699	.85	.66	87	
701111 3 2	52.88	297.09	699	.75	.58	87	
701111 3 2	52.96	297.12	699	.73	.57	87	
701111 3 2	53.01	297.13	699	.75	.58	87	
701111 3 3	53.18	297.19	699	.79	.61	87	
701111 3 4	53.36	297.24	699	.73	.56	87	
701111 3 5	53.41	297.26	699	.79	.61	87	
701111 3 6	53.60	297.32	699	.83	.64	87	
701111 3 6	53.66	297.34	699	.75	.58	87	
701111 3 6	53.75	297.37	699	.77	.59	87	
701111 3 7	53.94	297.43	699	.71	.54	87	
701111 3 8	54.13	297.49	699	.69	.53	87	
701111 3 9	54.20	297.51	699	.67	.51	87	
701111 312	54.78	297.69	699	.93	.71	87	
701111 313	54.92	297.74	699	.97	.74	87	
701111 313	54.97	297.76	699	.97	.73	87	
701111 313	55.01	297.77	699	.93	.70	87	
701111 313	55.06	297.79	699	.83	.63	87	
701111 314	55.14	297.81	699	.83	.63	87	
701111 314	55.28	297.86	699	.81	.61	87	
701111 315	55.36	297.89	699	.93	.70	87	
701111 316	55.53	297.94	699	.85	.64	87	
701111 317	55.77	298.02	699	.93	.70	87	
701111 317	55.83	298.04	699	.95	.71	87	
701111 319	56.10	298.13	699	.87	.65	87	
701111 319	56.19	298.17	699	.97	.72	87	
701111 321	56.58	298.30	699	.97	.72	87	
701111 322	56.66	298.33	699	.99	.73	87	
701111 844	56.58	144.22	257	1.16	.86	88	Period 9
701111 845	56.41	144.55	257	1.20	.89	88	
701111 846	56.29	144.79	257	1.30	.97	88	
701111 847	56.23	144.92	257	1.28	.95	88	
701111 847	56.16	145.06	257	1.28	.96	88	

DATE	TIME	ZA	AZ	STAR	SIG/UNC	SIG/CCR	RUN	
701111	849	56.01	145.37	257	1.32	.99	88	
701111	849	55.97	145.44	257	1.52	1.14	88	
701111	849	55.92	145.54	257	1.56	1.17	88	
701111	850	55.86	145.67	257	1.26	.94	88	
701111	851	55.77	145.85	257	1.38	1.03	88	
701111	852	55.57	146.30	257	1.30	.98	88	
701111	858	54.93	147.70	257	1.05	.80	88	
701111	859	54.83	147.92	257	1.07	.81	88	
701111	859	54.79	148.01	257	1.20	.91	88	
701111	859	54.76	148.09	257	1.24	.94	88	
701111	9 0	54.71	148.20	257	1.10	.84	88	
701111	9 0	54.68	148.27	257	1.16	.88	88	
701111	9 0	54.65	148.33	257	1.14	.87	88	
701111	9 1	54.56	148.55	257	1.07	.81	88	
701111	9 2	54.50	148.70	257	.99	.75	88	
701111	9 3	54.39	148.96	257	1.30	.99	88	
701111	9 3	54.33	149.09	257	1.10	.84	88	
701111	9 4	54.26	149.27	257	1.14	.87	88	
701111	9 4	54.20	149.40	257	1.16	.89	88	
701117	654	27.10	49.57	193	.89	.84	89	Period 10
701117	655	27.04	49.51	193	.73	.69	89	
701117	656	26.82	49.32	193	1.10	1.04	89	
701117	656	26.74	49.25	193	.89	.84	89	
701117	657	26.63	49.15	193	.77	.73	89	
701117	658	26.51	49.04	193	1.05	.99	89	
701117	659	26.38	48.92	193	.99	.94	89	
701117	7 2	25.88	48.44	193	.83	.79	89	
701117	7 3	25.75	48.30	193	.91	.86	89	
701117	7 4	25.51	48.05	193	.87	.83	89	
701117	7 4	25.46	48.00	193	.75	.71	89	
701117	7 5	25.31	47.84	193	.77	.73	89	
701117	7 6	25.21	47.73	193	.71	.68	89	
701117	7 7	24.97	47.46	193	.69	.66	89	
701117	7 9	24.79	47.25	193	.79	.75	89	
701117	7 9	24.68	47.13	193	.83	.79	89	
701117	712	24.28	46.65	193	.85	.81	89	
701117	713	24.13	46.45	193	.89	.85	89	
701117	713	24.04	46.34	193	.93	.89	89	
701117	716	23.72	45.91	193	.91	.87	89	
701117	717	23.56	45.71	193	.85	.81	89	
701117	718	23.28	45.31	193	.89	.85	89	
701117	719	23.18	45.17	193	.91	.87	89	
701117	722	22.77	44.55	193	1.05	1.01	89	
701117	722	22.71	44.45	193	.75	.72	89	
701117	723	22.63	44.34	193	.81	.78	89	
701117	723	22.56	44.22	193	.87	.84	89	
701117	724	22.38	43.94	193	.87	.84	89	
701117	726	22.15	43.55	193	.93	.90	89	
701118	252	32.97	305.45	777	.79	.72	90	Period 11
701118	253	33.02	305.44	777	.77	.71	90	

DATE TIME	ZA	AZ	STAR	SIG/UNC	SIG/CCR	RUN	
701118 253	33.06	305.42	777	.71	.65	90	
701118 253	33.10	305.41	777	.69	.63	90	
701118 254	33.26	305.36	777	.77	.70	90	
701118 254	33.32	305.34	777	.85	.78	90	
701118 255	33.38	305.32	777	.93	.85	90	
701118 255	33.44	305.30	777	.75	.69	90	
701118 256	33.58	305.25	777	.85	.78	90	
701118 257	33.73	305.21	777	.99	.90	90	
701118 257	33.76	305.20	777	1.01	.92	90	
701118 259	34.06	305.11	777	.69	.63	90	
701118 259	34.11	305.10	777	.71	.65	90	
701118 259	34.18	305.08	777	.69	.63	90	
701118 3 2	34.60	304.97	777	.71	.64	90	
701118 3 2	34.64	304.95	777	.81	.73	90	
701118 3 4	34.92	304.88	777	.67	.61	90	
701118 3 4	35.01	304.86	777	.93	.84	90	
701118 3 5	35.14	304.83	777	.99	.90	90	
701118 3 6	35.30	304.79	777	1.01	.91	90	
701118 3 6	35.36	304.78	777	.87	.79	90	
701118 3 6	35.40	304.77	777	.97	.88	90	
701118 3 7	35.46	304.76	777	.93	.84	90	
701118 3 8	35.75	304.69	777	.93	.84	90	
701118 3 9	35.84	304.68	777	.87	.78	90	
701118 3 9	35.94	304.65	777	.75	.67	90	
701118 311	36.22	304.60	777	.89	.80	90	
701118 312	36.35	304.57	777	.69	.62	90	
701118 312	36.40	304.57	777	.71	.64	90	
701118 312	36.44	304.56	777	.79	.71	90	
701118 314	36.78	304.50	777	.83	.74	90	
701118 315	36.85	304.49	777	.95	.85	90	
701118 315	36.91	304.48	777	.79	.71	90	
701118 316	37.04	304.46	777	.89	.80	90	
701118 316	37.09	304.45	777	.99	.88	90	
701118 916	15.20	341.92	193	.67	.66	91	Period 12
701118 917	15.26	341.38	193	.67	.66	91	
701118 918	15.30	341.08	193	.65	.64	91	
701118 920	15.43	339.93	193	.73	.72	91	
701118 921	15.57	338.90	193	.65	.64	91	
701118 922	15.61	338.56	193	.59	.58	91	
701118 922	15.64	338.32	193	.69	.68	91	
701118 923	15.69	337.98	193	.77	.76	91	
701118 923	15.72	337.75	193	.69	.68	91	
701118 924	15.80	337.23	193	.61	.60	91	
701118 927	16.00	335.93	193	.67	.66	91	
701118 927	16.04	335.66	193	.61	.60	91	
701118 928	16.11	335.20	193	.59	.58	91	
701118 930	16.25	334.40	193	.63	.62	91	
701118 930	16.30	334.14	193	.61	.60	91	
701118 933	16.60	332.51	193	.63	.62	91	
701118 934	16.65	332.26	193	.57	.56	91	

DATE TIME	ZA	AZ	STAR	SIG/UNC	SIG/CCR	RUN	
701118 934	16.71	331.97	193	.59	.58	91	
701118 937	16.95	330.83	193	.59	.58	91	
701118 938	17.04	330.40	193	.57	.56	91	
701118 938	17.13	330.01	193	.59	.58	91	
701118 940	17.34	329.12	193	.57	.56	91	
701118 942	17.49	328.48	193	.57	.56	91	
701118 943	17.61	328.04	193	.57	.56	91	
701118 944	17.76	327.46	193	.55	.54	91	
701118 947	18.05	326.41	193	.65	.63	91	
701118 948	18.17	326.00	193	.57	.56	91	
701118 952	18.65	324.42	193	.59	.57	91	
701118 952	18.75	324.13	193	.65	.63	91	
701118 954	18.97	323.48	193	.69	.67	91	
701118 957	19.29	322.58	193	.63	.61	91	
701118 957	19.40	322.29	193	.53	.51	91	
701118 958	19.44	322.17	193	.59	.57	91	
701118 959	19.55	321.89	193	.63	.61	91	
701118 959	19.66	321.61	193	.79	.77	91	
70111810 0	19.78	321.30	193	.65	.63	91	
70111810 1	19.93	320.94	193	.61	.59	91	
70111810 3	20.08	320.57	193	.63	.61	91	
701121 254	35.32	304.79	777	.67	.61	92	Period 13
701121 254	35.40	304.77	777	.83	.75	92	
701121 255	35.44	304.76	777	.75	.68	92	
701121 256	35.59	304.73	777	.65	.59	92	
701121 256	35.63	304.72	777	.61	.55	92	
701121 256	35.72	304.70	777	.67	.60	92	
701121 256	35.75	304.70	777	.71	.64	92	
701121 257	35.88	304.67	777	.61	.55	92	
701121 258	36.07	304.63	777	.63	.57	92	
701121 259	36.20	304.60	777	.61	.55	92	
701121 259	36.24	304.60	777	.61	.55	92	
701121 259	36.27	304.59	777	.65	.58	92	
701121 3 1	36.51	304.55	777	.63	.56	92	
701121 3 1	36.60	304.53	777	.67	.60	92	
701121 3 1	36.63	304.53	777	.67	.60	92	
701121 3 3	36.96	304.47	777	.69	.62	92	
701121 3 4	36.99	304.46	777	.69	.62	92	
701121 3 4	37.04	304.46	777	.69	.62	92	
701121 3 6	37.49	304.39	777	.67	.60	92	
701121 3 7	37.58	304.37	777	.67	.60	92	
701121 3 7	37.62	304.37	777	.69	.61	92	
701121 3 8	37.81	304.34	777	.77	.68	92	
701121 3 9	37.87	304.33	777	.77	.68	92	
701121 310	38.19	304.29	777	.71	.63	92	
701121 311	38.39	304.27	777	.73	.65	92	
701121 314	38.78	304.23	777	.69	.61	92	
701121 314	38.83	304.22	777	.81	.71	92	
701121 316	39.25	304.19	777	.69	.61	92	
701121 317	39.37	304.18	777	.69	.61	92	

DATE TIME	ZA	AZ	STAR	SIG/UNC	SIG/COR	RUN	
701121 318	39.49	304.17	777	.83	.73	92	
701121 319	39.78	304.14	777	.73	.64	92	
701121 320	39.96	304.13	777	.81	.71	92	
701121 321	40.09	304.13	777	.73	.64	92	
701121 321	40.14	304.12	777	.69	.60	92	
701121 322	40.24	304.12	777	.71	.62	92	
701121 324	40.52	304.10	777	.69	.60	92	
701121 324	40.58	304.10	777	.79	.69	92	
701121 324	40.62	304.10	777	.79	.69	92	
701124 236	34.19	305.08	777	.85	.77	93	Period 14
701124 237	34.43	305.01	777	.91	.83	93	
701124 238	34.58	304.97	777	.91	.83	93	
701124 242	35.24	304.81	777	.87	.79	93	
701124 243	35.39	304.77	777	.97	.88	93	
701124 244	35.55	304.74	777	.91	.82	93	
701124 247	36.12	304.62	777	.91	.82	93	
701124 247	36.22	304.60	777	.91	.82	93	
701124 249	36.46	304.55	777	.95	.85	93	
701124 250	36.76	304.50	777	.97	.87	93	
701124 251	36.88	304.48	777	1.01	.90	93	
701124 253	37.15	304.44	777	.99	.88	93	
701124 254	37.40	304.40	777	.95	.85	93	
701124 257	37.99	304.32	777	1.07	.95	93	
701124 259	38.19	304.29	777	.93	.82	93	
701124 3 2	38.85	304.22	777	.87	.77	93	
701124 3 4	39.14	304.20	777	.81	.71	93	
701124 3 7	39.73	304.15	777	.97	.85	93	
701124 3 8	39.86	304.14	777	.97	.85	93	
701124 311	40.41	304.11	777	1.03	.90	93	
701124 312	40.61	304.10	777	.89	.78	93	
701124 314	40.97	304.08	777	.97	.84	93	
701124 317	41.44	304.07	777	1.14	.99	93	
701124 319	41.81	304.07	777	.93	.80	93	
701124 320	41.93	304.06	777	1.05	.91	93	
70112410 0	23.04	315.04	193	.53	.51	94	Period 15
70112410 0	23.16	314.87	193	.61	.58	94	
70112410 1	23.19	314.82	193	.55	.53	94	
70112410 1	23.32	314.63	193	.53	.51	94	
70112410 2	23.35	314.60	193	.55	.53	94	
70112410 3	23.55	314.31	193	.59	.56	94	
70112410 4	23.68	314.14	193	.57	.55	94	
70112410 4	23.70	314.11	193	.57	.55	94	
70112410 5	23.93	313.80	193	.61	.58	94	
70112410 6	24.00	313.72	193	.61	.58	94	
70112410 6	24.06	313.63	193	.57	.54	94	
70112410 7	24.16	313.50	193	.61	.58	94	
70112410 8	24.29	313.34	193	.57	.54	94	
70112410 9	24.53	313.06	193	.53	.51	94	
7011241012	24.93	312.58	193	.55	.52	94	
7011241013	25.17	312.32	193	.59	.56	94	

DATE TIME	ZA	AZ	STAR	SIG/UNC	SIG/CCR	RUN	
7011241014	25.25	312.23	193	.63	.60	94	
7011241014	25.28	312.19	193	.65	.62	94	
7011241015	25.44	312.02	193	.73	.69	94	
7011241016	25.65	311.80	193	.69	.66	94	
7011241017	25.81	311.63	193	.67	.64	94	
7011241019	26.08	311.37	193	.69	.65	94	
7011241022	26.48	310.99	193	.61	.58	94	
7011241022	26.56	310.91	193	.57	.54	94	
7011241022	26.62	310.86	193	.57	.54	94	
7011241023	26.72	310.77	193	.65	.61	94	
7011241024	26.83	310.67	193	.59	.56	94	
7011241024	26.94	310.57	193	.63	.59	94	
7011241026	27.13	310.41	193	.63	.59	94	
7011241026	27.18	310.37	193	.59	.56	94	
7011241027	27.41	310.17	193	.67	.63	94	
7011241028	27.58	310.04	193	.55	.52	94	
7011241029	27.67	309.97	193	.61	.57	94	
7011241032	28.16	309.59	193	.61	.57	94	
7011241032	28.22	309.55	193	.61	.57	94	
7011241033	28.41	309.41	193	.61	.57	94	
7011241034	28.58	309.29	193	.63	.59	94	
7011241035	28.74	309.17	193	.63	.59	94	
7011241036	28.81	309.13	193	.65	.61	94	
7011241036	28.91	309.06	193	.57	.53	94	
7011241037	28.98	309.01	193	.57	.53	94	
7011241038	29.14	308.91	193	.67	.63	94	
7011241039	29.29	308.81	193	.59	.55	94	
7011241039	29.35	308.77	193	.65	.61	94	
7012 1 532	31.65	52.49	193	.81	.75	95	Period 16
7012 1 532	31.57	52.45	193	.93	.86	95	
7012 1 532	31.52	52.43	193	.77	.71	95	
7012 1 534	31.34	52.34	193	1.05	.97	95	
7012 1 535	31.16	52.25	193	.79	.73	95	
7012 1 536	30.92	52.13	193	.77	.71	95	
7012 1 537	30.78	52.06	193	.81	.75	95	
7012 1 537	30.84	52.09	193	.75	.69	95	
7012 1 538	30.67	52.00	193	.75	.70	95	
7012 1 538	30.53	51.92	193	.81	.75	95	
7012 1 539	30.42	51.86	193	.99	.92	95	
7012 1 540	30.30	51.80	193	1.07	.99	95	
7012 1 540	30.22	51.75	193	.89	.83	95	
7012 1 541	30.15	51.71	193	.93	.86	95	
7012 1 541	30.11	51.69	193	.89	.83	95	
7012 1 542	29.86	51.54	193	.95	.88	95	
7012 1 545	29.44	51.29	193	.81	.76	95	
7012 1 545	29.37	51.24	193	.83	.77	95	
7012 1 546	29.18	51.12	193	.81	.76	95	
7012 1 547	29.08	51.05	193	.73	.68	95	
7012 1 548	28.86	50.91	193	.87	.81	95	
7012 1 548	28.85	50.90	193	.99	.93	95	

DATE	TIME	ZA	AZ	STAR	SIG/UNC	SIG/CCR	RUN	
7012	1 549	28.75	50.83	193	.81	.76	95	
7012	1 550	28.61	50.74	193	.93	.87	95	
7012	1 550	28.56	50.70	193	.71	.67	95	
7012	1 551	28.42	50.60	193	.81	.76	95	
7012	1 552	28.30	50.51	193	.89	.84	95	
7012	1 552	28.21	50.45	193	.87	.82	95	
7012	1 554	27.87	50.19	193	.75	.71	95	
7012	1 556	27.65	50.02	193	.93	.88	95	
7012	2 151	31.93	305.84	777	.81	.75	96	Period 17
7012	2 152	32.03	305.80	777	.81	.75	96	
7012	2 154	32.37	305.67	777	.77	.71	96	
7012	2 154	32.45	305.64	777	.75	.69	96	
7012	2 155	32.63	305.57	777	.87	.80	96	
7012	2 156	32.71	305.54	777	.87	.80	96	
7012	2 157	32.97	305.45	777	.87	.80	96	
7012	2 159	33.24	305.36	777	.95	.87	96	
7012	2 2 0	33.40	305.31	777	.83	.76	96	
7012	2 2 0	33.49	305.28	777	.87	.79	96	
7012	2 2 4	34.10	305.10	777	.97	.88	96	
7012	2 2 6	34.46	305.00	777	.89	.81	96	
7012	2 2 6	34.57	304.97	777	.93	.84	96	
7012	2 958	27.80	309.86	193	1.29	1.21	97	Period 18
7012	2 959	27.86	309.82	193	1.10	1.03	97	
7012	2 959	27.99	309.72	193	1.06	1.00	97	
7012	210 0	28.06	309.66	193	1.14	1.07	97	
7012	210 1	28.33	309.46	193	.96	.90	97	
7012	210 2	28.38	309.43	193	1.02	.96	97	
7012	210 2	28.49	309.35	193	.90	.84	97	
7012	210 3	28.53	309.32	193	.98	.92	97	
7012	210 3	28.57	309.29	193	.94	.88	97	
7012	210 4	28.68	309.22	193	.88	.82	97	
7012	210 4	28.73	309.18	193	.96	.90	97	
7012	210 4	28.80	309.13	193	1.08	1.01	97	
7012	210 5	28.98	309.01	193	1.20	1.12	97	
7012	210 8	29.37	308.76	193	1.37	1.28	97	
7012	210 9	29.60	308.61	193	1.20	1.12	97	
7012	210 9	29.65	308.59	193	1.37	1.28	97	
7012	21010	29.76	308.52	193	1.14	1.06	97	
7012	21010	29.79	308.50	193	1.24	1.16	97	
7012	21011	29.97	308.39	193	1.12	1.04	97	
7012	21012	30.13	308.30	193	1.35	1.26	97	
7012	21013	30.22	308.25	193	1.24	1.15	97	
7012	21014	30.39	308.15	193	1.16	1.08	97	
7012	21015	30.61	308.03	193	1.02	.95	97	
7012	21017	30.86	307.90	193	1.12	1.04	97	
7012	21017	30.92	307.87	193	1.29	1.19	97	
7012	21017	30.99	307.83	193	1.16	1.07	97	
7012	21018	31.16	307.75	193	1.12	1.04	97	
7012	21019	31.21	307.72	193	1.06	.98	97	
7012	21019	31.33	307.66	193	.98	.91	97	

DATE	TIME	ZA	AZ	STAR	SIG/UNC	SIG/CCR	RUN	
7012	21020	31.44	307.61	193	1.06	.98	97	
7012	21020	31.49	307.58	193	1.26	1.16	97	
7012	8 713	14.71	12.49	193	.69	.68	98	Period 19
7012	8 714	14.66	11.71	193	.73	.72	98	
7012	8 715	14.63	11.27	193	.65	.64	98	
7012	8 717	14.56	10.03	193	.55	.54	98	
7012	8 718	14.52	9.24	193	.67	.66	98	
7012	8 718	14.51	9.01	193	.63	.62	98	
7012	8 718	14.50	8.84	193	.65	.64	98	
7012	8 721	14.41	6.89	193	.61	.60	98	
7012	8 722	14.40	6.60	193	.65	.64	98	
7012	8 722	14.39	6.25	193	.61	.60	98	
7012	8 725	14.33	3.99	193	.67	.66	98	
7012	8 728	14.30	1.82	193	.69	.68	98	
7012	8 730	14.29	.99	193	.57	.56	98	
7012	8 731	14.29	.05	193	.51	.50	98	
7012	8 733	14.29	358.70	193	.63	.62	98	
7012	8 734	14.30	357.76	193	.57	.56	98	
7012	8 735	14.31	357.00	193	.61	.60	98	
7012	8 738	14.35	355.18	193	.69	.68	98	
7012	8 739	14.38	354.02	193	.55	.54	98	
7012	8 741	14.42	353.10	193	.59	.58	98	
7012	8 741	14.42	352.92	193	.53	.52	98	
7012	8 742	14.45	352.23	193	.53	.52	98	
701211	628	17.39	31.10	193	1.19	1.16	99	Period 20
701211	628	17.34	30.91	193	1.05	1.03	99	
701211	629	17.33	30.84	193	1.07	1.05	99	
701211	630	17.14	30.03	193	1.11	1.09	99	
701211	631	17.11	29.91	193	1.03	1.01	99	
701211	631	17.06	29.68	193	1.25	1.22	99	
701211	632	16.93	29.08	193	1.15	1.12	99	
701211	633	16.88	28.88	193	1.09	1.07	99	
701211	634	16.80	28.47	193	1.31	1.28	99	
701211	634	16.75	28.23	193	1.21	1.18	99	
701211	636	16.53	27.14	193	1.23	1.20	99	
701211	636	16.51	27.02	193	1.15	1.13	99	
7012111033		54.55	211.44	257	1.56	1.19	100	Period 21
7012111033		54.57	211.48	257	1.48	1.13	100	
7012111035		54.69	211.76	257	1.44	1.09	100	
7012111035		54.75	211.89	257	1.70	1.29	100	
7012111037		54.98	212.41	257	1.56	1.18	100	
7012111038		55.13	212.75	257	1.44	1.09	100	
7012111041		55.42	213.39	257	1.83	1.38	100	
7012111041		55.45	213.45	257	1.89	1.42	100	
7012111043		55.64	213.86	257	1.36	1.02	100	
7012111043		55.70	213.98	257	2.18	1.64	100	
7012111046		55.98	214.57	257	1.36	1.02	100	
7012111046		56.06	214.74	257	1.79	1.34	100	
7012111047		56.14	214.90	257	1.79	1.34	100	
7012111048		56.33	215.29	257	2.14	1.59	100	

DATE TIME	ZA	AZ	STAR	SIG/UNC	SIG/CCR	RUN	
7012111049	56.45	215.52	257	1.95	1.45	100	
7012111051	56.59	215.81	257	1.87	1.39	100	
7012111051	56.61	215.85	257	1.91	1.42	100	
701217 253	48.26	54.44	193	.93	.76	103	Period 22
701217 253	48.20	54.44	193	.97	.79	103	
701217 254	48.05	54.46	193	.79	.65	103	
701217 255	47.97	54.47	193	.83	.68	103	
701217 255	47.92	54.47	193	.81	.66	103	
701217 256	47.76	54.49	193	.85	.70	103	
701217 257	47.62	54.51	193	.97	.80	103	
701217 258	47.30	54.54	193	.81	.67	103	
701217 259	47.11	54.56	193	.75	.62	103	
701217 3 0	46.94	54.58	193	.85	.70	103	
701217 3 1	46.90	54.58	193	.71	.59	103	
701217 3 1	46.85	54.58	193	.91	.75	103	
701217 3 1	46.81	54.59	193	.95	.79	103	
701217 3 2	46.66	54.60	193	.79	.65	103	
701217 3 2	46.62	54.60	193	.73	.60	103	
701217 3 4	46.24	54.64	193	.73	.61	103	
701217 3 5	46.18	54.64	193	.75	.62	103	
701217 3 5	46.14	54.64	193	.79	.66	103	
701217 3 6	45.89	54.66	193	.73	.61	103	
701217 3 7	45.79	54.67	193	.85	.71	103	
701217 3 7	45.72	54.67	193	.83	.69	103	
701217 3 9	45.53	54.68	193	.91	.76	103	
701217 3 9	45.45	54.69	193	.71	.59	103	
701217 310	45.36	54.69	193	.83	.70	103	
701217 310	45.24	54.70	193	.77	.65	103	
701217 311	45.18	54.70	193	.79	.66	103	
701217 312	44.85	54.72	193	.67	.56	103	
701217 314	44.66	54.73	193	1.02	.86	103	
701217 315	44.43	54.74	193	1.11	.94	103	
701217 316	44.31	54.74	193	.91	.77	103	
701217 316	44.26	54.74	193	.85	.72	103	
701217 317	44.05	54.75	193	.69	.58	103	
701217 317	44.01	54.75	193	.79	.67	103	
701231 5 6	17.77	32.58	193	.74	.72	104	Period 23
701231 5 6	17.75	32.51	193	.72	.70	104	
701231 5 7	17.65	32.11	193	.82	.80	104	
701231 5 7	17.61	31.97	193	.85	.83	104	
701231 5 8	17.58	31.86	193	.87	.85	104	
701231 5 8	17.50	31.56	193	.89	.87	104	
701231 5 9	17.42	31.23	193	.85	.83	104	
701231 510	17.33	30.85	193	.84	.82	104	
701231 510	17.28	30.66	193	.85	.83	104	
701231 511	17.16	30.12	193	.70	.68	104	
701231 513	17.03	29.57	193	.80	.78	104	
701231 514	16.92	29.05	193	.82	.80	104	
701231 514	16.90	28.97	193	.97	.95	104	
701231 514	16.85	28.73	193	.84	.82	104	

DATE	TIME	ZA	AZ	STAR	SIG/UNC	SIG/CCR	RUN	
701231	515	16.78	28.41	193	.97	.95	104	
701231	515	16.75	28.24	193	.91	.89	104	
701231	518	16.53	27.12	193	.78	.76	104	
701231	519	16.42	26.52	193	.84	.82	104	
701231	520	16.26	25.65	193	.86	.84	104	
701231	521	16.17	25.12	193	.84	.82	104	
701231	522	16.12	24.81	193	.78	.76	104	
701231	523	15.99	24.04	193	.82	.80	104	
701231	524	15.91	23.53	193	.72	.71	104	
701231	525	15.84	23.07	193	.80	.78	104	
701231	527	15.66	21.84	193	.80	.79	104	
701231	528	15.64	21.64	193	.86	.84	104	
701231	528	15.58	21.21	193	.76	.75	104	
701231	530	15.48	20.43	193	.88	.86	104	
701231	530	15.43	20.03	193	.82	.81	104	
701231	531	15.38	19.59	193	.86	.84	104	
701231	533	15.26	18.63	193	.80	.79	104	
701231	534	15.21	18.17	193	.86	.84	104	
701231	534	15.19	17.97	193	.88	.86	104	
701231	535	15.12	17.24	193	.84	.83	104	
71	126 457	16.14	335.05	193	.53	.52	105	Period 24
71	126 458	16.19	334.78	193	.49	.48	105	
71	126 458	16.21	334.65	193	.55	.54	105	
71	126 459	16.30	334.12	193	.57	.56	105	
71	126 459	16.32	333.99	193	.55	.54	105	
71	126 459	16.36	333.77	193	.49	.48	105	
71	126 5 0	16.40	333.55	193	.57	.56	105	
71	126 5 1	16.47	333.21	193	.59	.58	105	
71	126 5 1	16.51	332.95	193	.57	.56	105	
71	126 5 2	16.65	332.24	193	.63	.62	105	
71	126 5 3	16.69	332.07	193	.57	.56	105	
71	126 5 3	16.71	331.95	193	.63	.62	105	
71	126 5 4	16.80	331.54	193	.55	.54	105	
71	126 5 4	16.86	331.25	193	.57	.56	105	
71	126 5 5	16.92	330.97	193	.61	.60	105	
71	126 5 6	16.97	330.73	193	.61	.60	105	
71	126 5 6	17.05	330.38	193	.59	.58	105	
71	126 517	18.24	325.74	193	.85	.83	105	
71	126 518	18.32	325.47	193	.85	.83	105	
71	126 519	18.44	325.08	193	.85	.83	105	
71	126 526	19.41	322.25	193	1.14	1.11	105	
71	126 527	19.48	322.07	193	1.10	1.07	105	
71	126 527	19.57	321.84	193	.97	.94	105	
71	126 529	19.81	321.23	193	1.14	1.11	105	
71	126 531	20.10	320.53	193	1.12	1.09	105	
71	126 532	20.17	320.37	193	1.14	1.10	105	
71	126 532	20.22	320.26	193	1.18	1.14	105	
71	126 533	20.26	320.16	193	1.10	1.07	105	
71	126 533	20.31	320.06	193	1.12	1.08	105	
71	126 534	20.44	319.75	193	.91	.88	105	

DATE TIME	ZA	AZ	STAR	SIG/UNC	SIG/CCR	RUN	
71 126 534	20.51	319.60	193	1.07	1.04	105	
71 126 536	20.79	319.00	193	1.01	.98	105	
71 126 537	20.88	318.81	193	1.01	.98	105	
71 126 538	21.00	318.57	193	1.16	1.12	105	
71 126 539	21.23	318.12	193	1.10	1.06	105	
71 126 540	21.36	317.87	193	1.12	1.08	105	
71 126 542	21.56	317.49	193	1.10	1.06	105	
71 126 543	21.71	317.23	193	1.16	1.12	105	
71 126 544	21.84	316.99	193	1.01	.97	105	
71 126 544	21.92	316.84	193	1.01	.97	105	
71 126 545	22.00	316.71	193	1.10	1.06	105	
71 126 545	22.07	316.59	193	1.05	1.01	105	
71 126 548	22.44	315.97	193	1.10	1.06	105	
71 126 548	22.52	315.83	193	1.22	1.17	105	
71 126 549	22.60	315.72	193	1.14	1.10	105	
71 126 549	22.66	315.62	193	1.07	1.03	105	
71 126 550	22.75	315.48	193	1.05	1.01	105	
71 126 550	22.81	315.39	193	1.05	1.01	105	
71 126 552	23.10	314.95	193	1.18	1.13	105	
71 126 552	23.14	314.90	193	1.14	1.09	105	
71 126 553	23.19	314.83	193	1.10	1.05	105	
71 126 553	23.23	314.77	193	1.03	.99	105	
71 126 554	23.39	314.54	193	1.07	1.03	105	
71 126 554	23.43	314.48	193	1.05	1.01	105	
71 126 555	23.59	314.25	193	1.05	1.01	105	
71 126 558	23.91	313.83	193	1.07	1.02	105	
71 126 558	23.99	313.73	193	1.23	1.18	105	
71 126 559	24.07	313.63	193	1.13	1.08	105	
71 126 6 0	24.31	313.32	193	1.19	1.14	105	
71 126 6 1	24.51	313.08	193	1.01	.96	105	
71 126 6 2	24.66	312.89	193	1.11	1.06	105	
71 126 6 3	24.71	312.83	193	1.07	1.02	105	
71 126 6 4	24.84	312.68	193	1.05	1.00	105	
71 126 6 4	24.92	312.59	193	1.25	1.19	105	
71 126 6 5	25.00	312.50	193	1.01	.96	105	
71 126 6 5	25.08	312.41	193	.93	.89	105	
71 126 6 6	25.28	312.20	193	1.09	1.04	105	
71 126 6 7	25.40	312.07	193	1.01	.96	105	
71 126 6 8	25.52	311.94	193	1.29	1.23	105	
71 126 6 8	25.57	311.89	193	1.19	1.13	105	
71 126 6 9	25.63	311.82	193	1.09	1.03	105	
71 126 6 9	25.77	311.68	193	1.05	1.00	105	
71 126 612	26.15	311.30	193	1.21	1.15	105	
71 126 612	26.26	311.19	193	1.23	1.16	105	
71 126 912	57.09	307.37	193	1.49	1.10	106	Period 25
71 126 913	57.14	307.38	193	1.41	1.04	106	
71 126 913	57.26	307.42	193	1.35	.99	106	
71 126 914	57.28	307.42	193	1.33	.98	106	
71 126 914	57.38	307.45	193	1.41	1.04	106	
71 126 915	57.45	307.47	193	1.37	1.00	106	

DATE	TIME	ZA	AZ	STAR	SIG/UNC	SIG/CCR	RUN
71	126 916	57.62	307.52	193	1.33	.97	106
71	126 916	57.71	307.55	193	1.31	.96	106
71	126 916	57.78	307.57	193	1.27	.93	106
71	126 918	58.02	307.64	193	1.37	1.00	106
71	126 918	58.07	307.66	193	1.58	1.15	106
71	126 919	58.13	307.67	193	1.35	.98	106
71	126 919	58.17	307.68	193	1.47	1.07	106
71	126 919	58.24	307.71	193	1.33	.96	106
71	126 920	58.30	307.72	193	1.13	.82	106
71	126 921	58.55	307.80	193	1.33	.96	106
71	126 922	58.79	307.87	193	1.25	.90	106
71	126 924	59.01	307.94	193	1.21	.87	106
71	126 925	59.17	307.99	193	1.35	.97	106
71	126 925	59.28	308.03	193	1.25	.89	106
71	126 926	59.39	308.06	193	1.21	.86	106
71	126 927	59.60	308.13	193	1.39	.99	106
71	126 928	59.66	308.15	193	1.27	.90	106
71	126 928	59.74	308.18	193	1.07	.76	106
71	126 928	59.78	308.19	193	1.17	.83	106
71	126 929	59.90	308.23	193	1.11	.79	106
71	126 930	60.04	308.27	193	1.15	.81	106
71	126 931	60.18	308.32	193	1.35	.95	106
71	126 931	60.23	308.34	193	1.37	.97	106
71	126 931	60.30	308.36	193	1.21	.85	106
71	126 934	60.65	308.48	193	1.25	.88	106
71	126 934	60.77	308.52	193	1.11	.78	106
71	126 934	60.80	308.53	193	1.35	.94	106
71	126 935	60.87	308.56	193	.97	.68	106
71	126 936	60.98	308.59	193	1.19	.83	106
71	126 936	61.02	308.61	193	1.23	.86	106
71	126 936	61.11	308.64	193	1.23	.85	106
71	126 938	61.36	308.73	193	1.27	.88	106
71	126 939	61.50	308.77	193	1.29	.89	106
71	126 939	61.57	308.80	193	1.35	.93	106
71	126 939	61.61	308.81	193	1.41	.97	106
71	126 940	61.65	308.83	193	1.45	1.00	106
71	126 940	61.70	308.85	193	1.39	.96	106
71	126 941	61.90	308.92	193	1.21	.83	106
71	126 942	61.98	308.95	193	1.21	.83	106
71	126 943	62.28	309.06	193	1.29	.88	106
71	126 944	62.35	309.09	193	1.31	.89	106
71	126 944	62.39	309.10	193	1.25	.85	106
71	126 944	62.46	309.13	193	1.21	.82	106
71	126 945	62.51	309.14	193	1.31	.89	106
71	126 946	62.67	309.20	193	1.19	.81	106
71	126 946	62.79	309.25	193	1.25	.85	106
71	126 947	62.95	309.31	193	1.27	.86	106
71	126 948	62.97	309.32	193	1.35	.91	106
71	126 948	63.01	309.33	193	1.35	.91	106
71	126 949	63.14	309.38	193	1.19	.80	106

DATE TIME	ZA	AZ	STAR	SIG/UNC	SIG/CCR	RUN	
71 126 950	63.43	309.49	193	1.25	.84	106	
71 126 951	63.47	309.51	193	1.31	.88	106	
71 126 951	63.51	309.52	193	1.33	.89	106	
71 126 951	63.55	309.54	193	1.45	.97	106	
71 126 951	63.60	309.56	193	1.37	.91	106	
71 126 955	64.14	309.77	193	1.14	.75	106	
71 126 955	64.19	309.79	193	1.20	.79	106	
71 126 955	64.25	309.82	193	1.24	.82	106	
71 126 956	64.29	309.83	193	1.16	.76	106	
71 126 956	64.37	309.87	193	1.34	.88	106	
71 126 956	64.43	309.89	193	1.20	.79	106	
71 126 958	64.64	309.98	193	1.18	.77	106	
71 126 958	64.62	309.96	193	1.18	.77	106	
71 126 958	64.75	310.02	193	1.34	.88	106	
71 126 959	64.83	310.05	193	1.26	.82	106	
71 126 959	64.86	310.07	193	1.24	.81	106	
71 127 250	21.70	42.77	193	.71	.68	107	Period 26
71 127 250	21.62	42.62	193	.71	.68	107	
71 127 251	21.57	42.53	193	.73	.70	107	
71 127 251	21.53	42.46	193	.93	.90	107	
71 127 252	21.45	42.30	193	.81	.78	107	
71 127 253	21.32	42.05	193	.81	.78	107	
71 127 253	21.25	41.92	193	.83	.80	107	
71 127 254	21.13	41.68	193	.83	.80	107	
71 127 254	21.08	41.59	193	.83	.80	107	
71 127 256	20.87	41.16	193	.89	.86	107	
71 127 256	20.82	41.07	193	.81	.78	107	
71 127 256	20.78	40.97	193	.85	.82	107	
71 127 258	20.60	40.60	193	.79	.76	107	
71 127 258	20.54	40.47	193	.71	.69	107	
71 127 259	20.45	40.27	193	.65	.63	107	
71 127 3 2	20.07	39.39	193	.77	.75	107	
71 127 3 2	19.95	39.12	193	.81	.79	107	
71 127 3 3	19.89	38.96	193	.61	.59	107	
71 127 3 4	19.75	38.63	193	.71	.69	107	
71 127 3 4	19.69	38.46	193	.77	.75	107	
71 127 3 6	19.53	38.06	193	.65	.63	107	
71 127 3 6	19.44	37.83	193	.69	.67	107	
71 127 3 7	19.37	37.63	193	.59	.57	107	
71 127 3 7	19.28	37.40	193	.69	.67	107	
71 127 3 8	19.18	37.13	193	.63	.61	107	
71 127 3 9	19.10	36.89	193	.67	.65	107	
71 127 311	18.78	35.97	193	.61	.59	107	
71 127 312	18.73	35.81	193	.59	.57	107	
71 127 312	18.66	35.59	193	.65	.63	107	
71 127 313	18.57	35.34	193	.67	.65	107	
71 127 313	18.53	35.21	193	.69	.67	107	
71 127 314	18.43	34.88	193	.57	.56	107	
71 127 315	18.29	34.42	193	.69	.67	107	
71 127 316	18.24	34.25	193	.57	.56	107	

DATE TIME	ZA	AZ	STAR	SIG/UNC	SIG/CCR	RUN	
71 127 317	18.09	33.74	193	.53	.52	107	
71 127 317	18.05	33.60	193	.57	.56	107	
71 127 318	17.97	33.33	193	.55	.54	107	
71 127 319	17.90	33.05	193	.55	.54	107	
71 127 319	17.83	32.80	193	.57	.56	107	
71 127 322	17.57	31.82	193	.57	.56	107	
71 127 322	17.51	31.57	193	.61	.60	107	
71 127 323	17.44	31.31	193	.55	.54	107	
71 127 324	17.29	30.66	193	.55	.54	107	
71 127 324	17.25	30.51	193	.49	.48	107	
71 127 325	17.14	30.05	193	.53	.52	107	
71 127 327	16.99	29.38	193	.53	.52	107	
71 127 328	16.89	28.90	193	.65	.64	107	
71 127 329	16.82	28.57	193	.63	.62	107	
71 128 837	63.86	227.28	257	.89	.59	108	Period 27
71 128 837	63.90	227.33	257	.83	.55	108	
71 128 838	63.97	227.42	257	.73	.48	108	
71 128 838	64.06	227.53	257	.91	.60	108	
71 128 839	64.14	227.63	257	.91	.60	108	
71 128 839	64.18	227.68	257	.91	.60	108	
71 128 840	64.34	227.89	257	.83	.55	108	
71 128 841	64.51	228.10	257	.83	.54	108	
71 128 841	64.56	228.17	257	.79	.52	108	
71 128 843	64.75	228.40	257	.73	.48	108	
71 128 844	64.89	228.58	257	.87	.57	108	
71 128 844	64.93	228.63	257	.89	.58	108	
71 128 844	65.01	228.73	257	.81	.53	108	
71 128 845	65.11	228.85	257	.95	.62	108	
71 128 846	65.21	228.98	257	.95	.62	108	
71 128 846	65.25	229.03	257	.91	.59	108	
71 128 847	65.37	229.17	257	.87	.56	108	
71 128 850	65.94	229.85	257	.91	.58	108	
71 128 850	65.98	229.90	257	.87	.56	108	
71 128 851	66.07	230.00	257	.89	.57	108	
71 128 851	66.11	230.04	257	.95	.60	108	
71 128 852	66.19	230.14	257	.93	.59	108	
71 128 852	66.32	230.30	257	1.01	.64	108	
71 128 853	66.43	230.43	257	.87	.55	108	
71 128 854	66.52	230.52	257	.99	.62	108	
71 128 854	66.60	230.62	257	1.01	.64	108	
71 128 855	66.68	230.71	257	.95	.60	108	
71 128 856	66.85	230.90	257	1.01	.63	108	
71 128 856	66.89	230.95	257	.97	.61	108	
71 128 856	66.97	231.05	257	.95	.59	108	
71 128 859	67.44	231.58	257	.93	.58	108	
71 128 9 0	67.54	231.69	257	.87	.54	108	
71 128 9 0	67.60	231.75	257	.99	.61	108	
71 128 9 0	67.64	231.79	257	1.01	.62	108	
71 128 9 1	67.71	231.87	257	1.01	.62	108	
71 128 9 1	67.78	231.95	257	.97	.60	108	

DATE TIME	ZA	AZ	STAR	SIG/UNC	SIG/CCR	RUN	
71 128 9 2	67.99	232.18	257	1.03	.63	108	
71 128 9 3	66.10	232.30	257	.97	.59	108	
71 128 9 3	68.17	232.38	257	.91	.55	108	
71 128 9 5	68.35	232.58	257	.91	.55	108	
71 128 9 5	68.44	232.67	257	1.02	.62	108	
71 128 9 6	68.55	232.79	257	1.01	.61	108	
71 128 9 6	68.65	232.90	257	.99	.60	108	
71 128 9 9	69.09	233.37	257	1.10	.66	108	
71 128 910	69.25	233.53	257	.97	.58	108	
71 128 911	69.38	233.67	257	1.10	.65	108	
71 128 911	69.41	233.70	257	1.10	.65	108	
71 128 911	69.51	233.80	257	1.12	.66	108	
71 128 913	69.72	234.02	257	1.14	.67	108	
71 128 913	69.78	234.08	257	1.16	.68	108	
71 127 419	14.32	356.82	193	.61	.60	16	Period 28
71 127 420	14.33	356.00	193	.63	.62	16	
71 127 421	14.35	355.00	193	.65	.64	16	
71 127 422	14.36	354.77	193	.67	.66	16	
71 127 422	14.37	354.60	193	.65	.64	16	
71 127 422	14.37	354.31	193	.65	.64	16	
71 127 423	14.39	353.73	193	.65	.64	16	
71 127 425	14.43	352.75	193	.65	.64	16	
71 127 425	14.44	352.34	193	.65	.64	16	
71 127 427	14.49	351.31	193	.69	.68	16	
71 127 427	14.51	350.97	193	.69	.68	16	
71 127 428	14.53	350.46	193	.71	.70	16	
71 127 539	21.71	317.22	193	.65	.63	17	Period 29
71 127 539	21.77	317.11	193	.69	.66	17	
71 127 541	21.95	316.79	193	.69	.66	17	
71 127 541	21.99	316.73	193	.71	.68	17	
71 127 542	22.10	316.54	193	.69	.66	17	
71 127 542	22.21	316.35	193	.67	.64	17	
71 127 543	22.29	316.21	193	.75	.72	17	
71 127 543	22.35	316.11	193	.71	.68	17	
71 127 545	22.58	315.75	193	.71	.68	17	
71 127 546	22.69	315.58	193	.61	.59	17	
71 127 546	22.73	315.52	193	.67	.64	17	
71 127 547	22.89	315.27	193	.61	.59	17	
71 127 547	22.94	315.19	193	.67	.64	17	
71 127 548	23.03	315.06	193	.69	.66	17	
71 127 548	23.13	314.91	193	.65	.62	17	
71 127 618	27.84	309.83	193	.81	.76	18	Period 30
71 127 619	27.97	309.74	193	.79	.74	18	
71 127 620	28.05	309.67	193	.63	.59	18	
71 127 621	28.35	309.45	193	.89	.83	18	
71 127 622	28.46	309.37	193	.77	.72	18	
71 127 622	28.50	309.34	193	.77	.72	18	
71 127 623	28.67	309.23	193	.77	.72	18	
71 127 624	28.75	309.17	193	.77	.72	18	
71 127 624	28.79	309.14	193	.75	.70	18	

DATE TIME	ZA	AZ	STAR	SIG/UNC	SIG/CCR	RUN	
71 127 626	29.04	308.97	193	.81	.76	18	
71 127 626	29.18	308.88	193	.75	.70	18	
71 127 627	29.33	308.78	193	.77	.72	18	
71 127 628	29.37	308.76	193	.71	.66	18	
71 127 629	29.54	308.65	193	.71	.66	18	
71 127 629	29.62	308.60	193	.69	.64	18	
71 127 630	29.72	308.54	193	.75	.70	18	
71 127 717	37.82	305.65	193	.65	.58	19	Period 31
71 127 717	37.87	305.64	193	.65	.58	19	
71 127 718	37.95	305.63	193	.67	.59	19	
71 127 719	38.16	305.59	193	.67	.59	19	
71 127 719	38.22	305.58	193	.63	.56	19	
71 127 720	38.31	305.57	193	.65	.58	19	
71 127 720	38.39	305.56	193	.65	.58	19	
71 127 721	38.58	305.53	193	.71	.63	19	
71 127 722	38.73	305.51	193	.69	.61	19	
71 127 723	38.81	305.50	193	.67	.59	19	
71 127 723	38.90	305.49	193	.61	.54	19	
71 127 724	38.97	305.48	193	.75	.66	19	
71 127 724	39.09	305.47	193	.81	.71	19	

APPENDIX C

COMMENTS ON CORRELATION ANALYSIS

APPENDIX C

COMMENTS ON CORRELATION ANALYSIS

In this report, a great deal of emphasis is placed on correlation analysis. In particular, the concept of a correlation coefficient between the sets of observed values for two variables is often used. This concept has been discussed by Topping (1960). Some examples of correlation coefficients and the rather idealized data distributions for which they apply are presented in Figures C1 to C3. In each figure, perfect correlation (corr = 1.0) would correspond to the data equation $X \propto Y$. A perfect anticorrelation (corr = -1.0) would correspond to the data equation $X \propto -Y$. Each correlation coefficient is accompanied by a level of confidence based on a table quoted by Fischer and Yates. The table is included for the reader's reference.

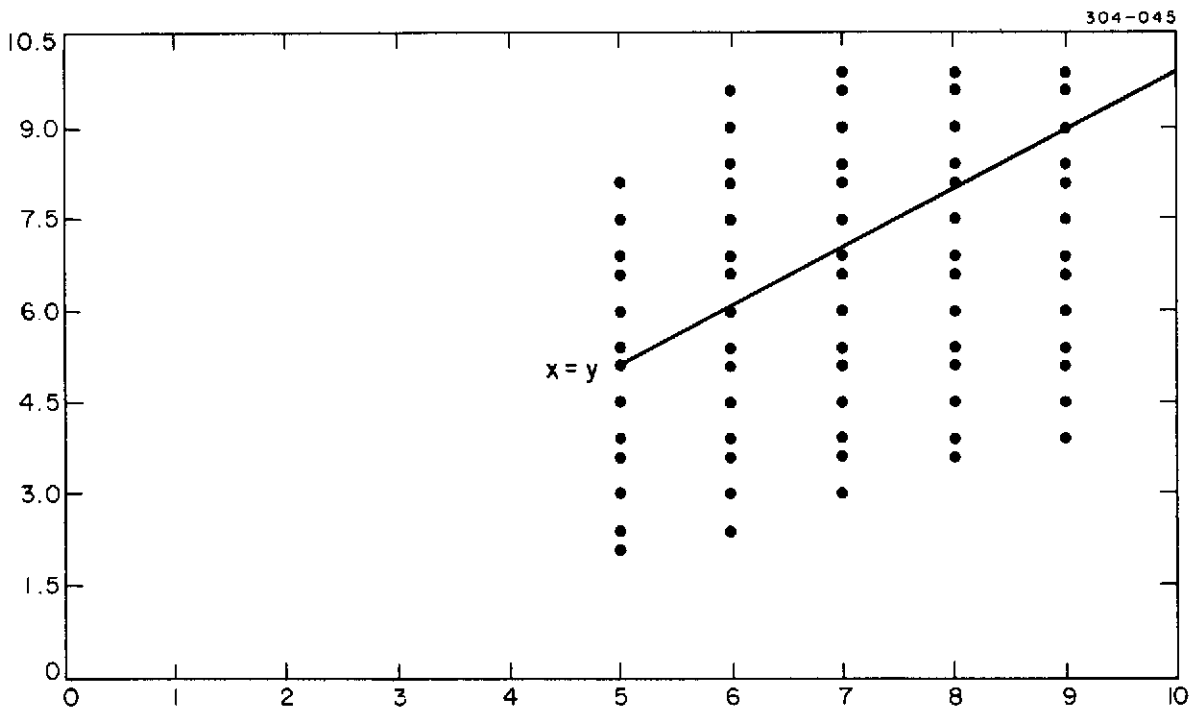

Figure C1. Example of data distribution with corresponding correlation coefficients.

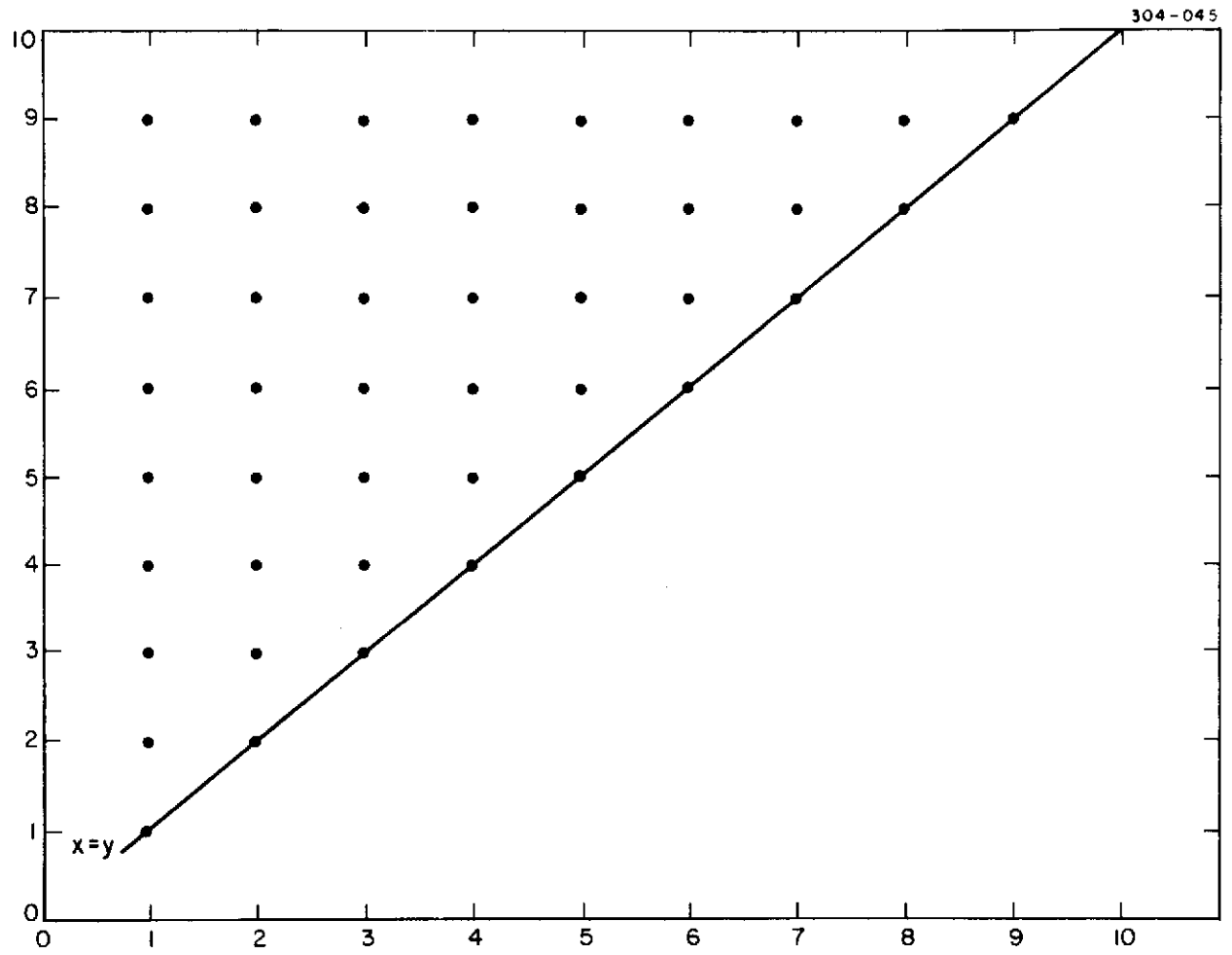

Figure C2. Example of data distribution with corresponding correlation coefficients.

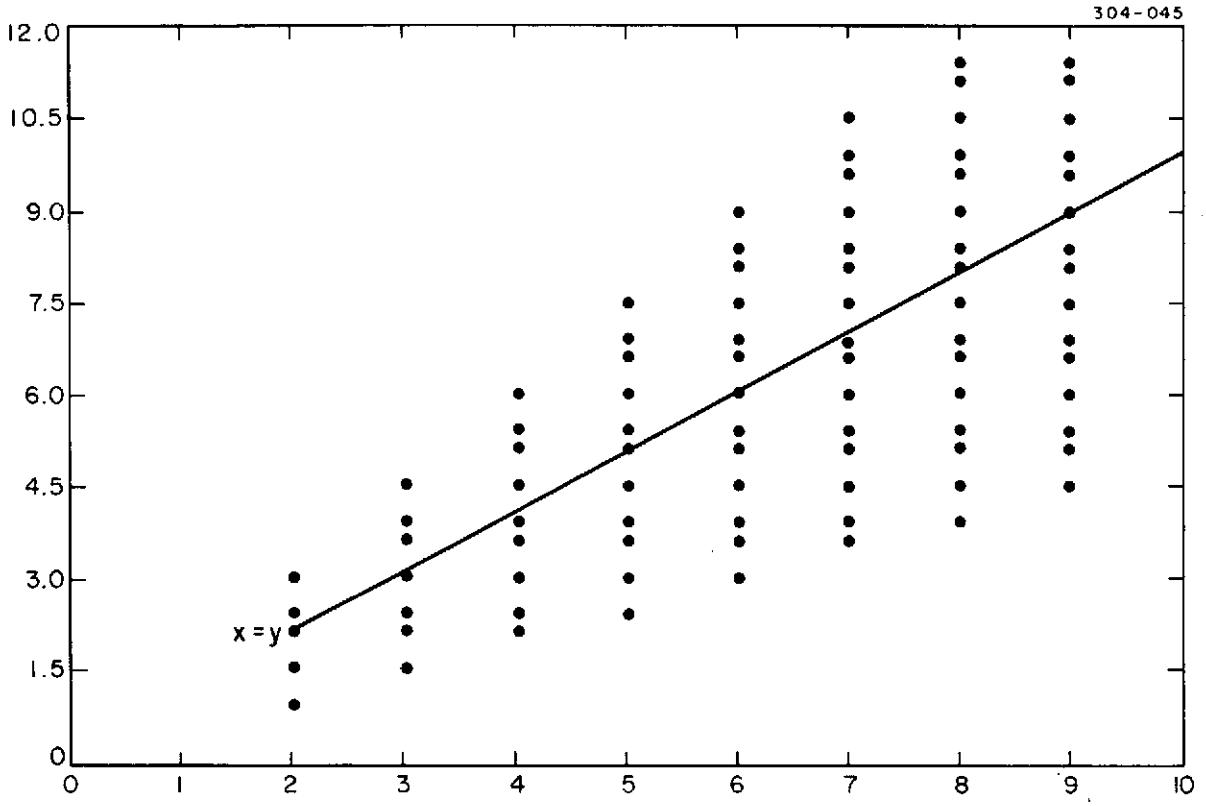

Figure C3. Example of data distribution with corresponding correlation coefficients.

Correlation Coefficients

The table* gives values of the correlation coefficient r that have certain probabilities of being exceeded for observations of variables whose parent distributions are independent. The number of pairs of observations is N. To illustrate: for a sample of 10 pairs of observations on unrelated variables, the probability is 0.10 that it will have $r \geq 0.549$, and the probability is 0.001 that $r \geq 0.875$.

N	Probability				
	0.10	0.05	0.02	0.01	0.001
3	0.988	0.997	0.999	1.000	1.000
4	0.900	0.950	0.980	0.990	0.999
5	0.805	0.878	0.934	0.959	0.992
6	0.729	0.811	0.882	0.917	0.974
7	0.669	0.754	0.833	0.874	0.951
8	0.621	0.707	0.789	0.834	0.925
10	0.549	0.632	0.716	0.765	0.872
12	0.497	0.576	0.658	0.708	0.823
15	0.441	0.514	0.592	0.641	0.760
20	0.378	0.444	0.516	0.561	0.679
30	0.307	0.362	0.423	0.464	0.572
40	0.264	0.312	0.367	0.403	0.502
60	0.219	0.259	0.306	0.337	0.422
80	0.188	0.223	0.263	0.291	0.366
100	0.168	0.199	0.235	0.259	0.327

*Adapted from Table VI of Statistical Treatment of Experimental Data, by H. D. Young, McGraw-Hill Book Co., New York, 1962, p. 164.

BIOGRAPHICAL NOTES

MICHAEL R. PEARLMAN received his B.S. in physics from the Massachusetts Institute of Technology in 1963 and his Ph.D. in physics from Tufts University in 1968.

Dr. Pearlman joined the staff of Smithsonian Astrophysical Observatory in September 1968 as a scientist in the Satellite Geophysics Group. From February 1971 to July 1972, he was a Visiting Scientist in the Office of Geodetic Satellites at the National Aeronautics and Space Administration Headquarters in Washington, D. C. Since July 1972, Dr. Pearlman has been Chief of the Experimental Geophysics Department in the Observatory's Earth Dynamics Program. He is currently working primarily on laser satellite tracking.

JACK L. BUFTON received his B.S. in engineering physics from Lehigh University in 1966 and his M.S. in physics from the University of Maryland in 1970.

Mr. Bufton joined the staff of the Goddard Space Flight Center in June 1966. Since that time he has worked primarily in research and development programs to measure the effects of atmospheric turbulence on laser propagation. His current efforts in the Laser Technology Branch at Goddard include direct measurement of high-altitude turbulence strength with temperature sensors and participation in atmospheric-propagation experiments with balloon-borne laser systems.

DONALD HOGAN received a B.S. degree in navigation from the Massachusetts Maritime Academy in 1957 and has attended Boston University, the University of New Mexico, and Pima College in Tucson.

Before joining Smithsonian Astrophysical Observatory in 1963, he was Operations Officer in communications and electronics in the Navy. After being on the observing staff at SAO field stations in New Mexico and Iran, Mr. Hogan transferred to Mt. Hopkins in 1967, where he became Manager of the Observer Services Division. In June 1973, he was appointed Support Supervisor of the Mt. Hopkins Observatory.

DeWAYNE KURTENBACH received a B.S. degree in mathematics and electronics from Southern State College in Springfield, South Dakota, in 1961. He has also attended the University of Arizona and Pima College in Tucson.

Before coming to the Smithsonian Astrophysical Observatory in 1969, he taught mathematics and electronics at the high-school level.

Mr. Kurtenbach joined the Observer Services Division at Mt. Hopkins in 1969. In June 1973, he transferred to the technical support group at Mt. Hopkins.

KENNETH GOODWIN received an Associates Degree in electrical engineering in 1962 from New York State University and has attended New Mexico State University.

Mr. Goodwin joined Smithsonian Astrophysical Observatory in 1962 and has been an observer and EECo timing specialist at SAO field stations in New Mexico, Spain, and Arizona. He has also been a laser leader and has worked on Project Scanner.

In early 1969, Mr. Goodwin joined the Observer Services Division at Mt. Hopkins. He left the Observatory in July 1973.

NOTICE

This series of Special Reports was instituted under the supervision of Dr. F. L. Whipple, Director of the Astrophysical Observatory of the Smithsonian Institution, shortly after the launching of the first artificial earth satellite on October 4, 1957. Contributions come from the Staff of the Observatory.

First issued to ensure the immediate dissemination of data for satellite tracking, the reports have continued to provide a rapid distribution of catalogs of satellite observations, orbital information, and preliminary results of data analyses prior to formal publication in the appropriate journals. The Reports are also used extensively for the rapid publication of preliminary or special results in other fields of astrophysics.

The Reports are regularly distributed to all institutions participating in the U. S. space research program and to individual scientists who request them from the Publications Division, Distribution Section, Smithsonian Astrophysical Observatory, Cambridge, Massachusetts 02138.